University of Naples “Federico II”

Department of Chemical Sciences

Doctoral Thesis

Alessandro Emendato

Structures and interactions of amyloidogenic polypeptides in biomimetic environments.

Tutor: Prof. Delia Picone

Supervisor: Prof. Nadia Rega

2014-2017

"Muad'Dib learned rapidly because his first training was in how to learn. And the first lesson of all was the basic trust that he could learn. It's shocking to find how many people do not believe they can learn, and how many more believe learning to be difficult. Muad'Dib knew that every experience carries its lesson."

Dune, Frank Herbert, 1965

Table of Contents

Abbrevations 1
Chapter 1 – Introduction 2
1.1 Protein aggregation 2
1.2 Aim of the thesis 4
1.3 Amyloid β peptide 5
1.3.1 Alzheimer's Disease 7
1.3.2 The Amyloid Cascade Hypothesis 8
1.3.3 Abeta amyloid peptides structure 11
1.3.4 Abeta peptides membrane interaction 17
1.3.5 Glycation 24
1.4 Hemopressin 29
1.5 Sweet Proteins 32
1.6 Thesis outline 34
Chapter 2 – Abeta peptides recombinant expression 36
2.1 Work outline 36
2.2 Abeta40 expression and purification protocol 36
2.3 Experimental Section 40
2.3.1 Materials 40
2.3.2 Transformation 40
2.3.3 Abeta peptides expression 41
2.3.4 Inclusion bodies purification procedure 41
2.3.5. Ion exchange chromatography 41
2.3.6 MW fractionation step 42
Chapter 3 - Interaction between Abeta42 with model phospholipid bilayers 43
3.1 Work outline 43
3.2 Sample conditions design 44

3.3 CD spectroscopy 45
3.4 Electron Paramagnetic Resonance 48
3.5 Membrane Leakage 53
3.6 Conclusions 54
3.7 Experimental Section 56
3.7.1 Materials 56
3.7.2 Liposome preparation 56
3.7.3 Peptide samples preparation 56
3.7.4 CD spectroscopy 57
3.7.5 ESR spectroscopy 57
3.7.6 Leakage experiments 58
Chapter 4: Effect of glycation on structure and aggregation properties of Abeta peptides 59
4.1 Work outline 59
4.2 Aqueous environment 61
4.2.1 Reaction kinetics 61
4.2.2 Effects on secondary structure 65
4.3 Apolar environment 69
4.4 Conclusions 72
4.5 Experimental Section 73
4.5.1 Materials 73
4.5.2 Samples preparation 73
4.5.3 Fluorescence spectroscopy 73
4.5.4 Circular Dichroism spectroscopy 74
Chapter 5 – High-resolution analysis of hemopressin peptides conformation 75
5.1 Work Outline 75
5.2 CD spectroscopy screening 76
5.2.1 Aqueous environment 76
5.2.2 Apolar environments 77

5.3 NMR analysis 80
5.3.1 Aqueous environments 80
5.3.2 Apolar environments 83
5.4 Conclusions 91
5.5 Experimental section 92
5.5.1 Materials 92
5.5.2 CD spectroscopy 92
5.5.3 NMR spectroscopy 93
Chapter 6 – Aggregation propensity study of the sweet protein Y65R-MNEI 94
6.1 Work outline 94
6.2 Thermal stability 94
6.3 Thioflavin T assays 96
6.4 Atomic Force Microscopy 98
6.5 Conclusions 100
6.6 Experimental Section 100
6.6.1 Materials 100
6.6.2 Circular Dichroism 101
6.6.3 ThioflavinT assay 101
6.6.4 Atomic Force Microscopy 101
Final Remarks 103
Appendix A – Hemopressin peptides chemical shifts tables 106
A-I Hp in NaP pH 3.0 106
A-II Hp in NaP pH 7.4 107
A-III RVD-Hp in NaP pH 3.0 108
A-IV RVD-Hp in NaP pH 7.4 109
A-V Hp in HFIP/NaP 50/50 % v/v pH 3.0 110
A-VI Hp in HFIP/NaP 50/50 % v/v pH 7.4 111
A-VII RVD-Hp HFIP/NaP 50/50 % v/v pH 3.0 112
A-VIII RVD-Hp HFIP/NaP 50/50 % v/v pH 7.4 113

Appendix B – PhD Course Activity Summary 114
References 120

Abbrevations

Abeta – Amyloid beta peptide.

AbetaNG – Non glycated Abeta.

AbetaG – Glycated Abeta.

AD – Alzheimer disease.

AFM – Atomic force microscopy.

AGEs – Advanced glycation end products.

ANTS – 8-aminonaphthalene-1,3,6-trisulfonic acid.

APP – Amyloid precursor protein.

CD – Circular dichroism spectroscopy.

Chol – Cholesterol.

COSY – Correlation spectroscopy.

CSI – Chemical shift index.

DMSO – Dimethyl sulphoxide.

DOPC – 1,2-dioleoyl-sn-glycero-3-phosphocholine.

DPX – p-xylene-bis-pyridinium bromide.

E.Coli – Escherichia Coli.

EM – Electron microscopy.

ESR – Electron spin resonance.

FTIR – Fourier transform infrared spectroscopy.

GM1 – Monosialic ganglioside.

ThT – ThioflavinT.

HFIP – Hexafluoroisopropanol.

HN – Amide proton.

Hp – Hemopressin.

HSQC – Heteronuclear single quantum coherence spectroscopy.

IBs – Inclusion bodies.

IPTG – Isopropyl β-D-1-thiogalactopyranoside.

LB – Luria-Bertani broth.

Ld – Fluid-disordered phase.

Lo – Fluid-ordered phase.

LUV – Large unilamellar lipid vesicle.

MD – Molecular dynamics.

MGO – Methylglyoxal.

MW – Molecular weight.

n-PCSL – Spin-labeled phosphocholines.

NaP – Sodium phosphate buffer solution.

NMR – Nuclear magnetic resonance spectroscopy.

NOESY – Nuclear Overhauser effect spectroscopy.

RVD-Hp – RVD-Hemopressin.

PAGE – Polyacrylamide gel electrophoresis.

POPC – 1-palmitoyl-2-oleoyl-sn-glycero-3-phosphocholine.

POPS – 1,2-diacyl-sn-glycero-3-phospho-L-serine.

PUFA – Polyunsaturated fatty acids.

TFE – Trifluoroethanol.

ROESY – Rotating-frame Overhauser spectroscopy.

S – Lipid segmental order parameter.

SDS – Sodium dodecyl sulphate.

SM – Sphingomyelin.

TFA – Trifluoroacetic acid.

Tm – Melting temperature.

TOCSY – Total correlation spectroscopy.

Chapter 1 – Introduction

1.1 Protein aggregation

The importance of protein aggregation has increasingly gained interest in the last 20 years, due to the discovery that the formation of amorphous or fibril-like protein aggregates are involved in many different cellular processes.

Data gathered on this topic in the recent years show that an increasing number of pathologies are associated with protein aggregation and that aggregation often occurs through misfolding rather than just unfolding. A very important class of protein aggregation related diseases are amyloidoses, of which the more studied are Alzheimer's disease, Huntington's disease, Bovine Spongiform Encephalopathy, familial amyloid polyneuropathy and Parkinson's disease [1]. Extensive studies show that all amyloid diseases are characterized by assemblies containing extremely insoluble protein fibrillar aggregates that share similar morphological features but comprise many different proteins with no obvious sequence similarity, called amyloid fibrils (see Table 1-1) [2,3].

The interest in protein aggregation is, however, not limited to its medical implications. Many more proteins than those known to be implicated in human diseases have been found to lead to amyloid fibrils, suggesting the hypothesis that most, if not all, amino acid sequences might be able to misfold in a similar ordered way. This evidence places protein misfolding into a much wider perspective [4].

It has also been recently shown that protein aggregation is not always dangerous: formation of essential cellular bodies such as melanosomes and dendritic cell aggresome-like structures depends on protein aggregation [5]. Moreover, some cellular protein interactions involve the formation of amyloid-like structures and

several protein and peptide hormones are stored in the cell in amyloid-like structures [6].

One of the main features of all amyloid protein deposits, both functional and disease-related, is their ability to display positive apple green birefringence under polarized light after binding amyloidophilic dyes such as Congo red [7,8] or ThioflavinT (ThT) [9]. Electron Microscopic (EM) examination of amyloid fibrils revealed that fibrils are 5-10 nm in width and of indefinite length [10,11]. X-ray diffraction analysis revealed a so-called cross-β diffraction pattern [12], showing that the fibrils are ordered in a β–pleated sheet conformation, with the direction of the polypeptide backbone perpendicular to the fibrils' axis. The structural similarity of amyloid fibrils suggests that the key elements of the aggregation process may be common to all proteins involved. However, the molecular basis underlying amyloid aggregation are still poorly understood [13], making more difficult the identification of the therapeutic targets for treating amyloid diseases. Moreover, recent studies have shown that the amyloid toxicity could be related to the formation of soluble oligomeric species during the amyloid fibrils formation process, with the latter relatively inert compared to their oligomeric counterparts [14]. Whether oligomers are precursors to fibrils or form along a separate pathway is a subject of current research and academic debate [15]. Therefore, it is critical to understand the mechanisms of these processes at a molecular level, in order to find a rationale for the structure-related toxicity of amyloid fibrils.

Diseases	Involved proteins
Alzheimer's Disease	Amyloid β-protein
Parkinson's disease	α-Synuclein
Creutzfeldt–Jakob disease	Prion protein
Huntington's disease	Huntingtin
Familial Amyloid Polyneuropathy	Transthyretin
Diabetes type 2	Amylin
Amyotrophic lateral sclerosis (ALS)	Superoxide dismutase (SOD)

Table 1-1 *List of some amyloid-based diseases and their related proteins.*

1.2 Aim of the thesis

This thesis aims to provide structural and biophysical insights on the molecular mechanism underlying amyloid aggregation. Three polypeptides were chosen as models for these studies, differing in size and molecular origin, but sharing the capability to form fibrillar aggregates, although starting from different conformations, therefore likely through different mechanisms. The main model is represented by amyloid beta peptides, in particular the 40 and the 42 residues peptides, henceforth called Abeta40 and Abeta42, which are related to Alzheimer disease. The ability to switch from α-helical conformation in membrane and apolar environment [16,17] to β-sheet fibril structure in aqueous solution characterizes these peptides The second model is Hemopressin, a short peptide that shows very promising pharmacological application, hampered by its aggregation propensity; this peptide is unstructured in aqueous buffers, but it forms amyloid fibrils in specific conditions in vitro [18]. The third model is an engineered protein, called Y65R-MNEI, derived from monellin, very interesting for its potential biotechnological application as ipocaloric sweetener. Its structures is very close to that of the parent protein MNEI which, at native state, is a soluble globular protein rich in β-sheet. MNEI is a well-known model for protein folding studies; moreover, after a partial unfolding event, it is also able to form amyloid fibrils [19].

These molecules were studied at different levels of deepness in literature, with many different biophysical techniques. The choice of these three models allowed me to study the amyloid aggregation process at different stages, using a combination of biophysical techniques widely used in protein aggregation studies. In particular, the effect of different physico-chemical parameters (temperature, ionic strength, pH and solvent polarity), of the interaction with membrane model systems and of the effect of non-enzymatic post-translational modification on the aggregation properties of these molecules was investigated. A literature review about the chosen models and a more detailed work outline are reported in this chapter.

1.3 Amyloid β peptide

Abeta peptide was first identified by Glemer and Wong in 1984 as the principal component of amyloid deposits present in the brain of patients affected by Alzheimer Disease [20]. Abeta has a peptide length of 39-43, with the majority of amyloid found in senile plaques having a peptide length of 40 and 42 residues [21,22]. The sequence of the two main Abeta peptides, Abeta40 and Abeta42, are shown in figure 1.1.

NH2-DEAFRHDSGY^{10}EVHHQKLVFF^{20}AEDVGSNKGA^{30}IIGLMVGGVV^{40}IA-COOH

Figure 1.1 *Abeta peptides aminoacidic sequences: Abeta40 sequence is coloured in red, the two more C-term residues present in Abeta42 are coloured in blue.*

Abeta40 is more soluble and aggregates slowly, while Abeta42 is a "sticky" β-amyloid peptide that rapidly forms insoluble clumps [23]. Abeta peptides are encoded by a gene on chromosome 21 as part of a larger transmembrane protein, named amyloid precursor protein (APP) [23]. The function of APP is unclear at this point, but research has suggested that APP may have a role as an autocrine factor to stimulate the proliferation of fibroblasts [24] and as a modulator of cell adhesion. In addition, APP is implicated in the regulation of intracellular calcium [25] metal ion homeostatsis [26], and cell growth [24]. Recently, Sanders and colleagues demonstrated that APP

may have a cholesterol-binding site with E693 and N698 accepting and donating hydrogen bonds to bind cholesterol, thus providing evidence that APP may have a role in cholesterol regulation and metabolism [27].

Proteolytic cleavage of APP occurs in two distinct manners: via either the α-secretase pathway or the β-secretase pathway [28]. The former pathway involves neuronal secretion of sAPPα by a putative α-secretase enzyme that precludes the formation of full-length Aβ, as the cleavage occurs at level of the peptide bond corresponding to Abeta residues 16 and 17. Traditionally the α-secretase pathway has been called the non-amyloidogenic pathway since full-length Abeta cannot be formed anymore. Full-length Abeta is generated when N-terminus of APP is sequentially cleaved by a β-secretase and γ-secretase, releasing the amyloidogenic peptide in the extracellular space, traditionally called amyloidogenic pathway. APP metabolism by the β-secretase pathway was initially proposed to be an abnormal proteolytic processing event specific to, and with a causative role, in AD. However, proteolysis of APP via the β-secretase pathway has been found to be a normal process, which occurs ubiquitously in both AD and non-demented individuals [29]. The location of the γ-secretase cleavage site is variable, which causes the C-terminus of Aβ to vary between amino acids 39 and 43. A schematic view of this process is shown in figure 1.2.

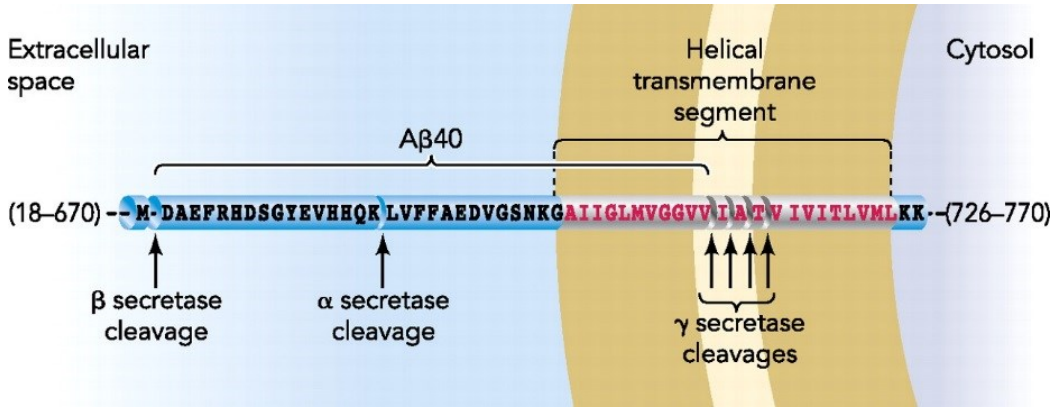

Figure 1.2 *Schematic view of APP proteolytic cleavage [30].*

This heterogeneous cleavage pattern can be explained by assuming that γ-secretase activity is due to multiple enzymes, or even that Abeta generation occurs in different cellular sites, where environmental conditions affect enzymes specificity [31].

1.3.1 Alzheimer's Disease

Alzheimer's disease is a neurodegenerative disorder that results in progressive cognitive impairment, including dementia, personality changes, judgment, language skills and memory loss, eventually resulting in the death of the individuals.

The pathology which would later be identified as AD was first described by Alois Alzheimer in 1907 [32]. A significant period of time elapsed between the time that Dr. Alzheimer identified the disease until any significant progress was made in the study of AD: it was not until the mid- to late 1980's that the Abeta peptides were shown to be correlated with AD symptoms [21,33].

Pathologically, AD is identified post-mortem by the presence of extracellular amyloid plaques and intracellular neurofibrillary tangles. Research by Selkoe and others has shown that Abeta peptides are the primary constituent in these amyloid plaques, while hyper-phosphorylated tau protein is the primary constituent in neurofibrillary tangles [34]. Post mortem examinations of patients with AD symptoms have shown a

reduction in the physical size of the temporal and frontal lobes, hippocampus and amygdala, the regions involved in memory and learning process. This cerebral atrophy is the direct result of neuronal apoptosis and synaptic atrophy appearing concurrently with the presence of amyloid plaques and tau tangles [35]. In addition, inflammatory cytokines formed by degenerating neurons and activated microglia around the amyloid plaques may contribute to the symptoms associated with AD [35].

The exact mechanism by which Abeta produces neurodegenerative symptoms remains unclear, although several mechanisms have been suggested. The interaction between oligomeric Abeta peptides and lipid membranes is thought to have a central role in AD pathology [36-38]. Free radical production [39] and changes in lipid metabolism has been identified [40]. Other mechanisms that have been proposed are: induction of cell apoptosis [41] and the production of toxic levels of hydrogen peroxide [42].

1.3.2 The Amyloid Cascade Hypothesis

The notion that Abeta peptides are the causative agents in the etiology of AD has been a controversial one [43]. However, few researchers have managed to present alternative hypotheses that explain the majority of pathological and biophysical phenomena that are manifested in the progression of AD. The amyloid cascade hypothesis has been revised over time even though the basic precepts of the hypothesis remain intact (Figure 1.3).

Few years after the identification of Abeta peptides as the major constituent in amyloid plaques, Hardy and Higgins proposed their hypothesis [44], suggesting that Abeta aggregation is the causative agent of AD and that all other phenomenon such as neurofibrillatory tangles, tau phosphorylation, vascular damage, neuronal death, dementia, and finally death, follow, in that order, from the over- production of Abeta [34,45]. A schematic view of the process is reported in figure 1.3.

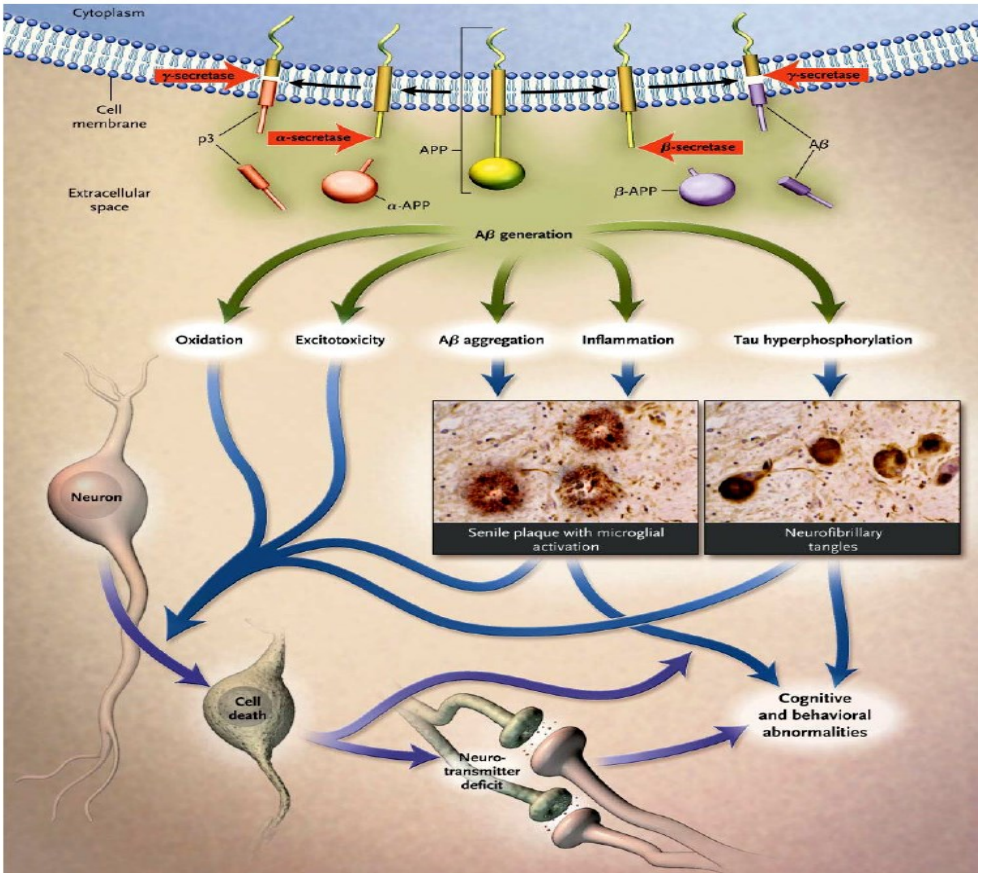

Figure 1.3 *Amyloid Cascade Hypothesis scheme [46].*

One of the recurring criticisms of the amyloid cascade hypothesis is that it fails to explain the unequal distribution of amyloid deposition in the brain; many people have been observed to have neuronal amyloid plaques during post mortem autopsy without demonstrating any Alzheimer's symptoms while they were alive [47]. Lastly, the amyloid cascade hypothesis is unable to explain why Alzheimer's is an age related disease or why there are considerable vascular pathologies related to AD [48].

A number of revisions to the amyloid cascade hypothesis have been accepted by the research community without compromising the underlying premise that Abeta peptides are the causative agents of AD. Firstly, it is now widely accepted that small

molecular weight aggregates are the most neurotoxic amyloid species rather than amyloid fibrils or amyloid plaques [49,50], leading some authors to refer to an "oligomer cascade hypothesis".

By the turn of the last century, many studies have shown that neuronal synapses were most affected by amyloid neurotoxicity by impairing potentiation as a result of the interaction between amyloid oligomers and the neuronal synapse [51,52]. In addition, recent studies shown that cytotoxicity is a generic effect of all amyloid oligomers [2] and is associated with the initial misfold of oligomers setting off the amyloid cascade [50,53].

A very nice analogy conceived by Selkoe figures the amyloid plaque like "jails" which neutralize toxic oligomers. Once the "jails" are full, there are too many oligomers for the "police" (neuroclearance mechanisms) to deal with and the oligomers can wreck their havoc on the brain. Attempting to prevent amyloid plaques would release the "bad guys" causing more damage (Selkoe, D. (n.d.). Amyloid hypothesis - beta oligomers and plaques. Retrieved 10 21, 2013, from DNA Learning Center: http://www.dnalc.org/view/2134-Amyloid-hypothesis-beta-oligomers-and-plaques.html).

Secondly, in late onset AD, the incorrect cleaving of APP into the more pathogenic Abeta42 form as opposed to the more stable Abeta40 has been linked to AD symptoms rather than the simply overproduction of them [47]. The amyloid cascade hypothesis assumes a linear progression of the disease; however, considerable evidence is mounting that different amyloid species with varying degrees of toxicities may lie along different reaction pathways. Factors such as metals catalyse the aggregation process along differing pathways.

1.3.3 Abeta amyloid peptides structure

The amyloid β peptide is considered as part of the Intrinsically Disordered Proteins, a class of protein characterised by lack of a unique 3D folding at physiological conditions; on the other hand, they show a very high structural polymorphism, which is largely dependent on the environment [54,55]. For these reasons, the field of structural studies of Abeta peptides is extremely complex and encompasses the structure of the soluble Abeta, its polymerization into intermediates and their assembly in amyloid fibrils that characterise the amyloid deposition in vivo. Structural studies of soluble Aβ have been performed using NMR, CD and FTIR methods to look at the structure of different regions of Abeta in various solvents. Atomic force microscopy (AFM) has proved a valuable tool to investigate the nature of the intermediates in the amyloid pathway. Transmission EM and fiber diffraction have been used to examine the structure of the amyloid fibrils, as well as methods of solid-state NMR and FTIR.

To structurally characterise the non-aggregated state of the Abeta peptides, tri-dimensional structures have been obtained using smaller fragments in aqueous solution or full-length peptides in non-physiological conditions (pH, presence of strong organic solvents or detergents) to avoid protein aggregation. The N-terminal 28-amino-acid fragment of Abeta was studied in detail by 1H-NMR in water–trifluoroethanol (TFE) solutions and was found to have a predominantly α-helical structure [56]. NMR structures of Abeta40 and Abeta42 have been determined respectively in the presence of sodium dodecyl sulphate (SDS) micelles [17] and in hexafluoroisopropanol (HFIP)/water mixture [16] (figure 1.4). All these NMR studies revealed the presence of a large helical region, however the current model representing the structure of Abeta42 in an apolar environment hints to the presence of two helical regions encompassing residues 8–25 and 28–38, connected through a flexible kink or a regular type I β-turn. Thus, Abeta generally forms stable α-helical

conformation in organic solvents or in micelles, although the specific conformation can be affected by pH, concentration and incubation time.

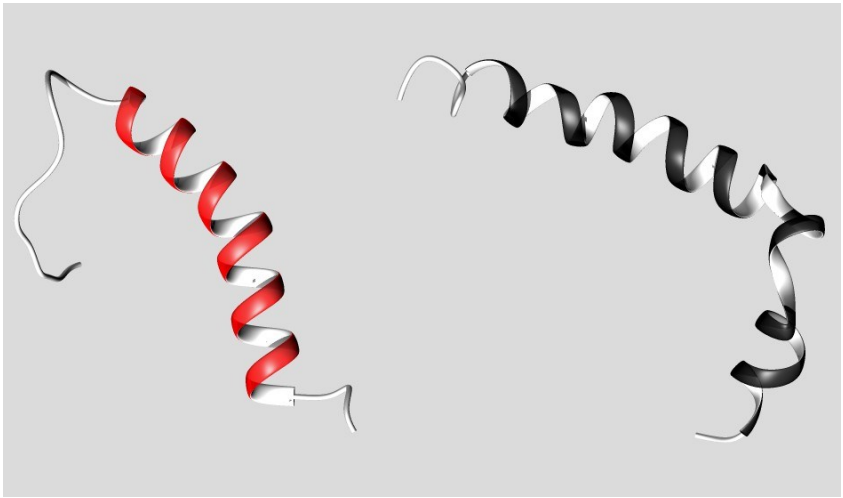

Figure 1.4 *Solution structural models of Abeta40 in SDS micelles (left side, red ribbon, pdb code 1BA4) and of Abeta42 in HFIP/water mixture (right side, black ribbon, pdb code 1IYT).*

This structure is modified when the water amount is increased [57], and the presence of a β-sheet appears in the C-terminal region. Peptide aggregation and precipitation was observed to occur following β-sheet formation in a time dependent manner, indicating that formation of β-sheet structure is directly related to peptide aggregation [57-59]. β-Sheet formation by Abeta was observed to be strongly dependent on environmental conditions, and such factors inducing these structural changes were identified over the last few years [60]. For example, it was found that β-sheet formation and peptide aggregation of Abeta40 have pH dependence and were most rapid at pH 5.5. The observation that β-sheet formation by Abeta was promoted at low pH is, particularly, of interest as the pH in AD brain has been found to be slightly lower than in normal brain, and this acidosis may result in enhanced peptide deposition. The longer Abeta42 isoform instead aggregates more rapidly at pH 7.4, demonstration that the presence of two extra residues at the C-terminal changes dramatically its aggregation properties with respect to the other isoform.

It may not necessarily be true that there is a distinct and reliable correlation between in vitro solution structure and Abeta deposition; however, particular conformational features in soluble, in vitro samples may contribute to a better understanding of Abeta deposition in AD. Studies on Abeta peptides in solution have revealed a common theme in which the soluble full length or fragments of the peptide convert from a α-helical structure or random coil structure to a β-structure upon aggregation.

The amyloid fibril appears to be a ubiquitous structure intrinsic to the protein backbone structure accessible to virtually any polypeptide sequence [4]. Despite a similar end structure, there seems to be no similarity among primary protein structure linking these proteins. Today, various methods including x-ray diffraction, NMR, AFM, and EM have shown that fibrils formed by different properties share similar properties. Mature amyloid fibrils are observed to be approximately 100Å in diameter and composed of 20–35Å wide protofilaments.

Recent advances have allowed researchers to solve the structure of amyloid fibrils, even if fibrils structure is characterized by a very high polymorphism, both chemical [61,62] and biological [63]. A multistep seeding approach can be used to select a single, more stable fibril morphology [64]. Abeta peptides have a β-sheet secondary structure that stack in a parallel or anti-parallel fashion to form β-sheets running perpendicular to the fibril axis [12,65]. This is referred to as a cross-β pattern [66].

One of the first amyloid fibrils structural model of Abeta42 was proposed by Riek group [61]. Figure 1.5 shows a 3D cartoon representation of a antiparallel structure of a single amyloid protofilament accordingly to Riek findings. A mature amyloid fibril is formed when these single protofilaments wrap around one another to form a multifilament fibril as shown in figure 1.6.

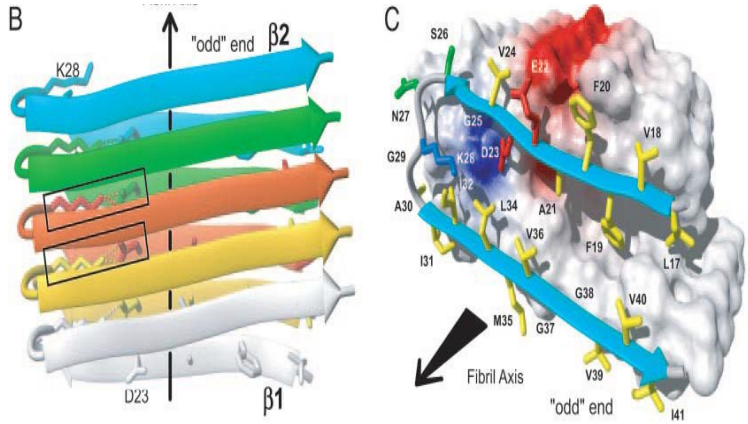

Figure 1.5 *Model of amyloid protofilament structure [61].*

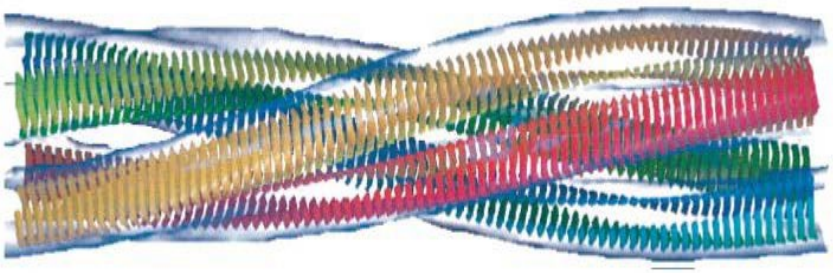

Figure 1.6 *Model of a mature amyloid fibril [61].*

This model has been characterized as each monomer having an unstructured N-terminal (1-16) region with two hydrophobic regions (16-23 and 28-35) connected by a loop region 24-27. An interior salt bridge forms between Asp23 and Lys28, detectable by both NMR and MD simulations. This salt bridge is imperative for the self-dimerization of Abeta and an important element of fibril structure [67]. Intermolecular interactions amongst the side chains are formed between the odd-numbered residues of the first strand of the n^{th} molecule and the even-numbered residues of the second strand of the $(n-1)^{th}$ molecule. These antiparallel sheets are held together by hydrogen bonds. All fibrils have been shown to form a left-handed helix [68,69].

Fibrils formed by Abeta40 and Abeta42 appear to have a similar structure on a molecular level [70]. However, fibrillar structure has been shown to differ when the fibrils are grown in different solutions [71]. Furthermore, the conformation of the less structured N-terminus of the monomer can alter the fibril structure even though the β-sheet motif remains intact [70].

In the past, amyloid fibrils were believed to be structures of beta sheets arranged in an antiparallel conformation. As a result of NMR spectra reported within the last 10 years, such opinion has shifted and a prevailing consensus has slowly emerged that the majority of Abeta fibrils are in fact stacked in a parallel conformation in most naturally occurring fibrils [66], though solid state NMR has shown anti-parallel β-sheet stacking under certain conditions in vitro [67].

Stacking of Abeta peptides into amyloid fibrils can be anti-parallel, made up of parallel dimers or parallel stacks of anti-parallel dimers [66]. A parallel β-sheet structure forms a linear chain with internuclear distance of approximately 4.8Å. In an antiparallel β-sheet structure, a planar zigzag pattern would emerge with internuclear distances exceeding 4.8Å. Tycko and colleagues compared fibrils formed from antiparallel β-sheets and fibrils formed from parallel b-sheets and found that antiparallel sheets nucleate faster and are metastable with respect to parallel structure conversion. Both are equally neurotoxic [72].

Parallel structures are more stable than antiparallel structures because they have more ordered residues, longer beta strand segments and possible better packing of hydrophobic side chains [72]. Antiparallel fibrils are thermodynamically metastable. Antiparallel structures eventually evolve towards parallel structures when grown together with parallel fibrils. If the rate of spontaneous nucleation of antiparallel structure is greater than the rate of spontaneous nucleation of parallel structures, antiparallel conformations will dominate leading to a greater proportion of relatively

short antiparallel fibrils [72]. These fibrils will eventually shrink and disappear, as monomers become more stable antiparallel fibrils.

Very recently, two different solid state NMR model of Abeta42 parallel fibrils came out, probably representing two different morphologies. One model shows a unique triple-β motif, which is made of three β-sheets encompassing residues 12–18, 24–33 and 36–40 [73]. The second model shows instead an S shape formed by four beta sheet with residues 15−42 comprising the amyloid fibril core and residues 1−14 appearing to be unstructured and the basic subunit of the mature fibrils exists as a dimer (figure 1.7) [62].

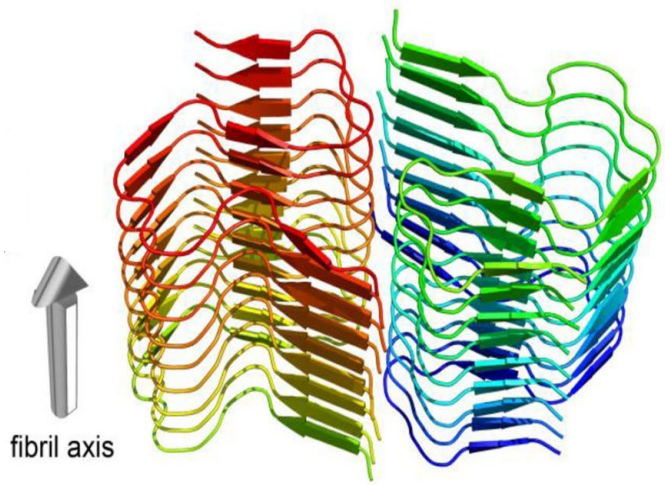

Figure 1.7 *Ribbon representation of the S shape tertiary structure of Abeta42 fibril core[62].*

1.3.4 Abeta peptides membrane interaction

The C-terminal end of Abeta peptides is part of the transmembrane domain of APP, and therefore the soluble peptide may retain affinity for the cellular membrane or certain features of the membrane. A potential cytotoxic mechanism involving the cytoplasmic membranes was suggested. Monomeric Abeta42 has been shown to tightly insert into membranes, with a small portion being peripherally associated with lysosomal membranes, leading to their destabilization and induction of toxicity [74]. Moreover, the amphipathic nature of amyloid oligomers has been suggested to contribute to their capacity to penetrate and insert into membranes, coat or lie on the surface of the membranes, or potentially act as cell-penetrating peptides [16,75]. Moreover, has been shown that lipid membranes are able to act as template for Abeta peptides aggregation [76], but it can also dissolve preformed amyloid fibrils into more toxic oligomers [77]. The importance of the membrane interaction in the Abeta peptides toxicity mechanism is widely accepted in the literature, but in vitro the effect of this interaction dramatically depends on membrane composition and experimental conditions.

To investigate the effect of membrane interaction on Abeta peptides aggregation, often simple, one-lipid species vesicles were used. It was demonstrated that in presence of neutral phosphatidylcholine vesicles, the lag time of Abeta40 aggregation was delayed and the half-time increased by 30%, dependent on lipid concentration [78]. Nucleation and elongation were also influenced by the presence of neutral lipid surfaces, and appeared to decrease when lipids were incubated with Abeta40. Secondary structural changes in Abeta conformation as a consequence of interaction with lipids have been demonstrated by CD spectroscopy [79]. The presence of various lipids, including egg yolk phosphatidylglycerol, bovine brain phosphatidylserine and phosphatidylethanolamine, induced the appearance of a strong 218 nm CD minima indicative of β-sheet structure. It was suggested that the headgroup charge of the

phospholipids contributes to the association between Abeta40 and the membrane via electrostatic interactions. The affinity of Abeta40 to the zwitterionic 1-palmitoyl-2-oleoyl-sn-glycero-3-phosphocholine (POPC) was found to be weaker than for the anionic 1-palmitoyl- 2-oleoyl-sn-glycero-3-phospho-rac-(1-glycerol) (POPG) [80], supporting the view that the headgroup charges mediate binding. Moreover, although POPC binding did not result in aggregation of the Abeta40, POPG liposomes significantly increased aggregation. The surface charge and hydrophobicity of the membranes can modulate the binding of the peptide to the membrane surface. Abeta40 preferentially binds to negatively charged phosphatidylglycerol membranes and composite membranes containing negatively charged lipids. On the other hand, the affinity between fibrillar Abeta40 and negatively charged membranes is lower with respect to neutrally charged membranes. The electrostatic forces were found to be more significant between monomeric Abeta40 and membranes, although hydrophobic forces were considered more important between fibrillar Abeta40 and membranes [81].

AFM studies have been used to monitor the assembly of Abeta42 on lipid bilayers composed of brain total extract, which provides a physiologically relevant ratio of acidic and neutral phospholipids. Small aggregates, about 5–7 nm in height, were initially found associated with the membrane and, after 7 h of in situ incubation, aggregates of about 5–15 nm in height were observed. Interestingly, this preparation of Abeta42 did not appear to ‘grow’ on the membrane bilayer [82]. To investigate the possibility that Abeta42 could form ion channels, it was incorporated into planar bilayers. AFM revealed multimeric complexes protruding above the lipid bilayer. The individual channels showed varying numbers of Abeta subunits, ranging from a two subunit arrangement to rectangular four subunit structures and hexagonal six subunit structures [36]. Electrophysiological records supported the view that Abeta42 was creating channels that allowed the passage of calcium ions [36]. By contrast to the conclusion that Abeta42 is able to form pores, was shown that size exclusion

chromatography-purified oligomers caused an increased conductance across mixed-lipid bilayers in a concentration-dependent manner [83]. The results showed that conductance was nonselective for different ions and was inconsistent with specific pore formation. Further studies indicated that Abeta42 caused increased conductance by interacting with the membrane surface, possibly by spreading the lipid headgroups apart, leading to membrane thinning, and thus lowering the membrane dielectric barrier and increasing conductance [84].

Studies using lipid vesicles encapsulating self-quenching fluorescent dyes such as calcein and fluorescein have been used to study the effect of Abeta assembly on membrane integrity. The addition of Abeta42 to 1,2-dimyristoyl-sn-glycero-3-phosphocholine large unilamellar lipid vesicles (LUVs) encapsulating calcein demonstrated that early oligomeric soluble species cause permeation of the membranes and the release of the encapsulated fluorescent dye [85]. It was also demonstrated that, as the Abeta42 peptide assembles into fibres in solution, the propensity to cause membrane permeation decreases, and mature fibres show a lack of ability to cause permeation. Interestingly, early oligomeric Abeta42 added to the vesicles elongates to form amyloid fibrils that appear to be associated with the membranes on EM [85]. This was suggested to cause mechanical disruption of the lipid membrane because of the growth of amyloid fibrils on membrane surface [86]. Moreover, it was suggested that Abeta42 is able to influence the cohesion of the components of the membranes [87].

In AD, the cholesterol content of certain regions of the brain can be markedly different from the same regions in non-demented brains; in particular, the cholesterol content is reduced by about 33% [88]. This reduction could significantly affect the fluidity of the neuronal membranes and make them more susceptible to Abeta peptides-induced permeation. Moreover, the decrease in cholesterol／phospholipid ratio in AD brains

may affect the cleavage of APP and cause an elevation in generated Abeta peptides [89].

The cholesterol content of membranes may play a role in modulating Abeta peptides penetration, because > 20% w/w cholesterol induces a membrane transition from a liquid-disordered (ld) to liquid-ordered phase (lo). As example, the Abeta fragment 25–35 is unable to intercalate into the membrane bilayer in presence of cholesterol [90]. However, it was shown that Abeta40 spontaneously inserts into monolayers containing a 30% mol/mol cholesterol to phospholipid ratio and, in this context, adopts an α-helical structure. Below this molar ratio, Abeta40 prefers to associate with the membrane surface region with a greater β-sheet content [91].

The cholesterol to phospholipid ratio has been reported to affect the affinity of Abeta peptides binding to synthetic lipid membranes. It was suggested that this increase in peptide-membrane affinity was a result of the involvement of cholesterol in altering membrane fluidity and structure [92]. Oligomeric, but not monomeric, Abeta42 was shown to insert into POPC/cholesterol membranes. Oligomer insertion was also found to occur in negatively-charged monolayers but not in the absence of cholesterol [93]. The inclusion of < 30% mol/mol cholesterol in POPC membranes gave rise to channel activity induced by the addition of Abeta40, whereas no channel activity was observed in membranes containing only POPC [94]. It was suggested that cholesterol-rich membranes prevented the fibrillization of Abeta40 by increasing the incorporation of the peptide within the phospholipid bilayer [95].

Another key feature of Abeta peptides and membranes interaction is the preferential binding with Gangliosides. Gangliosides are a group of glycosphingolipids composed of a hydrophilic sialic acid terminal sugar exposed to the external environment and a hydrophobic ceramide moiety that is embedded within the membrane [96]. Gangliosides are involved in a variety of cell functions, including as cell type-specific markers, as differentiation and developmental markers, and as receptors and

mediators of cell adhesion [97], and they comprise 5–10% of the outer membrane leaflet [98]. The affinity between gangliosides and Abeta peptides can vary, but is in the micromolar range for the most common gangliosides present in the membranes; the highest affinity is toward the monosialic ganglioside GM1 [99]. The presence of gangliosides within the membrane bilayer induces structural transitions in Abeta peptides. Upon dilution of Abeta peptides in aqueous environment, they initially adopt a random coil structure but, upon the interaction with GM1, the peptides undergo a transition into a mixed α/β conformation at pH 7 and into a β conformation at pH 6 [100]. Moreover, it was shown that neither the ceramide, nor sialic acid moieties could induce the structural transitions of Abeta peptides alone, implying that the association with the carbohydrate backbone and sialic acid is critical to induce structural transitions to Abeta peptides [100]. Fibrillization studies of Abeta40 in the presence of GM1 in the membrane showed that GM1 speeds up this process [101]. Electrostatic interactions may play a pivotal role in mediating Abeta–GM1 interactions (Abeta peptides are slightly positively charged and the GM1 headgroup is negatively charged); increasing the pH to 7.2 (where the peptides are negatively charged) leads to a decrease in peptides insertion because the interaction becomes repulsive [98]. The interaction with gangliosides-clustered domains is also important in this complex scenario [102].

From the body of data present in literature, a model of Abeta peptides interaction with gangliosides have been proposed: when gangliosides are uniformly distributed on membranes, the protein remains soluble and does not interact with membranes. Once a ganglioside cluster is generated due to a high cholesterol concentration in membrane, Abeta peptides specifically bind to it. After binding, they undergoe a conformational transition from an α-helix-rich structure to a β-sheet-rich one with increasing protein density on the membrane. The β-sheet form serves as a seed for the formation of amyloid cytotoxic fibrils [103,104]. A schematic representation of this model is shown in figure 1.8.

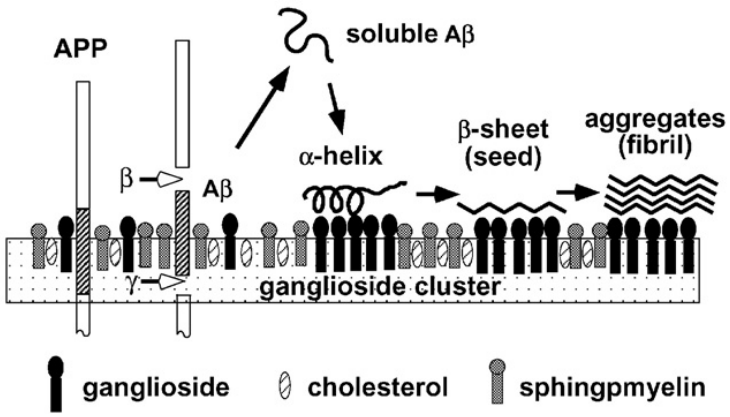

Figure 1.8 *Schematic representation of Abeta peptides interaction with gangliosides cluster.*

From this huge amount of data present on Abeta peptides/liposomes interaction briefly summarized here, three structurally different models of membrane-mediated toxicity have been proposed for Abeta: the carpeting model; the ion channel model; the detergent model, all shown in figure 1.9. In carpeting model, Abeta peptides accumulate on one leaflet of the membrane surface, resulting in an asymmetric pressure between the two leaflets and leakage of small molecules [105]. This model is believed to be of minor physiological relevance for amyloid diseases because it is strictly related to the formation of amyloid fibrils, and doesn't take in account the toxicity of soluble Abeta oligomers [86]. The formation of stable pores and ion channels is the second model proposed for amyloid-induced toxicity. The disruption of Ca^{2+} homeostasis has been recognized as a potential toxic mechanism associated with AD, and was shown to be involved in the amyloid cascade hypothesis, where elevated Ca^{2+} was suggested to be a consequence of both tau-phosphorylation and cell death [44]. The formation of Ca^{2+} channels in lipid bilayers was proposed in AD cytotoxicity because the incorporation of Abeta40 into planar phosphatidylserine bilayers formed channels that generated linear current–voltage relationships in symmetrical solutions [106,107]. Computational modelling of Abeta42 insertion into a lipid bilayer that approximately matches the thickness of 1,2-dioleoyl-sn-glycero-3-

phosphocholine bilayers showed that the transmembrane pore is formed by six hexamers, which span the bilayer and merge to form a more stable 36-stranded β-barrel arrangement [108]. This model is the most accepted because the parallel β-barrels formed by the N-terminal segments of the peptide form the lining of the pores and could account for the cationic selectivity observed for metal ions such as Zn^{2+} [109]. The third proposed model is based on the detergent-like effects of amyloid-forming peptides on lipid membranes. This mechanism of permeation is proposed to occur through the membrane association of the peptides in the form of micelle-like structures. Membrane permeation occurs at high local concentrations of the peptide on the membrane surface, either after the surface is covered with peptide monomers or oligomers, or through the association between membrane-bound amyloid [110]. The initial interaction is electrostatically driven, because the peptide preferentially binds to either the phospholipid headgroup or receptors on the membrane surface, then it aligns with the hydrophilic surface facing the phospholipid head groups. The peptide hydrophobic residues are buried inside the hydrophobic core of the membrane, and this is followed by disintegration of the membrane by disruption of the bilayer curvature. The detergent effect results from the surfactant-like properties associated with the amphiphilic peptide causing a reduction in membrane surface tension, where it forms a hole by the removal of lipid from the bilayer [105].

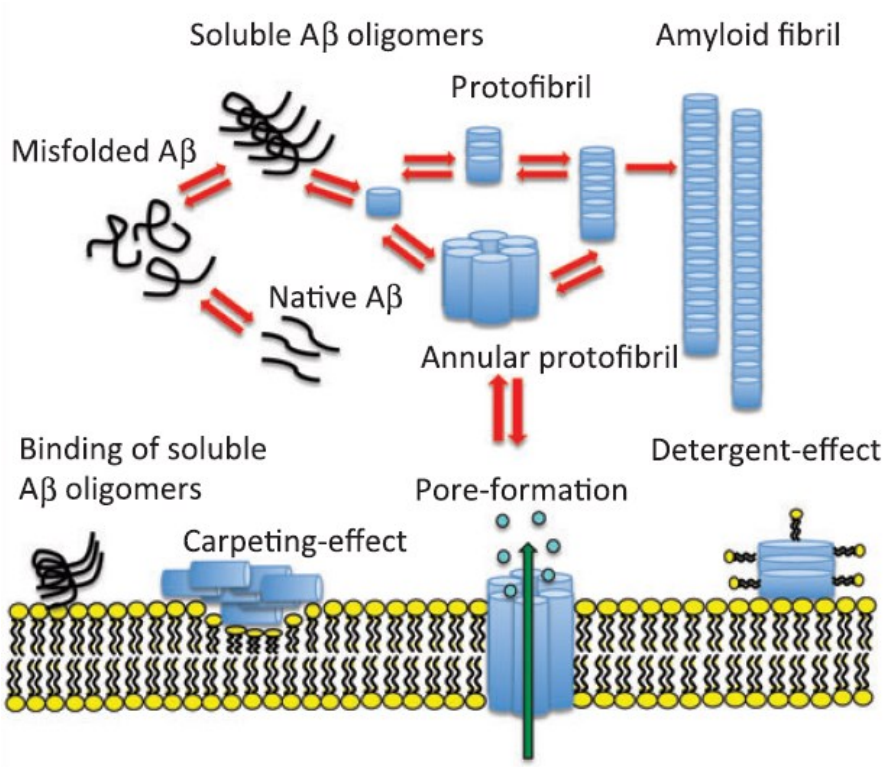

Figure 1-9 *Possible Abeta peptides membrane-disrupting mechanisms.*

The toxicity associated with Abeta peptides may not correspond exclusively to a single mechanism but more likely to an interplay of these mechanisms. Each mechanism may be involved in the disruption of biological membranes, either at a particular stage during the assembly of the amyloid-forming peptide or during a particular pathway taken during the peptide fibrillization.

1.3.5 Glycation

The term Glycation is referred in the recent literature as covalent, non-enzymatic modification of proteins by saccharides, well distinguished from the equivalent enzymatic reaction, called glycosylation [111]. Protein glycation involves the non-enzymatic reaction of a reducing sugar or sugar derivative with a protein. The reaction needs a free carbonyl function to be carried out; no sugars that has aldehyde or ketone

groups converted to stable ketal and acetal groups of glycosidic bonds are able to give this kind of reaction. The linking sites between the sugar and proteins are proteins nucleophilic sites, lysines and arginines side chains and N-terminal amine. In addition, cysteine side chains could be affected. Glycation of proteins occurs by a complex series of sequential and parallel reactions collectively called the Maillard reaction [112]. Many different adducts may be formed, some of which are fluorescent and coloured ‘‘browning pigments’’.

Several studies have shown that glycation stabilizes and promotes the formation of aggregated forms of proteins centrally involved in AD, such as Abeta and tau [113-115]. Plaques extracted from AD brains contained 3-fold more glycated proteins than preparations from healthy, age-matched controls [116]. Therefore, glycation may be responsible for the increase in the crosslinking of these proteins and consequent formation of stable oligomeric forms. In the case of AD, glycation not only directly modulates the aggregation of these proteins, but also up regulates the expression of APP, increasing the levels of Abeta42 [117]. Strikingly, there is an age- and stage-dependent accumulation of glycated products in AD brains. Glycated proteins levels in the cerebrospinal fluid of AD patients are increased and might constitute promising biomarkers for this disease [118]. To better understand the specific role of glycation in AD, the toxicity of normal and glycated Abeta peptides was evaluated in primary hippocampal neurons. The hypothesis that glycation exacerbates the toxicity of Abeta was confirmed, indicating that this kind of modification plays a role in Abeta toxicity mechanism [119].

The study of proteins modifications induced by glycation reaction is a topic relative new in proteins research. The reaction between lysine side chain and N-terminal amino groups by glucose was the major glycation process studied in the earlier literature. For this reason, the reaction was classified into two steps, early and advanced glycation processes. Glucose reacts with amino groups to initially form a

glycosylamine, which dehydrates to form a Schiff's base. The Schiff's base undergoes an Amadori rearrangement to form N-(1-deoxy-D-fructos-1-yl)amino acids or fructosamine [112]. This reaction stage is considered the early glycation process. Glycosylamine, Schiff's base and fructosamines are considered to be early stage glycation adducts. In later reaction steps, fructosamine is degraded and forming many stable end-stage adducts called advanced glycation end products (AGEs) [120]. However, this classification fails when unattached glucose is converted in reactive α-oxoaldehydes, which are potent glycating agents and react with proteins to form AGEs directly. The Schiff's base adduct may also react via non-Amadori rearrangement reaction pathways to α-oxoaldehydes which also leads to the formation of AGEs. Moreover, these reactive α-oxoaldehydes can be formed also by the degradation of glycolytic intermediates and lipid peroxidation. A scheme of the reaction is shown in figure 1.10.

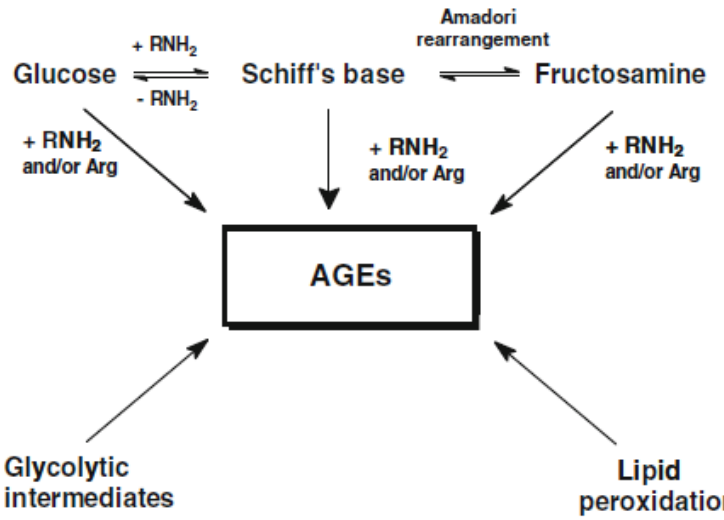

Figure 1.10 *Scheme of the possible glycation events [121].*

Important α-oxoaldehyde or dicarbonyl glycating agents are glyoxal, methyglyoxal (MGO), and 3-deoxyglucosone, shown in figure 1.11. In the physiological setting, one of the important saccharides participating in glycation of mammalian metabolism is glucose, and some of the most important saccharide derivatives are the reactive dicarbonyl metabolites such as MGO.

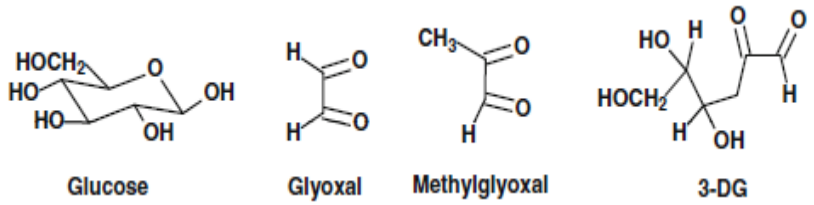

Figure 1.11 *Common glycation agents in physiological environment.*

Another classification of glycation products has been made related to the mechanism of AGE formation. Glycoxidation is a term widely used for glycation processes in which oxidation is involved and the AGEs thereby formed have been called glycoxidation products [122]. The AGEs pentosidine and carboxylmethylysine are examples of glycoxidation products. Where aldehyde substrates of glycation are formed by lipid peroxidation, the end-stage adducts have been called advanced lipoxidation adducts. In figure 1.12 some possible glycation product are shown.

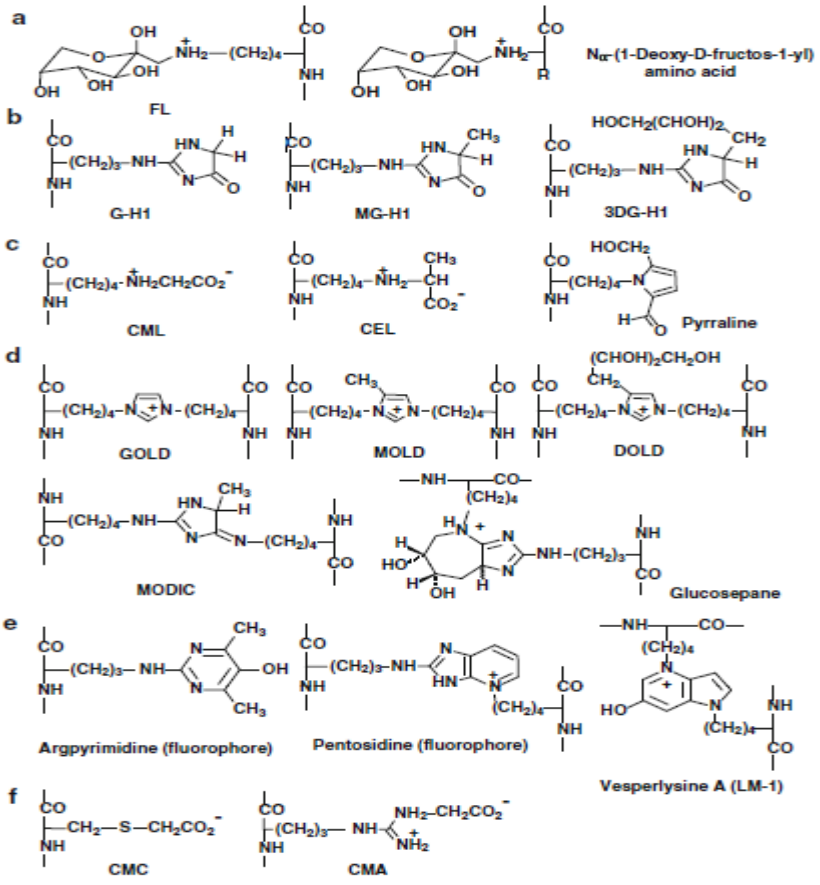

Figure 1-12 *Possible glycation products.* ***a*** *Early glycation adducts formed by glycation with glucose: fructosamines. R indicates the amino acid side chain.* ***b–f*** *Advanced glycation endproducts.* ***b*** *Hydroimidazolones.* ***c*** *Monolysine adducts.* ***d*** *Imidazolium and other crosslinks.* ***e*** *Fluorophores.* ***f*** *Other Structures.*

Protein glycation causes low-level endogenous damage to the proteome, modifying protein properties in unpredictable ways [123]. The enzymatic defence against glycation consists of enzymes that repair early glycated proteins and prevent glycation by metabolising dicarbonyl glycating agents: fructosamine 3-kinase [124], fructosamine 3-kinase-related protein [125]; and aldoketo reductases 1A4, 1B1 and 1B3 [126]. The imbalance of glycating agents and enzymatic defence against glycation in favour of glycating agents has been termed carbonyl stress and is thought

to contribute to ageing and disease [127]. By a clinical point of view, formation and steady state accumulation of glycated proteins have been linked to disease development and progression, particularly diabetes and its vascular complications [128], renal failure [129], cardiovascular disease, Alzheimer's disease [130,131], mood affective disorders such as anxiety and Schizophrenia [132], Parkinson's disease [133] and other diseases are emerging.

Recently, type 2 diabetes mellitus has been identified as an important risk factor for AD, increasing the risk up to 60% [134]. Interestingly, both AD and diabetes lead to a desensitization of insulin receptors in the brain [135]. This causes not only glucose homeostasis impairment, but also impairment of the neuroprotective actions of insulin, facilitating the development of AD. Remarkably, administration of insulin to AD patients improves the ratio of Abeta40/Abeta42 (marker of decreased toxicity), enhances cortical activation, and improves performance in cognitive tasks [136]. Moreover, diabetes drugs reduce the formation of Abeta plaques and brain inflammation. In a triple transgenic mouse model of AD, a high-sucrose diet that induces several metabolic alterations found in diabetes is responsible for a significant increase in Abeta peptides levels [137]. This evidence further supports an important interplay between diabetes and AD. These findings highlight the importance of glycation in the context of AD.

1.4 Hemopressin

Hemopressin is a nonapeptide derived from hemoglobin α-chain able to interact with cannabinoid CB1 receptor [138]. It was first isolated from rat brain homogenates in the 2003 [139].

This peptide acts a CB1 receptor endogenous inverse agonist, and exerts antinociceptive, hypotensive and anoretic activity in rat and mice models [140,141]. It shows a similar binding affinity and the same binding pocket of rimonabant, a well-known CB1 ligand [138,142]. Before the discovery of this peptide, the cannabinoid

receptor ligands were previously thought to be small and lipophilic molecules. Therefore, the finding of a peptide modulator of the cannabinoid receptor sparked interest for pharmaceutical development based on a hemopressin scaffold.

N-terminally extended isoforms of hemopressin, RVD-hemopressin and VD-hemopressin, were identified and reported to be CB1 agonists [143]. Only two or three residues are different between these peptides, but this difference appears to determine whether the hemopressin peptides exhibit antagonistic or agonistic activity, eliciting opposite effects at the CB1 receptor. Is still unclear whether hemopressin is an endogenous peptide or instead a cleavage product of the longer RVD-hemopressin peptide. The Asp-Pro peptide bond is one of the most labile bonds, especially under acidic conditions [144], which were used in the extraction of rat brains when hemopressin was originally identified. Indeed, a subsequent mass spectrometry study of mouse brain extracts under not acidic conditions did not identify hemopressin but instead only found the N-terminally extended peptides amongst others. The sequence of RVD-hemopressin is shown within the hemoglobin α-chain sequence in figure 1.13.

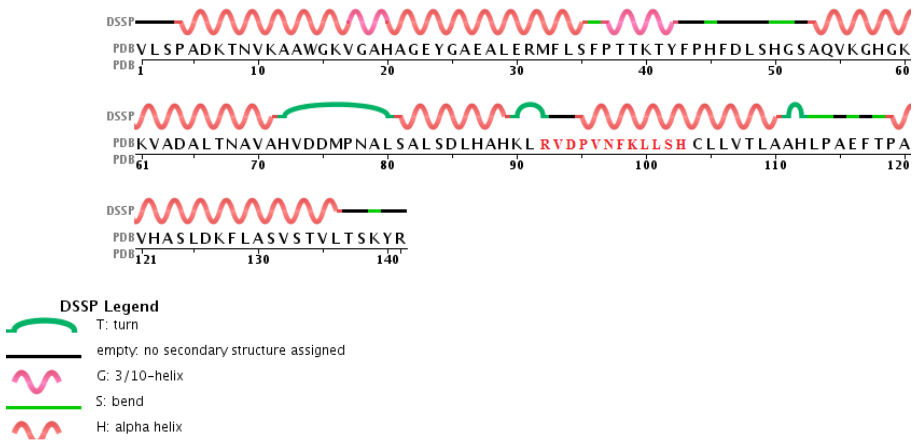

Figure 1.13 *Hemopressin sequence highlighted in the hemoglobin α-chain sequence. PDB code 2M6Z.*

Unfortunately, works using hemopressin in obesity and pain therapy has been hampered by the lack of reproducibility associated to its usage in pharmacological assays [143]. In certain conditions (1 mM peptide in 25 mM phosphate, 50 mM NaCl, pH 7.4), hemopressin is able to self-assembly into amyloid like nanostructured fibrils [18], which may contribute to its inconsistent activity. Moreover, no fibrillation was observed in RVD-hemopressin at the same concentration, underscoring the unique ability of hemopressin to form fibrils, shown in Figure 1.14.

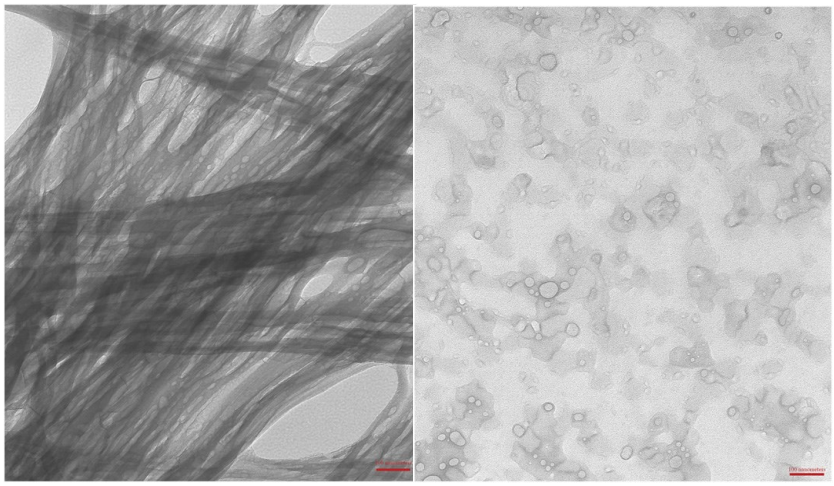

Figure 1.14 *TEM images of Hemopressin (Panel A) and RVD-Hemopressin (Panel B) in 25 mM phosphate, 50 mM NaCl, pH 7.4 [18].*

Although the high peptide concentrations in these experiments may not be considered physiologically relevant, they are certainly pharmacologically relevant; high concentrations of peptide are generated during peptide synthesis, purification, and are used in peptide formulations and pharmacological assays as stock concentration. Because hemopressin is a naturally occurring peptide found within the brain, a better understanding of the physiological role of its self-assembly is needed. The distinct differences in aggregation properties and in the biological activity between these peptides suggest that the three additional residues, RVD, cause structural differences

or ionic interactions that prevent fibril formation and change the interaction with the CB1 receptor. To the best of my knowledge, very few information on hemopressin peptides conformation are available in literature. Comparing the conformation assumed by hemopressin peptides in their monomeric form would be helpful to understand the different aggregation propensities of the two peptides.

1.5 Sweet Proteins

Sugars or small non-caloric sweeteners are the classes of molecules commonly associated to the sweet taste, but also some proteins can exhibit this kind of property. Some of them are indeed intensely sweet, orders of magnitude sweeter than sugar [145]. Proteins that exhibit this kind of property are found in unrelated tropical plants and, apart from the origin, they have no functional, sequence or three-dimensional structure similarity [146]. They are able to interact with the same receptor that binds small sweet molecules, called human taste receptor T1R2-T1R3, a heterodimeric G-protein coupled receptor located on specialised cells on the tongue [147,148]. To date, about ten sweet or sweet taste-modifying proteins were identified. Among them, the most known and studied proteins are: monellin [149], thaumatin [150], brazzein [151], miraculin [152]. Monellin, isolated from the African plant Dioscoreophyllum cumminsii, is one of the most potent sweeteners known, being about 90,000 times sweeter than sucrose on a molar basis [145]. Monellin is formed by two separate peptide chains that fold in a single domain through non-covalent interactions [149]. It shows an α/β architecture with a cystatin-like fold, with one helix that is embraced in a coiled antiparallel β-sheet [153]. Due to the similar folding, monellin is considered a member of the cystatin superfamily [154], even if it didn't show any protease inhibitory function. This protein is also a widely used model for protein folding studies [155].

Monellin chains dissociate when heated above 50 °C, when the protein loses sweetness as well, a clear indication that the correct folding is a prerequisite for

sweetness. Single chain constructs were engineered in order to overcome the low thermal stability. One of these, obtained by joining the two chains by the insertion of a Gly-Phe dipeptide linker, is called MNEI. This protein retains the sweetness and the same three-dimensional architecture (Figure 1.15) of the parent protein, but shows a greatly increased thermal stability [156].

Figure 1.15 *Molecular model of MNEI, pdb code 1fa3.*

Moreover, based on a hypothesis of the interaction between sweet proteins and the receptor called "wedge model" [157], even sweeter mutant of MNEI were designed, such as the single point mutant Y65R-MNEI [158,159].

Both native double chain monellin and MNEI are able to form amyloid fibrils after an initial denaturation event, i.e. when incubated at very high temperature [19,160]. So far, amyloid fibrils were never detected for the other MNEI mutants, such as Y65R-MNEI. During food processing, extreme temperature and pH conditions are often used; these conditions could trigger sweet proteins aggregation, hampering their biotechnological application in food industry.

1.6 Thesis outline

In this thesis, the effect of different environments on the amyloid aggregation process of three molecular models (Abeta peptides, hemopressin and sweet protein Y65R-MNEI) was studied by an integrated biophysical experimental approach. Considering the body of data already published on the amyloid fibril formation process, different aspects were studied for each molecule, therefore using different techniques. This approach allowed studying the amyloid aggregation process from different points of view. The results will be presented, divided by the topic, as follows:

- In chapter 2, an expression and purification protocol for production of recombinant Abeta peptides Abeta40 and Abeta42 in *E.Coli* is presented; Abeta40 peptide obtained in such a way were used for the experiments presented in chapter 4.
- In chapter 3, the interaction between Abeta42 and biomimetic lipid vesicles was investigated. The effect of this interaction was studied by different techniques: the changes in Abeta42 conformation upon interaction with the lipids were studied by CD spectroscopy, a very useful technique to investigate proteins secondary structure. On the other hand, changes in bilayers microstructure upon interaction with the peptide were studied by Electron Spin Resonance (ESR), using in particular the spin labelling approach; in this way, local information about fluidity changes in both hydrophilic polar head and hydrophobic lipid tail regions were obtained. Moreover, membrane permeabilization induced by monomeric Abeta42 was studied by a fluorescence based content-mixing assay, designed to investigate this kind of activity.
- In chapter 4, the effect of a non-enzymatic post-translational modification, i.e. glycation reaction, on the structure and the aggregation properties of Abeta40 and Abeta42 was studied. This reaction leads to the formation of a fluorescent

product, which was exploited to follow the reaction kinetic by fluorescence spectroscopy. Changes in peptide structure and aggregation properties caused by these modifications were studied by respectively CD and ThT binding fluorescence assay. ThT is a fluorophore able to selectively bind cross β-sheet structures; this binding leads to changes in ThT spectroscopic properties, which can be followed to study amyloid fibril formation kinetics.

- In chapter 5, the effect of pH and solvent polarity on hemopressin and RVD-hemopressin conformation was studied. An initial condition screening was performed by CD, followed by a high-resolution structural analysis performed by bi-dimensional NMR spectroscopy. Particular attention was paid in comparing the conformation assumed by hemopressin peptides in each condition, in order to understand the different aggregation propensities of the two peptides.
- In chapter 6, the effect of temperature, pH and ionic strength on the aggregation properties of the sweet protein Y65R-MNEI was investigated. Protein stability as a function of temperature was studied by CD thermal denaturation experiments. For each condition considered, the protein aggregation kinetics was investigated by ThT binding assay. The morphology of protein aggregates obtained in each condition was studied by AFM, one of the few techniques that can give a direct observation of protein aggregates shapes and dimensions.

Chapter 2 – Abeta peptides recombinant expression

2.1 Work outline

In this chapter it is reported a protocol for expression in *E.Coli* and purification of recombinant Abeta peptides. Despite decades of research about this topic, the production of these peptides is not yet an established routine, due to the high aggregation propensity of these peptides that makes them very tricky molecules to work with. The protocol I applied is based on an already published one [161].

The two plasmids expressing Abeta40 and Abeta42 peptides were gently provided by Professor Bernd Reif of Technical University of Munich. The peptides are expressed without any fusion protein and they have the N-term methionine, but is documented that this residue doesn't change Abeta peptides structure and aggregation properties [161]. The peptides are isolated in the inclusion bodies from the bacteria hosts. Then, the purification protocol is made of three main steps: inclusion bodies purification, ion exchange chromatography and molecular mass fractionation, followed by dialysis and freeze-drying. The same protocol was used for both peptides, but was completely successful only for the shorter and more soluble peptide, Abeta40, presented in this chapter.

2.2 Abeta40 expression and purification protocol

The *E.coli* BL21 (DE3) strain was used for this expression. Competent cells were transformed with Abeta40 gene containing plasmid (pET28a), kanamycin resistant, confirmed by sequencing before the experiments.

E.Coli cells growth and Abeta40 overexpression induction were performed using standard protocols; upon induction with IPTG, the cells were then harvested by centrifugation.

Due to Abeta40 exogenous nature and very high aggregation propensity, it is usually embedded in *E.Coli* inclusion bodies (IBs) when expressed as wild-type peptide, without any solubility-boosting tag attached to it [161]. Therefore, the first step of the purification protocol consists on IBs isolation and purification, performed by three sonication-centrifugation steps. At each step, proteins content was checked by SDS-PAGE, shown in figure 2.1. In order to dissolve the purified IBs, a very high urea concentration (8 M) was necessary.

The IBs solution was then diluted before the ion exchange chromatography. The separation was performed in batch, avoid the occurrence of local high concentration spots that could accelerate peptide aggregation, that hampers final peptide yield. A weak anion exchanger resin (DEAE) was used, and the peptide eluted by increasing stepwise the NaCl concentration. All fractions obtained were loaded on a SDS-PAGE (figure 2.1); the results indicate that the peptide is quite concentrated from 50 to 150 mM NaCl buffers, and seems very pure.

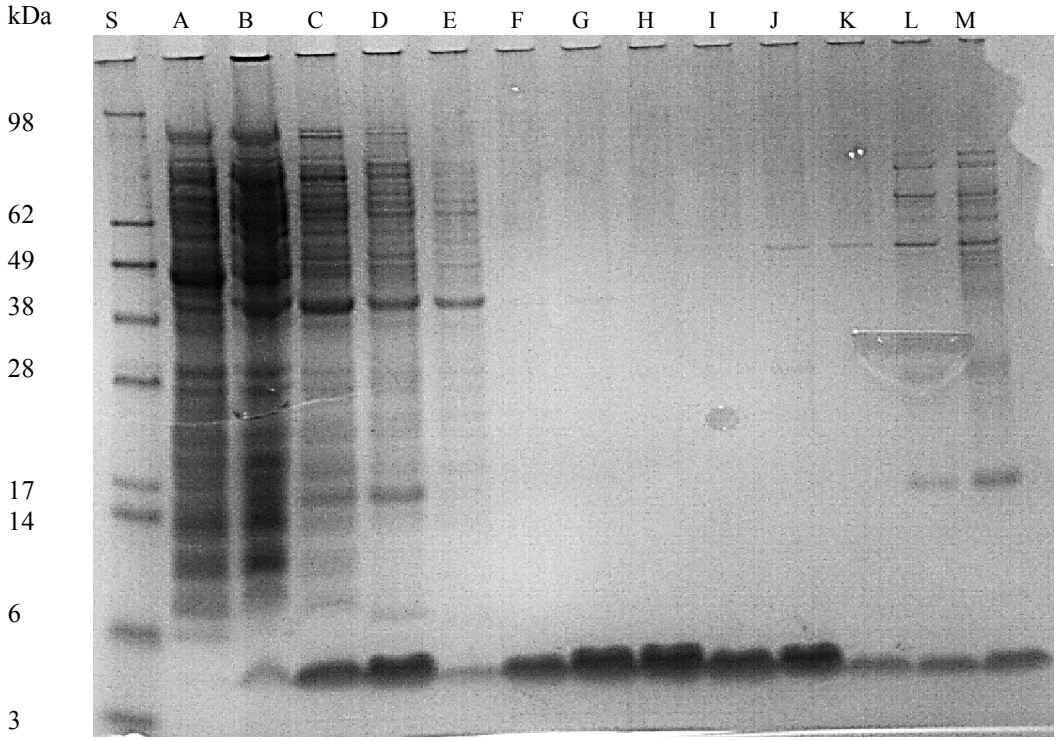

Lane S: MW standards mixture. Lane A: 1° IBs wash. Lane B: 2° IBs wash. Lane C: 3° IBs wash. Lane D: dissolved IBs. Lane E: DEAE flow through. Lane F: 50 mM NaCl. Lane G: 75 mM NaCl. Lane H: 100 mM NaCl. Lane I: 125 mM NaCl. Lane J: 150 mM NaCl. Lane K: 200 mM NaCl. Lane L: 300 mM NaCl. Lane M: 500 mM NaCl.

Figure 2.1 *SDS-PAGE of all Abeta40 purification steps; the fractions in which the peptide is more concentrated are the ones ranging from 50 to 150 mM NaCl.*

In order to double check peptide purity, the fraction from 50 to 150 mM NaCl were concentrated 10-fold by filtration using a 3.5 kDa cutoff Vivaspin tube. Actually, some high molecular weight proteins (more than 10 kDa) were detected after fractions concentrations (data not shown). In order to get rid of them, all the collected fractions were filtrated in a second step through a 10 kDa cutoff Vivaspin concentrator, as also described by the reference paper [161].

After the MW fractionation step, the fractions from 50 to 150 mM NaCl were pooled and dialysed against ultrapure water using a 3.5 kDa cutoff dialysis tube overnight in order to desalt the peptide. The solution obtained was then freeze-dried, and peptide purity and identity was checked by spectroscopy (UV, CD) and mass spectrometry (figure 2.2). The final yield was 20 mg of Abeta40 per litre of culture.

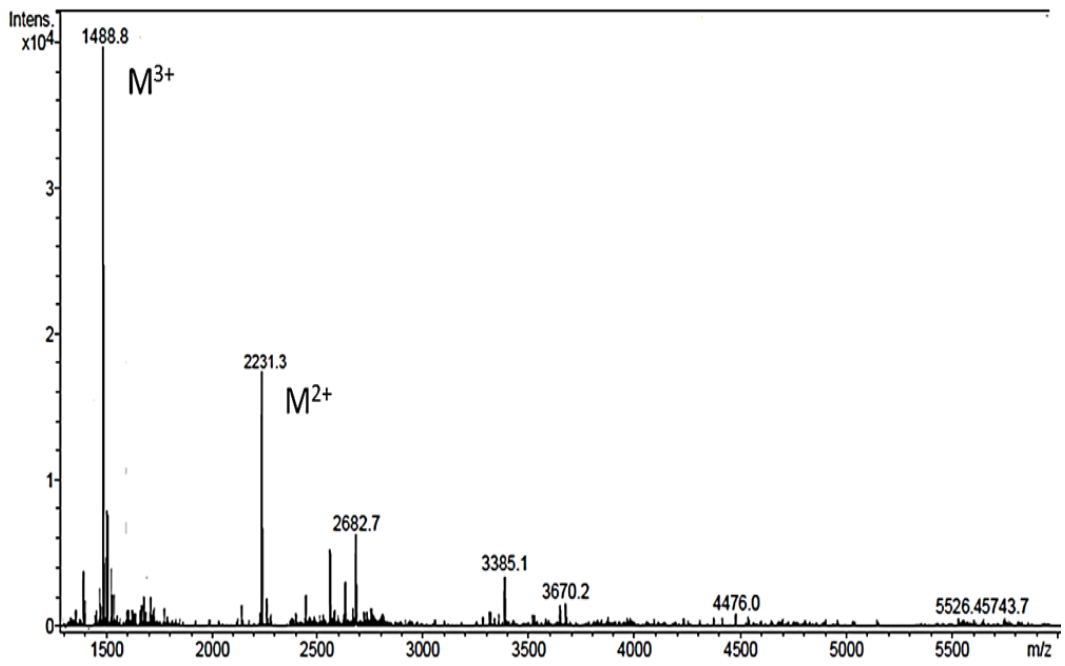

Figure 2.2 *Purified Abeta40 electrospray mass spectrum; the peaks corresponding to the double and triple ionized peptide are marked. Theoretical average mass: 4461 Da.*

In conclusion, a good expression system and purification protocol were set up for Abeta40 recombinant production; the studies on glycation reaction effects on Abeta40 aggregation properties reported in chapter 4 were performed using the recombinant peptide expressed by the protocol here described. On the other hand, some issues came out for Abeta42 expression. Even if the plasmid expressing for Abeta42 had the correct gene sequence, and the band position in the SDS-PAGE control experiment was coherent with the expected MW, it wasn't detectable either by mass spectrometry

or NMR spectroscopy. Moreover, spectroscopic investigation gave very unreproducible and weird results. Probably in this protocol Abeta42 co-purify with other non-proteinaceous impurities, which hampers its solubility in aqueous environment and its ionization efficiency, altering peptide biophysics properties. Henceforth in this thesis, all data regarding Abeta42 were obtained using a synthetized peptide sample produced by Professor Remo Guerrini of University of Ferrara [16].

2.3 Experimental Section

2.3.1 Materials

Plasmids (pET28a) containing genes expressing Abeta40 and Abeta42 were gently provided by Professor Bernd Reif of Technical University of Munich. Precasted 12% acrylamide gels were bought from Invitrogen (Carlsbad, California, USA). The ion exchange chromatography resin DEAE was bought from GE Healthcare (Little Chalfont, UK). Filtration systems and Vivaspin concentrator were bought from Merck (Darmstadt, Germany). All others laboratory reagents and solvents were bought from Sigma-Aldrich (Saint Louis, Missouri, USA).

2.3.2 Transformation

About 100 ng of plasmid DNA, containing the gene encoding for Abeta40 or Abeta42, were added to 100 µl of competent cells (*E.Coli* BL21 DE3 strain) in ice, and they were incubated for 30 minutes. Subsequently, the cells membranes were closed by the thermic shock procedure, placing the cells in a 42 °C water bath for 30 seconds; 900 ml of Luria-Bertani broth (LB) without any antibiotic were added and the cells were growth at 37 °C under shaking for 45 minutes. The cells were harvested using a bench centrifuge and plated on previously prepared LB-Agar plate containing 0.1 mg/ml kanamycin, for correctly transformed colonies selection, and growth on the plate overnight at 37 °C.

2.3.3 Abeta peptides expression

A single colony was picked from the LB-Agar plate and propagated overnight in 5 ml of LB containing 0.1 mg/ml kanamycin. 1 mL from this culture were diluted to 1 l of the same medium in a 4 l flask, and incubated at 37 °C under 200 rpm agitation, until the optical density at 600 nm (OD600nm) reached a value of 0.6/0.7. At this point, Abeta peptides production was induced by adding IPTG at the final concentration 1 mM, and the culture incubated for four hours at the same temperature and agitation speed. The cells were then harvested by centrifugation at 5000 g for 30 minutes at 4 °C, then the supernatant was discarded and the cell pellet frozen and stored at -80 °C.

2.3.4 Inclusion bodies purification procedure

The cells pellet was resuspended in 10 ml of Tris buffer 10 mM pH 8.0 containing 1 mM EDTA (Buffer A) and sonicated for 2 minutes, at power output 5 and duty cicle 50%, using an ultrasonic cells disruptor with a thin tip, taking the sample into an ice bath over the whole procedure. The suspension was centrifuged for 10 minutes at 18000 g and 4 °C. The supernatant, after checking its protein content by SDS-PAGE electrophoresis, was discarded. This procedure was repeated three times in order to properly purify the IBs from other, more soluble *E.Coli* endogenous proteins. 10 ml of Buffer A containing 8 M Urea was added to completely dissolve IBs and the suspension was sonicated (using the same parameters already mentioned) until a clear solution was obtained.

2.3.5. Ion exchange chromatography

The IBs dissolved were then diluted with Buffer A containing 8 M Urea to 40 ml total volume for the ion exchange chromatography. 20 ml of weak anion exchanger resin (DEAE Sepharose) were extensively washed with ultrapure water, equilibrated with Buffer A containing 8 M Urea and mixed with the IBs solution. This suspension was

incubated, under gently agitation, for one hour, to allow peptides binding to the resin. Then the resin was recovered by gentle vacuum filtration using a Millipore 22 μm filter. Abeta peptides were then eluted by increasing stepwise the NaCl concentration; in details, 20 ml of Buffer A containing 0, 50, 75, 100, 125, 150, 200, 300, 500 mM NaCl were subsequently added to the resin. After every buffer addition, the suspension was incubated for 5 minutes under gentle agitation at room temperature before collecting the buffer solution by vacuum filtration. All these operations were performed in cold room at 4 °C.

2.3.6 MW fractionation step

The peptide was separated from the high molecular weight (>10000 Da) contaminants by a MW fractionation step performed using Millipore Vivaspin concentrator with a membrane cutoff of 10 kDa at 4000 rpm and 4 °C. The same procedure was used to concentrate the fractions before the SDS-PAGE experiment as well, but a different membrane cutoff (3.5 kDa) was used in this case.

Chapter 3 - Interaction between Abeta42 with model phospholipid bilayers

3.1 Work outline

Many experimental evidences indicate that the interactions with neuronal membranes play an important role in the Abeta42 toxicity [85,102], and the study of the interactions between Abeta peptides and membrane model systems is a very important topic in the recent literature, as discussed in more details in section 1.3.4.

AD is also elicited by the interplay of genetic, environmental and dietary factors [162,163]. The adherence to a Mediterranean diet profile, including fish, vegetables, fruits, coffee, and light-to-moderate alcohol intake, seems to reduce the incidence of this and other neurodegenerative pathologies [164]. The beneficial effects of fish are at least partially ascribed to the high content of polyunsaturated fatty acids (PUFA), and specifically of Omega-3 ones [165]. However, the effectiveness of these molecules is still controversial, and their mechanism of action remains elusive. Among other hypotheses, mainly based on the radical-scavenging and anti-inflammatory action of PUFA [166,167], it has been proposed that Omega-3 fatty acids, once converted to lipids, could alter the structure and functionality of neuronal membranes, whose involvement in AD etiology is widely accepted [168].

Docosahexaenoic acid (DHA) is found in extraordinarily high concentration in the plasma membranes of neural tissues, reaching up to 50% of the total acyl chains [169,170], and its decline has been associated with the loss of memory and learning, suggesting that the Omega-3 fatty acids modulate the membranes properties and influence the molecular mechanism of AD [171,172]. Recently, it has been proposed that Omega-3 lipids disturb the lipid packing in the membrane, favouring a deeper internalization of Abeta fragments among the lipid acyl chains [173], offering a

possible explanation for the inhibition of Abeta self-aggregation operated by Omega-3 fatty acids.

To get light in this complex scenario, the interaction of Abeta42 with bilayers whose lipid composition reproduces the main components of neuronal membranes [174,175], including both zwitterionic and anionic phospholipids, cholesterol, sphingomyelin and gangliosides has been investigated. Moreover, the effect of the inclusion of the Omega-3 lipid 1,2-didocosahexaenoyl-sn-glycero-3-phosphocholine [22:6(cis)PC] in the bilayer composition is analysed in detail.

An integrated experimental approach was applied for this study. The effect of complex lipid bilayers on Abeta42 conformation/self-aggregation was monitored by CD; the influence of Abeta42 interaction on the membrane microstructure and fluidity was studied by ESR measurements; the disrupting effect of this interaction on membrane integrity was studied by a previously established fluorescence-based membrane leakage assay.

3.2 Sample conditions design

Six different conditions were explored in this work, using always the same (20 μM) Abeta42 concentration. Two control conditions were used: HFIP/NaP 20 mM pH 7.4, 80/20 % v/v, and 20 mM NaP pH 7.4, in order to check peptide behaviour in apolar environment a polar environment respectively. Four different liposomes composition were studied: 0.4 mg/ml of lipid bilayers formed only by palmytoil-oleil-phosphocholine (POPC-LB); 0.4 mg/ml of neuronal membrane mimicking lipid bilayer (NML-LB), which includes zwitterionic and anionic phospholipids, cholesterol, sphingomyelin and gangliosides [175,176]; 0.4 mg/ml of NML-LB containing also 25% w/w of the unsaturated fatty acid 22:6(cis)PC (O3-LB); 0.4 mg/ml of NML-LB containing 10% w/w of 22:6(cis)PC (O3L-LB). The two last mixtures were prepared with two different amounts of 22:6(cis)PC to evaluate its specific potential effect on Abeta42 solubility and structure. The detailed liposome

compositions are reported in the experimental section. The chemical structure of all lipids used for this study are reported in figure 3.1.

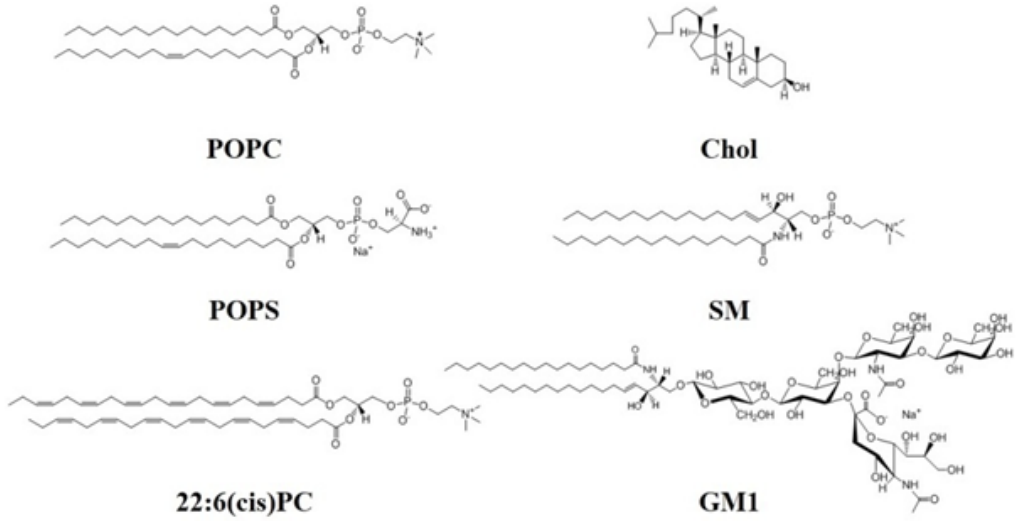

Figure 3.1 *Chemical structures of all lipids used in liposomes formulation.*

3.3 CD spectroscopy

In consequence of the generally low solubility of Abeta42 and fast aggregation in aqueous solutions, we have checked the peptide conformation in experimental conditions already known to induce canonical secondary structures in Abeta, i.e. HFIP/water mixture and phosphate buffer. Both the controls spectra gave the expected results, showing the typical shape of α-helix and β-sheet respectively, thus confirming the absence of pre-existing aggregates in the dry peptide film. Interestingly, in the presence of POPC-LB the spectrum of the peptide showed the shape of a β-structure, though the minimum was shifted at a slightly higher wavelength, according to the presence of aggregated forms [77]. In contrast, in the presence of more complex lipid bilayers (NML-LB, O3-LB and O3L-LB), only a low intensity CD signal was detected

and no regular secondary structure could be associated to the spectrum. The CD spectra of peptide upon dissolution in every condition are reported in figure 3.2.

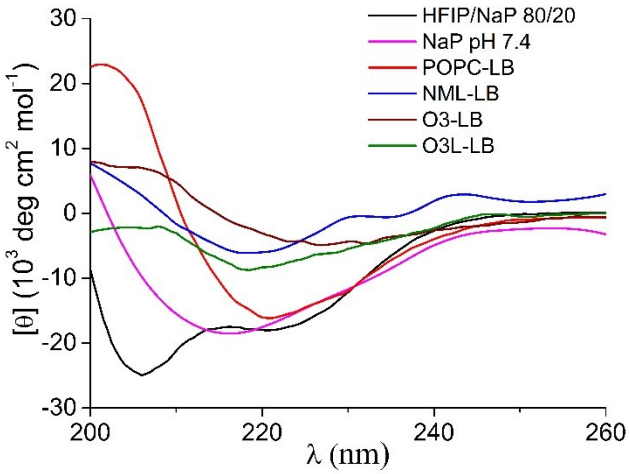

Figure 3.2 *CD spectra of Abeta42 just after dissolution in the conditions studied.*

Since the kinetics of aggregation/dissolution processes and conformational transitions of Abeta42 are quite slow, the CD spectra of the peptide in the different conditions were monitored over several days. The results obtained are reported in Figure 3.3 for each liposome conditions. The control experiments, not shown in the figure, gave the expected results: the spectrum in HFIP/water mixture was unaffected over the whole incubation time [16]; on the other hand, when the peptide was dissolved in phosphate buffer, the signal intensity decreased over time, becoming almost undetectable after 14 days, in agreement with the expected formation of insoluble aggregates in aqueous environments.

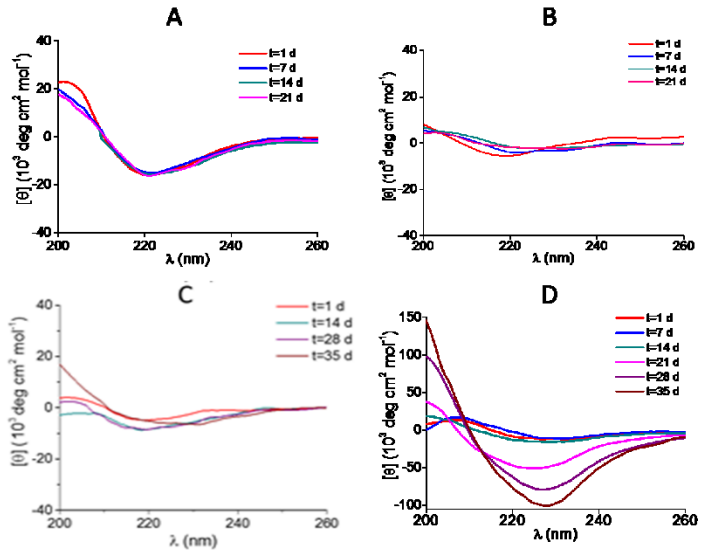

Figure 3.3 *CD spectra time evolution of Abeta42 interacting with different lipid bilayer:, POPC-LB (panel A); NML-LB (panel); O3L-LB (panel C); O3-LB (panel D).*

Figure 3.3 panel A shows that the shape and intensity of the spectra acquired in POPC-LB over time were constant, suggesting that the soluble aggregate concentration does not change. However, the presence of insoluble, CD silent forms cannot be excluded. In the presence of NML-LB bilayers, the low intensity of the CD signal indicates that only a small fraction of the peptide was dissolved (panel B), and no significant increase is appreciated over time. Yet, the spectrum shape changes during the incubation time, confirming that the lipid bilayer is able to interact with the peptide [85]. Unlike the previous cases, in the lipid bilayer O3-LB, the peptide slowly but extensively dissolves after several days, as highlighted by a consistent increase in the CD spectrum intensity. The spectrum assumes a shape similar to that observed in the presence of POPC, except for a further red-shift of the minimum, suggesting the presence of higher size soluble aggregates. Interestingly, the time necessary to appreciate changes in the CD spectrum decreases when the amount of Omega-3 lipid present in the lipid mixture increases. Indeed, while the presence of higher concentration of 22:6(cis)PC (panel D) induces the peptide film dissolution after 21

days incubation, at lower 22:6(cis)PC concentration (panel C) the spectrum shape changes slightly during 28 days incubation, but no clear trend can be appreciated, as in the case of NML-LB. These evidences suggest the presence of membrane interacting peptide aggregates slowly evolving over time when Omega-3 lipids is added in the lipid bilayer formulation [77]. However, the kinetics of this process critically depends on the amount of Omega-3 present in the lipid phase.

3.4 Electron Paramagnetic Resonance

The changes in lipid ordering and dynamics were studied using the spin label approach. Two spin-labeled phosphocholines were used as reporter: 5-PCSL and 14-PCSL. The former bears the radical in proximity of the polar head, just underneath the hydrophilic surface, while in the latter the label is close to the acyl chain terminus, thus spectra are representative of the inner apolar region behaviour.

The spectra of 5- and 14-PCSL in POPC bilayers are reported in figure 3.4, respectively panel A and panel B (black lines). 14-PCSL generates an almost isotropic three-line spectrum. In contrast, a clearly defined anisotropy is observed for 5-PCSL, as highlighted by the splitting of the low- and high-field signals. Thus, the rotational motion of the label is hindered in the relatively ordered external region of the bilayer, while it is almost free in the bilayer interior. A quantitative analysis of the spectra was accomplished by determining the lipid segmental order parameter (S), as reported in the literature [177]. The S value is 0.64 for 5-PCSL and 0.14 for 14-PCSL. These evidences indicate that POPC-LB presents a marked rigidity and ordering decrease in going from the lipid polar head to the acyl tails termini, as expected for membranes in the liquid crystalline disordered state (Ld) [178]. In the case of the NML-LB, both spin-labelled lipids show anisotropic spectra (figure 3.4). The S value is 0.74 for 5-PCSL and 0.41 for 14-PCSL, showing that these bilayers are more rigid than the previous ones, and the lipid ordering gradient in going from the polar head to the acyl tails termini is lower.

This indicates that NML-LB are in the liquid crystalline ordered state (Lo). Also in the presence of 22:6(cis)PC both spin-labelled lipids have anisotropic spectra; the two Omega3 containing lipid bilayers show the same lineshape, as example the spectra for the O3-LB mixture are shown in figure 3.4. No additional spectral component, evocative of domain formation [179], was detected. The rigidity of the membrane is only slightly reduced with respect to NML-LB even in the presence of the higher amount of Omega-3 lipids, as the S value is 0.68 for 5-PCSL and 0.38 for 14-PCSL. This indicates that inclusion of 22:6(cis)PC in the lipid mixture does not change the liquid crystalline organization of the bilayer, which remains in the Lo state. In a previous work was found that 22:6(cis)PC is able to drive the Lo/Ld transition in the case of a POPC/SM/Chol bilayer [173]. Moreover, Omega-3 lipid bearing two polyunsaturated acyl chains, like 22:6(cis)PC, are reported to drive the segregation of Chol, with formation of lipid domains [180,181]. The resistance of NML-LB to undergo any transition is probably ascribable to the presence of GM1, which is recognized as a major player in the modulation of later ordering within biological membranes [182], limiting domain growth.

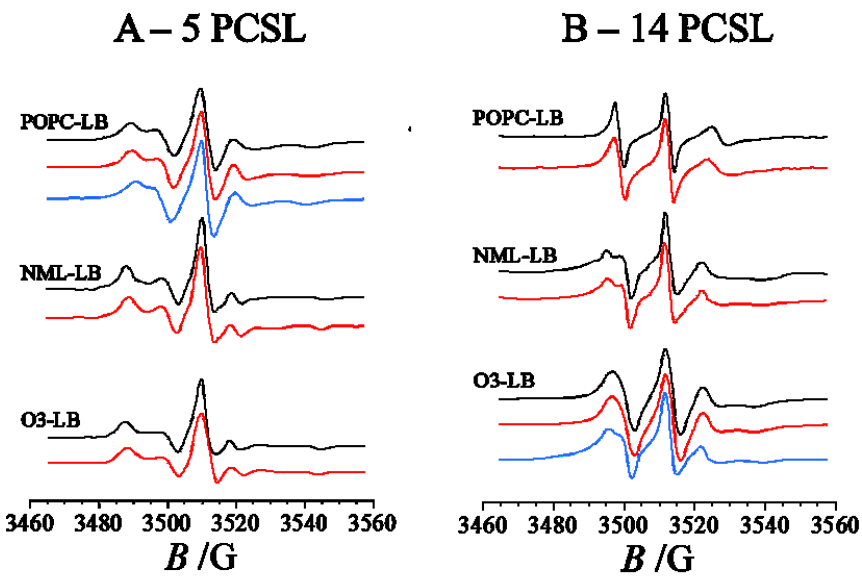

Figure 3.4 *EPR spectra of the two spin reporter used in this study, 5-PCSL (panel A) and 14-PCSL (panel B) of the investigated liposome compositions. Black lines: EPR spectra of liposomes without Abeta42. Red lines: EPR spectra just after peptide addition. Cyan lines: EPR spectra after 21 days of incubation.*

The presence of Abeta42 in the system affects the POPC-LB organization [173,183], as revealed by the spectra of 5- and 14-PCSL registered soon after samples preparation (Figure 3.4, red lines). In the case of 5-PCSL a slight reduction of the spectrum anisotropy is observed, as confirmed by the decrease of the S value by ~0.02. An opposite behaviour is observed for 14-PCSL: the spectrum anisotropy increases and S raises by ~0.04. However, no evidence of a second component in the spectrum is observed, as expected for membrane-penetrating peptides. Thus, the experimental evidences point to a positioning of the peptide close to the membrane interface, causing perturbation in the lipid dynamic and ordering that propagates to the bilayer inner core.

Even for NML-LB the presence of Abeta42 in the system causes a small reduction of the 5-PCSL spectrum anisotropy and a consequent slight S decrease of ~0.02.

However, almost no variation is found in the 14-PCSL spectrum. These results indicate a weak interaction of the peptide with the membrane interface, which does not affect the inner bilayer structure.

In the case of the Omega-3 lipid containing lipid bilayers, similarly to what observed for NML-LB, the presence of Abeta42 causes a reduction of the 5-PCSL spectrum anisotropy, as confirmed by the reduction of 0.02 in the S value, while no effect is registered for 14-PCSL. Thus, inclusion of 22:6(cis)PC does not affect peptide-membrane interaction in just-prepared samples.

The evolution over time of the 5- and 14-PCSL spectra in all the considered bilayers was followed both in the absence and in the presence of Abeta42. No spectra change was observed in the peptide absence. In the case of O3L-LB and O3-LB, this indicates that no 22:6(cis)PC oxidation occurs, in line with the long-term stability of Omega-3 lipids in liposomes reported in the literature [184]. For samples containing the peptide, significant changes of the spectra with time were observed, depending on the bilayer lipid composition. In the case of POPC a progressive reduction of the 5-PCSL spectrum anisotropy is observed, as shown by the trend of ΔS reported in figure 3.5. As an example, the spectra of the two spin labels in POPC-LB in the presence of the peptide after 21 days are shown in figure 3.4 (cyan lines). In contrast, the 14-PCSL S value remains almost constant (figure 3.5).

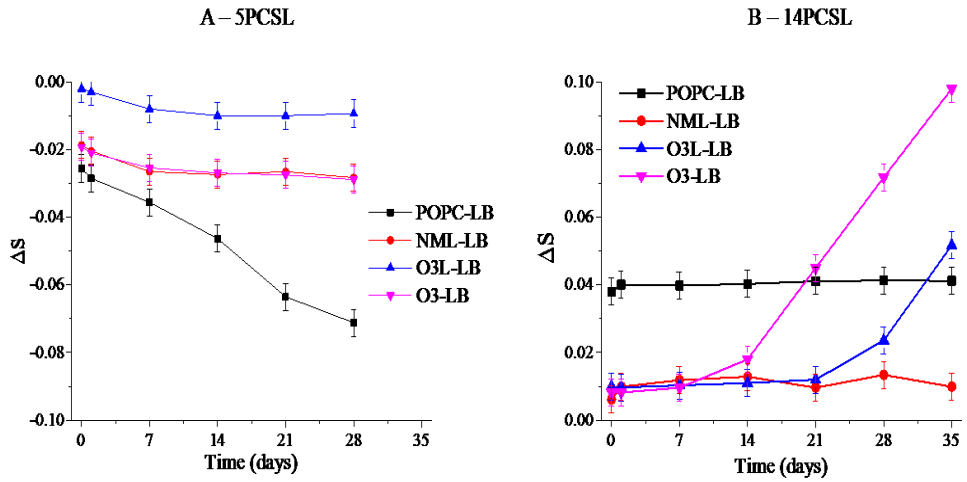

Figure 3.5 *Time course evolution of ΔS for the spin label 5PCSL (panel A) and for 14PCSL (panel B) for each lipid bilayers studied when interacting with Abeta42.*

The 5-PCSL and 14-PCSL spectra in NML-LB exposed to Abeta42 remain almost unaltered, indicating that the weak interaction of the peptide with the membrane does not strengthen with time.

In the presence of Omega-3 containing lipid bilayers, for both the formulations considered (O3L-LB and O3-LB), the 5-PCSL spectrum exposed to Abeta42 remains almost constant whilst, interestingly, in the case of 14-PCSL the spectrum anisotropy becomes markedly more evident after three weeks and, consequently, the S value significantly increases (figure 3.5). These results indicate an increasing membrane perturbation of the bilayer inner core due to the interaction with the peptide, modulated by the amount of Omega-3 lipids in the membrane, as it is elicited after a smaller time-lag for O3-LB than for O3L-LB systems.

Internalization of Abeta fragments has been observed in the case of POPC/SM/Chol bilayers enriched in 22:6(cis)PC, which, differently from the ones used in this study, are in the Ld state [173]. This could indicate that the peptide selectively interacts with Omega-3 lipids, almost independently of the lipid bilayer state.

3.5 Membrane Leakage

The leakage activity of the peptide towards the lipid compositions investigated was studied by a fluorescence based content-mixing assay [185]. Liposomes loaded with a fluorophore, 8-Aminonaphthalene-1,3,6-Trisulfonic Acid (ANTS), and its quencher, p-Xylene-Bis-Pyridinium Bromide (DPX), were titrated with Abeta42. In case of pore formation upon liposomes-peptide interaction, the two molecules are released in the bulk solution, resulting in molecules detaching and ANTS dequenching effect. In order to study the leakage activity of Abeta42 in its monomeric form, the peptide was dissolved in DMSO; in this solvent, Abeta42 aggregation is hindered, and it assumes a random-coil conformation. The data, shown in figure 3.6, indicate a very strong permeabilization effect towards all the three liposomes composition studied, with high leakage activity even if very low peptide/lipid ratios were explored. Omega3 lipid embedded in liposomes does not affect the Abeta42 leakage activity, that shows a similar permeabilization effect on both NML-LB and O3-LB. In case of POPC liposomes, pore formation by this interaction is clearly lower.

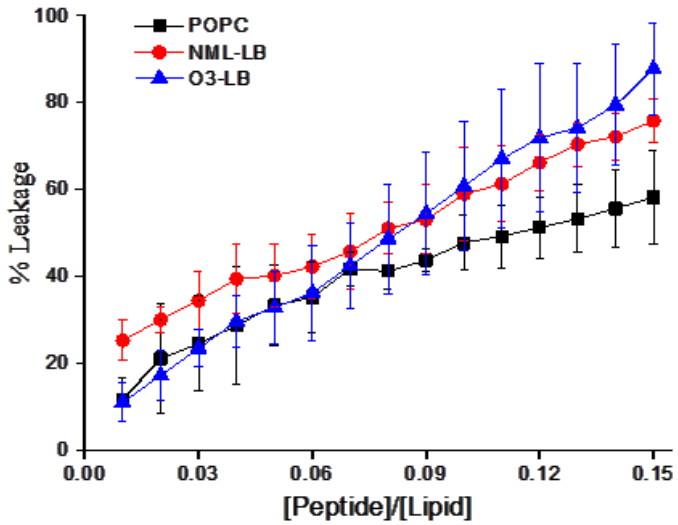

Figure 3.6 *Abeta42 leakage activity towards the studied lipid bilayers titration curves.*

3.6 Conclusions

In conclusion, by using CD spectroscopy, we have preliminarily verified that, in phosphate buffer and in the absence of lipids, the peptide adopts the expected β conformation and undergo the subsequent self-aggregation forming insoluble aggregates. The effect of single-component lipid bilayer has been also investigated by using POPC, a zwitterionic phospholipid abundant in eukaryotic cells, often chosen for membrane-peptide interaction studies. These results show that POPC-LB stabilize for several weeks a soluble, aggregated form of Abeta42, having a small but constant concentration. The CD spectrum is indeed very reproducible over time, but has a low intensity and shows a shift of the β sheet minimum toward higher lambda values, which can be the effect of a β aggregated but soluble structure, with a scattering [186] due to the presence of high molecular weight aggregates. ESR results show that these aggregates interact with the membrane interface, increasingly disturbing its organization, while the bilayer interior is only indirectly affected.

Interestingly, biomimetic lipid bilayers (NML-LB) do not present the ability to solubilize the peptide, although CD spectra suggest the presence of a small amount of peptide deprived of regular secondary structure also associated with the lipid phase. Our results indicate that, in the presence of GM1, large and likely heterogeneous aggregates interacting with the membrane interface quickly form. Furthermore, the experimental evidences clearly show that these insoluble aggregates are not able to penetrate in the lipid bilayer [187,188]. This could be connected with the rigidity of the lipid phase (in the Lo state), which in this case is much higher than that of POPC-LB (in the Ld state).

Inclusion of 22:6(cis)PC in the lipid composition does not affect the initial behavior of the membrane in the presence of Abeta42: only a limited perturbation of O3-LB interface is observed, probably due to a weak interaction with large, insoluble aggregates. However, CD data clearly show that, over time, an increasing fraction of

the peptide convert to soluble, lipid associated, aggregates, able to interact with the bilayer. The β-sheet minimum indeed undergoes a further shift toward high wavelength with respect to POPC-LB, suggesting an increasing of the scattering contribution in the spectra. Furthermore, ESR spectra indicate that these aggregates are significantly embedded in the bilayer, differently from the superficial interaction in case of NML-LB, as schematised in figure 3.7.

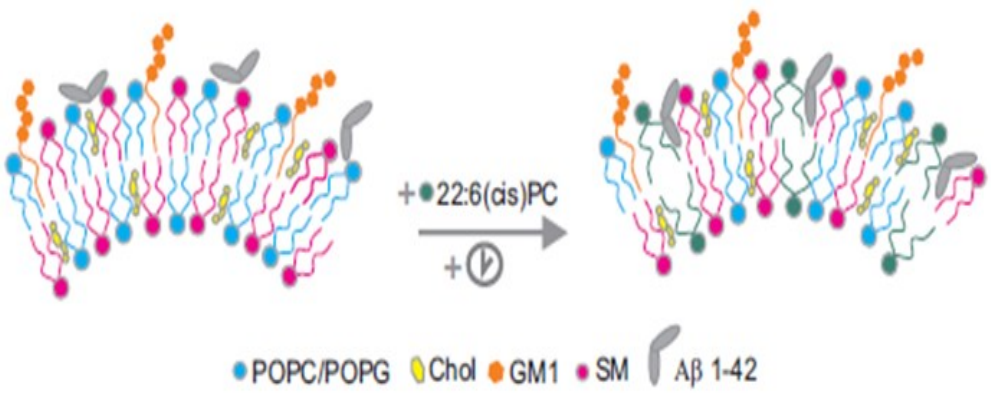

Figure 3.7 *Scheme of the different interaction model proposed for Abeta42 and neuronal membrane biomimetic lipid bilayers (left side), and Omega3 containing biomimetic bilayers (right side).*

The comparison of the data obtained by introducing two different 22:6(cis)PC amounts in the lipid bilayer formulation indicates that qualitatively the effect of Omega-3 lipid presence is independent by the amount of this component, however the extent of the perturbation and the kinetics of the process are enhanced when the Omega-3 lipid concentration increases. It is to be highlighted that the dramatic enhancement of the Abeta42 affinity for the membrane due to 22:6(cis)PC cannot be straightforwardly related to changes of the bilayer properties, considering that this lipid causes only a slight reduction of the bilayer ordering. This result could induce to speculate about a peptide molecular preference for the Omega-3 lipid, which, however, should be better investigated.

3.7 Experimental Section

3.7.1 Materials

The Abeta42 peptide was synthesised as previously reported [16]. The phospholipids POPC, POPS, SM, GM1 ovine brain sodium salt, 1,2-didocosahexaenoyl-sn-glycero-3-phosphocholine (22:6(cis)PC) and spin-labelled phosphatidylcholines (n-PCSL) with the label at different positions (n) in the sn-2 acyl chain were purchased from Avanti Polar Lipids (Alabaster, Alabama, USA). Chol, HFIP, TFA, ANTS, DPX and other laboratory reagents were purchased from Sigma-Aldrich (St. Louis, Missouri, USA).

3.7.2 Liposome preparation

Large unilamellar vesicles (LUVs) consisting of POPC (POPC-LB, where LB stands for lipid bilayers), POPC/POPS/Chol/SM/GM1 (8/2/9/1/1 mol/mol, henceforth indicated as neuronal membrane-like lipid bilayers, NML-LB), POPC/POPS/Chol/SM/GM1/22:6(cis)PC (4/2/9/1/1/5mol/mol, henceforth indicated as O3-LB) and POPC/POPS/Chol/SM/GM1/Omega-3 (6/2/9/1/1/2mol/mol, henceforth indicated as O3L-LB,), were prepared in 20 mM phosphate buffer pH 7.4, freshly degassed by Nitrogen purging, at total concentration of 0.4 mg/ml. The organic film rehydration/extrusion method, previously described [173], was adopted. Sonication steps and direct exposure to light were systematically avoided to minimize the oxidation processes. For ESR investigation, 1% w/w of the spin-label was added to the lipid mixture in organic solvent before drying.

3.7.3 Peptide samples preparation

The Abeta42 peptide was pretreated with TFA, in order to dissolve any fibrillar aggregates, as previously described [16]. The sample was then freeze-dried and redissolved in pure HFIP, and then the UV and CD spectra were recorded to assess

the acid treatment success. This solution was divided in aliquots of 100 μg each, and the solvent was dried under nitrogen flux to form a peptide film. These films were then rehydratated with 1 ml of 0.4 mg/ml liposome suspensions, yielding a lipid/peptide ratio of 25/1 mol/mol, and the samples were incubated at 4 °C as indicated and used for both CD and ESR experiments.

3.7.4 CD spectroscopy

CD spectra of Abeta42 (0.1 mg/ml final concentration) were taken using Jasco J-810 spectropolarimeter (Jasco international Co. Ltd, Tokyo, Japan) in the range of 200–260 nm using a 0.1 cm path length quartz cuvette at 20 °C in continuous scanning mode (20 nm/min, with a 4.0 s response and a 1.0 nm band width). Spectra corresponding only to the solvent or lipid bilayers in the absence of the peptide have been recorded thoroughly during the measurements and subtracted from the corresponding peptide/lipid bilayer spectrum. The data were accumulated over 3 runs, the presented data being the average. The results are expressed in term of molar ellipticity [θ], in unit of deg cm^2/mol.

3.7.5 ESR spectroscopy

ESR spectra of lipid and lipid/peptide samples were recorded in collaboration with Prof. Gerardino D'Errico on a 9 GHz Bruker Elexys E-500 spectrometer (Rheinstetten, Germany) at 20 °C. Capillaries containing the samples were placed in a 4 mm quartz sample tube. The instrumental settings were: sweep width, 120 G; resolution, 1024 points; modulation frequency, 100 kHz; modulation amplitude, 1.0 G; time constant, 20.5 ms, incident power, 5.0 mW. Several scans were accumulated to improve the signal-to-noise ratio. The quantitative analysis of the spectra was performed through a homemade, MATLAB-based software routine.

3.7.6 Leakage experiments

The ANTS/DPX assay [189] was used to monitor leakage induced by peptide interaction with vesicles. The fluorescence signal resulting from the de-quenching of ANTS released into the medium was observed through a HORIBA Fluoromax-4 spectrofluorimeter. The excitation wavelength was set to 360 nm, the emission wavelength red to 520 nm. The liposomes were titrated with a 1 mM Abeta42 solution in DMSO. The vesicles were completely lysed by the detergent Tween10, to obtain the maximal fluorescence value, which was set to 100% leakage. Fluorescence from intact vesicles in NaP 20 mM pH 7.4 buffer was set to 0% leakage, and results were normalized according to this scale. Liposomes were also titrated with the same volumes of NaP 20 mM pH 7.4 buffer and DMSO, in order to correct the dilution and DMSO effects. All experiments were repeated three times, and the average is reported. [185].

Chapter 4: Effect of glycation on structure and aggregation properties of Abeta peptides

4.1 Work outline

The effects of the glycation reaction on biological and biophysical properties of peptides and proteins is a very hot topic in the recent literature. Glycation could have very different effect on protein aggregation properties; it could both increase (as example albumin) and decrease (as example lysozime) the amyloid formation rate, depending if it promotes the formation of either on- or off-pathway oligomers [123]. Nevertheless, the effect of glycation and AGEs formation on biophysical properties of Abeta peptides is an intriguing topic that has not yet been addressed.

In this thesis, the effect of glycation reaction on structure and aggregation properties of Abeta peptides Abeta40 and Abeta42 was studied by an integrated combination of biophysical techniques. Methylglioxal (MGO), a three-carbon atom compound with two carbonyl function formed as a product of sugars autoxidation, was chosen as glycation agent. Its structure is shown in figure 4.1. MGO is too small to cyclise as other longer carbohydrates (such as glucose), leaving the carbonyl function always available for the reaction and therefore this compound shows a very high protein modification capacity, both in vitro and in vivo [190]. Both studied Abeta peptides have four possible glycation sites: the N-terminus, one arginine (5Arg) and two lysines (16Lys, 28Lys).

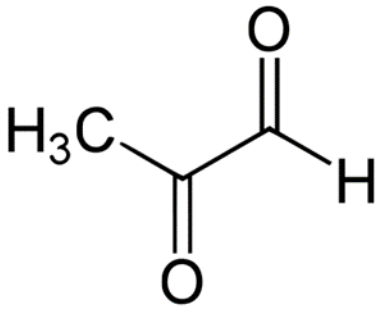

Figure 4.1 *Methylglioxal chemical structure.*

The reaction kinetic was studied by fluorescence spectroscopy, as one of the reaction product between MGO and arginine side chain, called argpyrimidine (see figure 1.13 for the chemical structure) has an aromatic moiety that shows fluorescence when excited at 340 nm [191], thus it can be exploited to follow the reaction progression. The effect on peptides secondary structure was studied by CD spectroscopy. Changes in the aggregation behaviour were monitored using the Thioflavin T (ThT) assay [9].

As the Abeta peptides conformation and solubility are strongly affected by the solvent polarity [57], the reaction was carried out in two different conditions. The first condition is phosphate buffer 200 mM pH 7.4, in order to simulate a polar environment, in which the Abeta peptides quickly adopt a beta conformation, leading to peptide self-assembly; moreover, it is known that phosphate is able itself to catalyse the glycation reaction [192]. The second condition is a HFIP/NaP 200 mM pH 7.4 mixture (80%/20% by volume), henceforth called HFIP mixture. This condition simulates a low polarity environment, in which even the most aggregation prone Abeta42 keeps a stable, soluble α-helical structure, so the glycation and aggregation processes are decoupled in this condition. The reaction was carried out in all cases at 37 °C, using a 100 fold molar excess of MGO.

The Abeta peptides were pre-treated in strong acidic condition in order to dissolve any pre-existent aggregates, prior to each experiment. They were divided into two

aliquots, and then dissolved at 100 μM final concentration in NaP 200 mM pH 7.4 (for more details, see experimental section), or at 50 μM final concentration in the HFIP/buffer mixture. In one aliquot, MGO was added at 10 mM final concentration (100-fold excess). This sample will be called glycated Abeta (Abeta40G and Abeta42G). The other sample was instead incubated without MGO, as control of peptide behaviour in this condition, and called non-glycated Abeta (Abeta40NG and Abeta42NG).

All experiments reported in this chapter were repeated three times. The spectra reported (both fluorescence and CD) are relative to one representative experiment. All reported kinetics are the average of all performed experiments.

4.2 Aqueous environment

4.2.1 Reaction kinetics

Abeta40G shows a very strong fluorescence signal when excited at 340 nm just after one day of incubation at 37 °C, with the maximum centred at 400 nm. Some recorded fluorescence spectra are reported in figure 4.2, showing that the fluorescence intensity, and therefore the argpyrimidine concentration, reaches a plateau after about three days of incubation. The kinetics of the reaction is clearer when plotting normalised fluorescence intensity at emission maximum (400 nm) against time, as reported in figure 4.2.

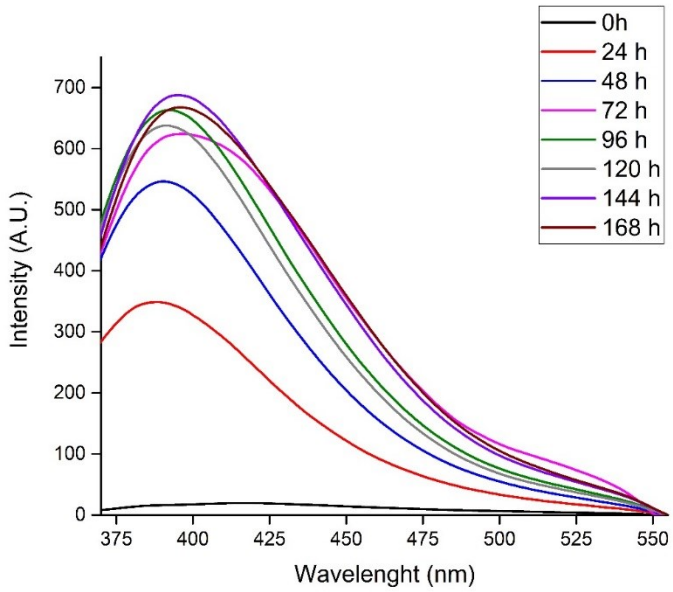

Figure 4.2 *Fluorescence emission spectra of Abeta40G.*

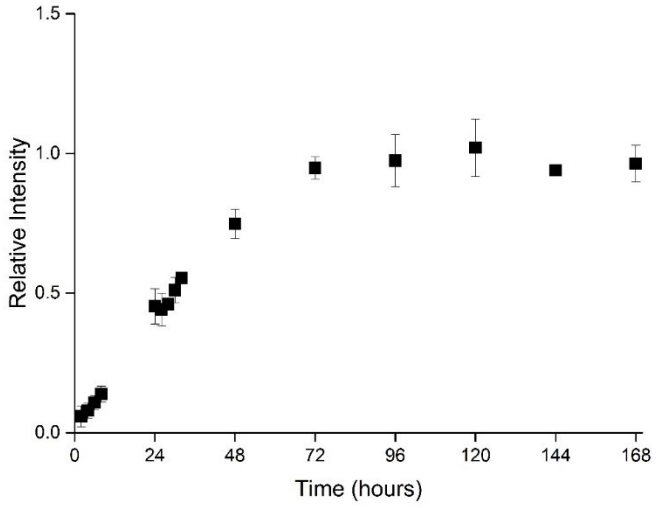

Figure 4.3 *Fluorescence intensity in correspondence of the emission maximum in function of time. When not visible the error bar is within the symbol.*

Control experiments were performed on AbetaNG and MGO in phosphate buffer, revealing no significant fluorescence intensity upon excitation at 340 nm. In fact, also the incubated MGO shows fluorescence, even if at different wavelengths. In figure 4.4, some excitation spectra of MGO are reported; they show a signal build up with time when excited at about 390 nm, probably due to some MGO self-polymerization adducts promoted by the high concentration. The MGO and AGEs excitation wavelengths are very different; no interference should arise on AGEs fluorescence.

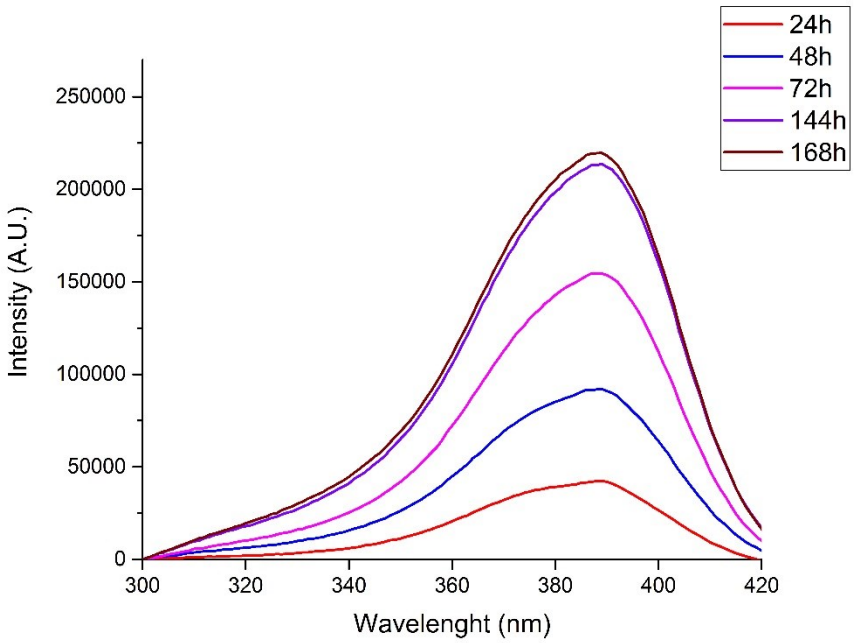

Figure 4.4 *Fluorescence excitation spectra of 10 mM MGO dissolved in phosphate buffer and incubated at 37 °C.*

The same experimental procedures were used to study the effect of glycation on the full-lenght amyloid peptide Abeta42. Also in this case, two aliquots were made, one with 10 mM MGO (Abeta42G) and one without the glycation agent (Abeta42NG).

The data reported in Figure 4.5 indicate some differences between AGEs formed by Abeta42 and Abeta40 since, during the reaction time course, there is a fluorescence signal build up when excited at 340 nm, but the emission maximum is red shifted with respect to the shorter peptide, being centred at 430 nm. This effect could be due to a different product or to a different conformation of Abeta42 in solution that could modify the environment of Arg5 because, as reported later in this chapter, the glycation does not hamper the transition to β-sheet structure. Even if the 5Arg is not in the fibril inner core according to the last structural model published [62], its chemical environment is likely to be different respect to Abeta40, which remains unstructured in the glycated peptide. The reaction is also slower, likely due to this conformational difference, and reaches plateau after about one week, as reported in figure 4.6.

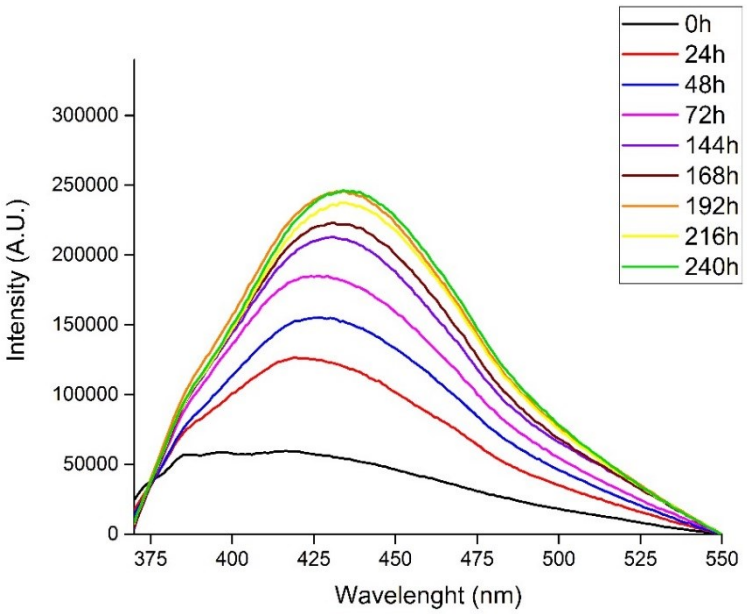

Figure 4.5 *Fluorescence emission spectra of Abeta42G.*

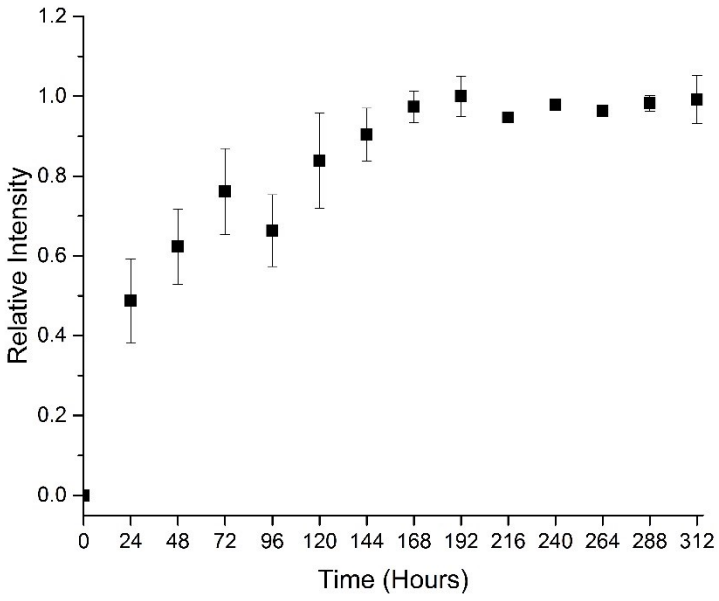

Figure 4.6 *Fluorescence intensity in correspondence of the emission maximum in function of time. When not visible the error bar is within the symbol.*

4.2.2 Effects on secondary structure

The effect on the secondary structure was monitored by CD spectroscopy both on glycated and non-glycated peptide. The AbetaNG undergoes a transition from a disordered conformation to a β-structure after two days, followed by a drop of the CD signal during the experiment timeframe that indicates peptide aggregation. On the other hand, AbetaG shows a random coil spectrum for the whole experiment timeframe; the signal slightly drops after four days of incubation, but the peptide is not able to undergo the transition to a β-structure anymore. Thus, the glycation boosts the solubility of Abeta40 and prevents the transition to β-structure. CD spectra of Abeta40NG and Abeta40G are shown separately in Figure 4.7 and Figure 4.8.

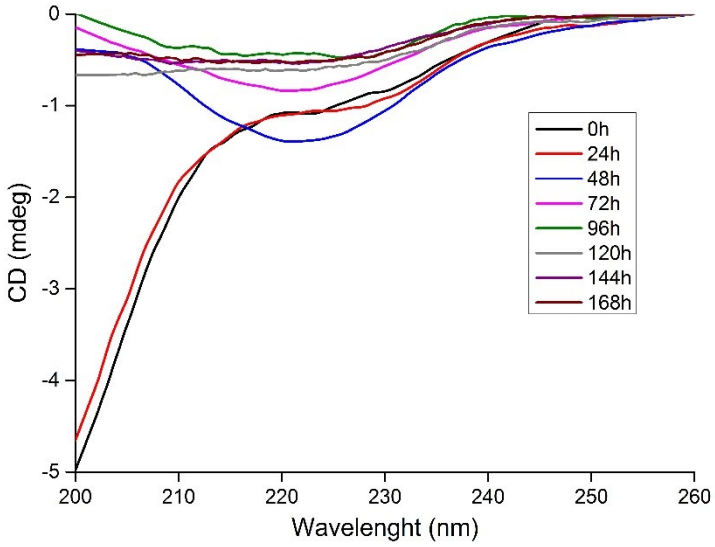

Figure 4.7 *CD spectra of Abeta40NG.*

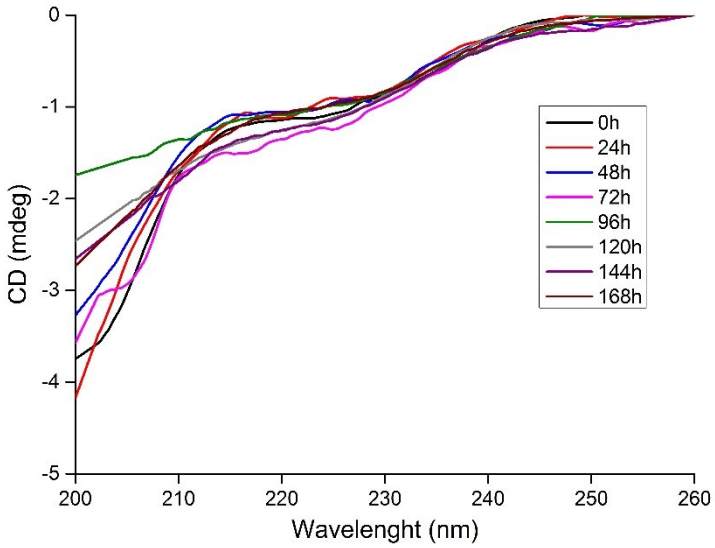

Figure 4.8 *CD spectra of Abeta40G.*

The CD spectra of Abeta42NG shows the usual behaviour: it is random coil when just dissolved in the buffer solution. After a lag phase, it forms β-sheet structures, whose minimum is red shifted during the incubation time respect to canonical β-sheet structure CD lineshape; this kind of behaviour is widely reported in literature and is related to the formation of β-structured soluble oligomers [77]; then the signal drops due to peptide aggregation. The CD spectra are shown in figure 4.9. As expected on the basis of fluorescence results, the effect of the glycation reaction on Abeta42 secondary structure is different with respect to Abeta40. In particular, also when modified by the reaction, the glycated peptide is able to undergo the transition to β-sheet structure, with the minimum slightly red shifted, but the spectra intensity and as lineshape remain stable for the whole timeframe of the experiment, as shown in figure 4.10. These results suggest that the structural modifications caused by glycation slow down the peptide aggregation as ; furthermore, the difference of the minimum position between Abeta42G and Abeta42NG could be related to the formation of different sized oligomers.

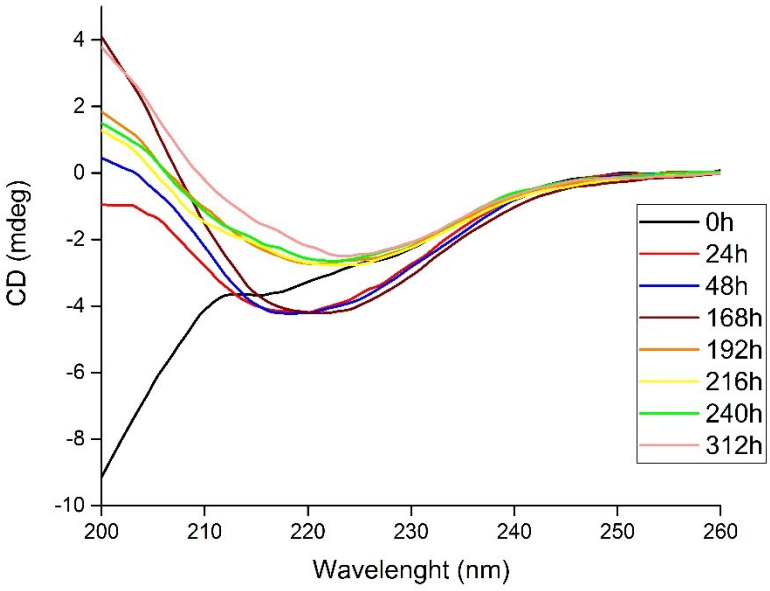

Figure 4.9 *CD spectra of Abeta42NG.*

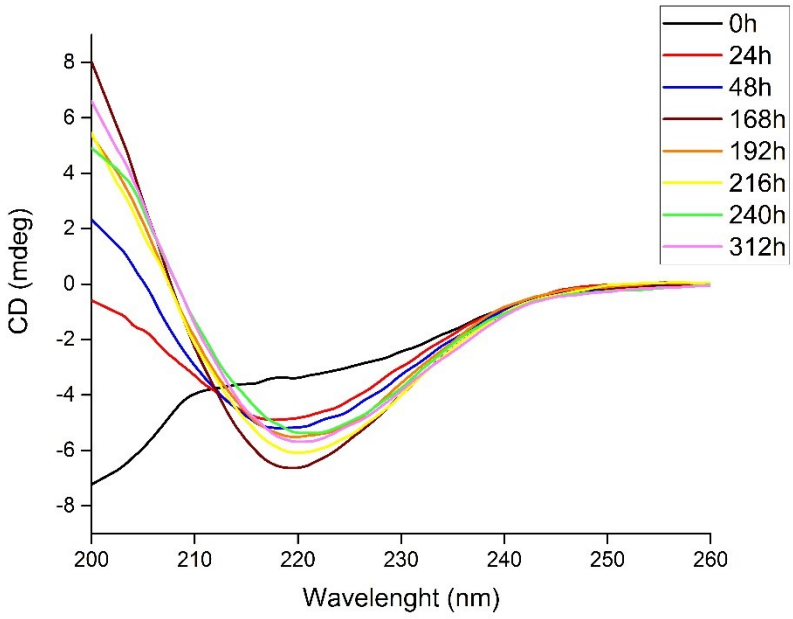

Figure 4.10 *CD spectra of Abeta42G.*

In addition, considering that Abeta42G is still able to adopt a β-sheet conformation (never observed for Abeta40G), and to form aggregates, its aggregation propensity was studied by ThT binding assay, and compared with that of Abeta42NG. There are two main differences between the two peptides: i) the plateau in the fluorescence signal is reached faster by Abeta42NG (two days) than by Abeta42G (three days); ii) the plateau signal of Abeta42NG is two times higher with respect to the glycated peptide. These data corroborates the hypothesis that glycation hampers Abeta42 peptide aggregation, by slowing it and possibly avoiding the formation of more mature aggregates.

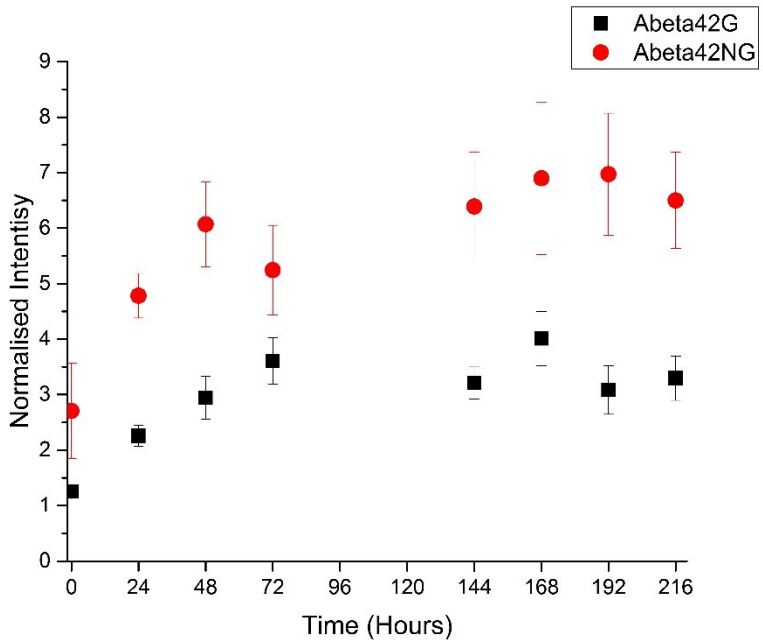

Figure 4.11 *ThT fluorescence normalised intensity (485 nm) in function of incubation time.*

4.3 Apolar environment

The glycation reaction was performed also in the HFIP mixture. Using this less polar solution, Abeta peptides adopts α-helical conformation and are not able to aggregate to amyloid fibrils, resulting in a very stable sample. The AGE fluorescence reaches

the maximum value after about one week for both peptides, but in case of Abeta40G, the signal slightly drops before reaching a plateau; both kinetics are shown in figure 4.12. In this condition, the excitation wavelength of MGO intrinsic fluorescence is blue shifted to about 340 nm, the same wavelength of AGEs excitation. In this solution, the contribution of MGO to the fluorescence signal is not negligible as in aqueous solution. The fluorescence spectra of Abeta40G and Abeta42G do not show any difference. During the incubation, together with the signal increase there is also a marked shift of AGEs emission maximum, from about 400 nm to 430 nm, for both peptides, indicating that the AGEs are changing during the incubation at 37 °C. A possible explanation could be that the rearrangement of glycation early-products into end-products is slower in apolar environment. More work is needed to further characterize this behaviour. As representative example, the Abeta42G fluorescence spectra and the same spectra subtracted MGO contributions are shown in figure 4.13.

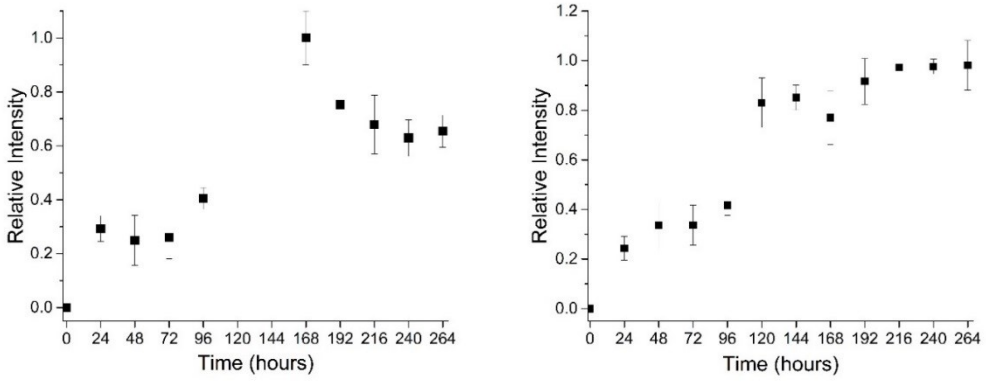

Figure 4.12 *Fluorescence intensity in correspondence of the emission maximum in function of time.*

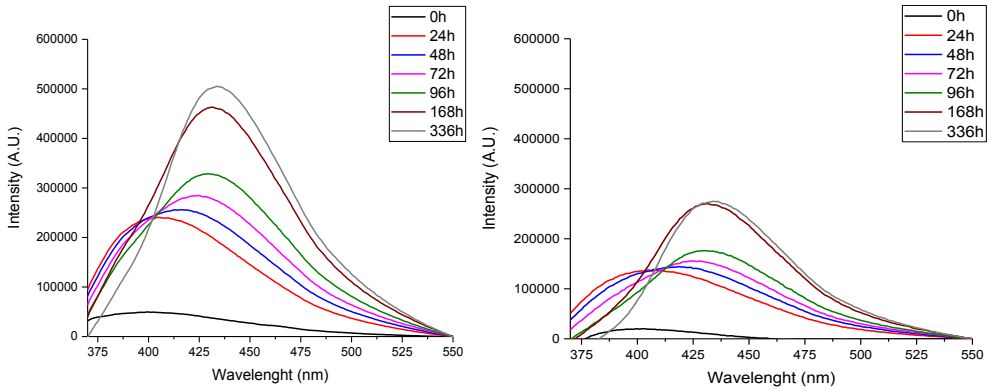

Figure 4.13 *Fluorescence emission spectra of Abeta42G in HIFP/phosphate buffer 80/20 v/v (left panel); Fluorescence emission spectra of Abeta42G after subtraction of MGO contribution (right panel).*

CD spectra of both peptides in this condition show a predominant α-helical structure, as expected [16]. There is no difference between unmodified and glycated Abeta peptides; as representative example, Abeta42G spectra are reported in figure 4.14. These results indicate that glycation does not modify the secondary structure features in this condition. Moreover, the CD signal is constant even after one month of incubation at 37 °C, confirming that the peptides are not able to aggregate in this kind of solution.

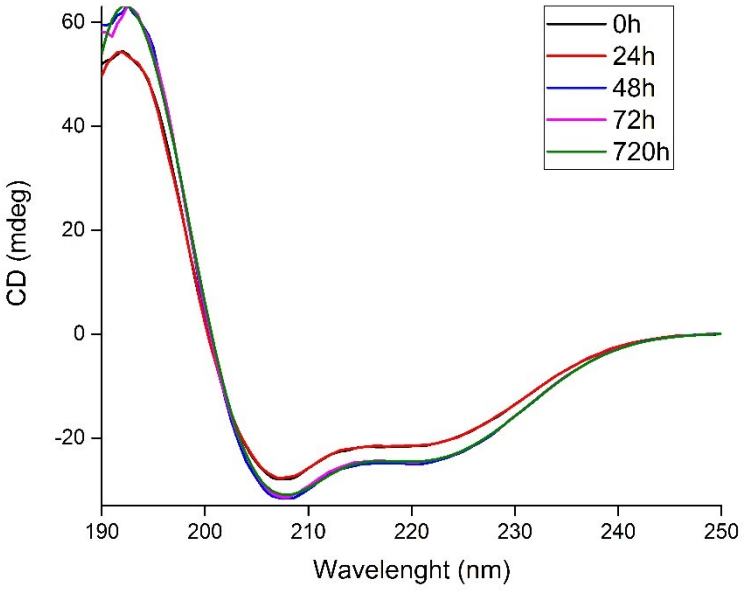

Figure 4.14 *CD spectra of Abeta42G in HFIP/NaP 200 mM pH 7.4.*

4.4 Conclusions

In conclusion, the glycation reaction was biophysically characterized for both amyloid peptides Abeta40 and Abeta42, in polar (aqueous phosphate buffer) and apolar (HFIP/phosphate buffer mixture) environment. The reaction kinetics and the effects on secondary structure were characterized in all conditions. The glycation is faster for the shorter peptide; this could be explained by considering an easier accessibility of the glycation sites . In fact, the glycation reaction completely hampers the transition to β-sheet structures for Abeta40, that remains in unstructured state for the whole experiment timeframe, and therefore arginine and lysine side chains are more available for the reaction. In case of Abeta42, glycated peptide is still able to form β-sheet structure, but CD data indicate that these species are different from the ones formed by the unmodified peptide and they are more soluble in water solution. ThT data for Abeta42G also indicate a slowed aggregation process after peptide glycation.

Still more work is needed to characterize glycation reaction in HFIP containing solution, but fluorescence data clearly indicate that the reaction take place also in this condition, without affecting peptides secondary structure. The HFIP mixture could be a very good model system to identify and structurally characterize AGEs formed by Abeta peptides with other biophysical techniques, thanks to the decoupling of glycation and aggregation processes.

4.5 Experimental Section

4.5.1 Materials

Recombinant Abeta40 was expressed in *E.Coli* as reported in chapter 2. Abeta42 was synthetized as previously described [16]. MGO was purchased from Sigma-Aldrich and further purified by steam distillation. All other laboratory reagents were purchased from Sigma-Aldrich (St. Louis, Missouri, USA).

4.5.2 Samples preparation

Before each experiment, Abeta peptides were treated with pure TFA in order to dissolve any pre-existent fibril aggregate [16], as reported also in section 3.7.3. The peptides were dissolved in phosphate buffer 200 mM pH 7.4 to the final concentration of 100 μM, or in HFIP/phosphate buffer 200 mM pH 7.4 mixture to the final concentration of 50 μM. Half of the aliquots were incubated at 37 °C without agitation (non glycated peptides, Abeta40NG and Abeta42NG), in the other half MGO was added in 100 fold molar excess, i.e. 10 mM in phosphate buffer experiments, and 5 mM in HFIP mixture experiments, and then incubated at 37 °C without agitation (glycated peptides, Abeta40G and Abeta42G).

4.5.3 Fluorescence spectroscopy

Fluorescence spectra were recorded on a Jasco FP 6600 and on HORIBA Fluoromax-4 spectrofluorimeters. For AGEs measurements, excitation wavelength was set to 340 nm, emission range from 370 to 550 nm, scanning speed 100 nm/min, both excitation

and emission slits were set to 5 nm. For excitation spectra measurements, emission wavelength was set to 430 nm, and a range from 300 to 420 nm was explored. AGEs fluorescence was measured directly, without dilute the samples. For ThT measurements, excitation wavelength was set to 440 nm, emission range from 460 to 600 nm, scanning speed 100 nm/min, both excitation and emission slits were set to 5 nm. Before each measurement, a sample aliquot was taken and diluted to 10 μM in phosphate buffer 20 mM pH 6.8 containing 30 μM ThT (3 fold molar excess of ThT). AGEs fluorescence emission intensity, after subtraction of non-glycated peptide and eventually MGO contributions, was internally normalized for each experiment, in order to be able to compare different experiments. ThT fluorescence emission intensity, after subtraction of sample without ThT contribution, was normalized with respect to the intensity of 30 μM solution of the same ThT batch, recorded in the same day of the experiment. All spectra were recorded at 20 °C.

4.5.4 Circular Dichroism spectroscopy

CD spectra were recorded on a Jasco spectropolarimeter. In phosphate buffer, a range from 200 to 260 nm was explored; due to buffer very high concentration, was not possible to explore lower wavelength because detector potential was too high. In HFIP mixture, a range from 190 to 250 nm was explored. The scanning speed was set to 20 nm/min, the average time to 4 seconds and the temperature to 20 °C for all experiments.

Chapter 5 – High-resolution analysis of hemopressin peptides conformation

5.1 Work Outline

Hemopressin (Hp) is a nonapeptide of sequence PVNFKLLSH derived from hemoglobin α-chain acting as CB1 receptor endogenous inverse agonist, and exerting antinociceptive, hypotensive and anoretic activity [140,141]. Its promising applications in obesity and pain therapy has been hampered by the lack of reproducibility associated to its usage in pharmacological assays, which can be related to its aggregation propensity. Under specific experimental conditions (1 mM peptide in 25 mM phosphate, 50 mM NaCl, pH 7.4), hemopressin is able to self-assembly into amyloid like nanostructured fibrils [18], which may contribute to its unreliable activity.

N-terminally extended isoforms of hemopressin, such as RVD-hemopressin (RVD-Hp), were identified and reported to be CB1 agonists [143]. Notably, RVD-Hp shows no fibrillation in the experimental conditions reported above [18], despite the high sequence identity with Hp.

Very little is known about hemopressin peptides conformation, which knowledge could be helpful in understanding the reasons for such different biological and biophysical properties that characterise these two peptides.

In this chapter, a conformational analysis of the hemopressin peptides Hp and RVD-Hp is reported. Conformational features were explored by a two-level approach: an initial screening was performed by CD spectroscopy; subsequently, a more detailed analysis was performed by high-resolution NMR spectroscopy. Furthermore, the influence of two parameters, i.e. pH and solvent polarity, was explored. In particular, almost neutral pH 7.4 and acidic pH 3.0 were studied. It has been reported that at

neutral pH, only Hp is able to form amyloid fibrils, while no aggregation occurs for the longer peptide; moreover at acidic pH, Hp loses its capacity to self-assemble [193]. The second parameter explored is the solvent polarity. The two peptides were titrated with a fluorinated alcohol, hexafluoroisopropanol (HFIP), a solvent often used to simulate low polarity environments, in which intrapeptide interaction are favoured with respect to peptide-solvent interaction, inducing more ordered conformations.

5.2 CD spectroscopy screening

5.2.1 Aqueous environment

A conformational screening was performed on both peptides by CD spectroscopy. Hp and RVD-Hp were dissolved in 20 mM NaP buffer at both pH 3.0 and pH 7.4, in order to assess the pH effect on peptides conformations. The CD spectra overlay is reported in figure 5.1.

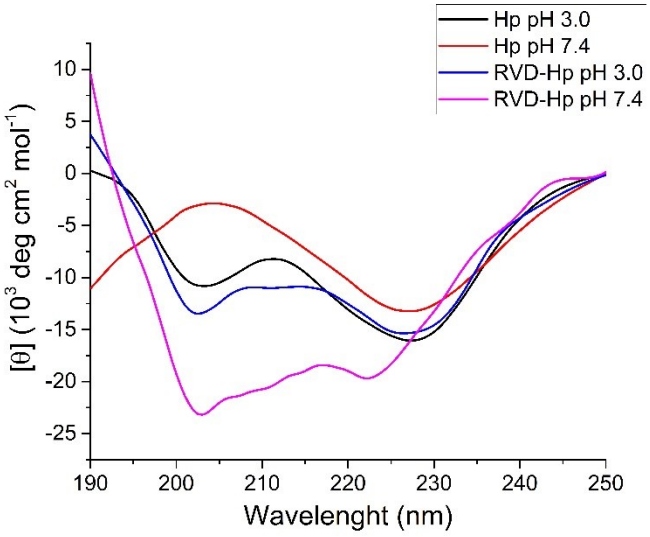

Figure 5.1 *CD spectra of hemopressin peptides in aqueous environments. The used buffer was NaP 20 mM for both pHs.*

Although CD signal is quite low, figure 5.1 shows that the shorter peptide, Hp, is sensible to pH condition. Indeed, when dissolved in acidic pH it shows a spectrum

corresponding to an α-helical conformation. The minima position are shifted with respect to the canonical position, (202 nm against 208 and 227 nm against 222), likely because the peptide explores different conformations in solution. On the other hand, at neutral pH the spectrum shape changes significantly, hinting at a conformational transition and possibly indicating that Hp assumes a β-sheet-like conformation. This is in agreement with the amyloid fibril formation observed for Hp at this pH, even if in different concentration and ionic strength conditions [18].

The spectrum of RVD-Hp instead is less sensible to pH condition. In both pHs explored, the longer peptide shows a spectrum that indicates a partial α-helical conformation. However, at neutral pH the CD intensity is higher and the spectrum minima are closer to the canonical values, indicating that a neutral pH stabilise the helical conformation for this peptide.

5.2.2 Apolar environments

The two peptides were titrated, at both pHs, with HFIP. The spectra obtained are shown in figure 5.2 and 5.3, respectively for Hp and RVD-Hp.

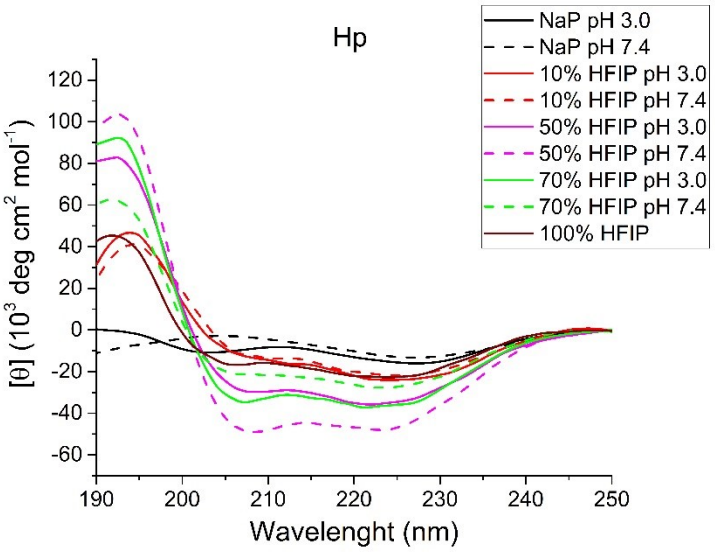

Figure 5.2 *CD spectra selection of Hp dissolved in different HFIP/ NaP 20 mM mixtures at two different pHs.*

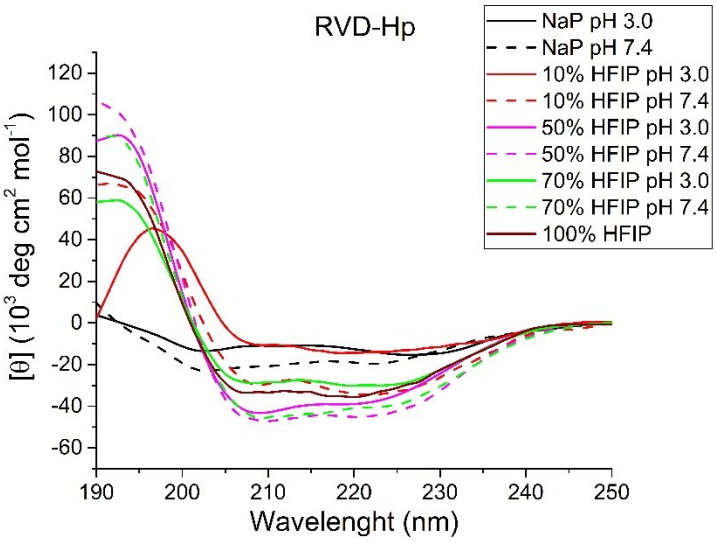

Figure 5.3 *CD spectra selection of RVD-Hp dissolved in different HFIP/20 mM NaP mixtures at two different pHs.*

The solvent polarity titration gave similar results for the two peptides. Even a low amount of HFIP, i.e. 10 % v/v, is enough to stabilise the helical conformation for both peptides, also for Hp at pH 7.4, whose spectrum changes dramatically with respect to the one measured without cosolvent (figure 5.1). The increase in the HFIP concentration is able to enhance the CD signal, further stabilising this conformation. The maximum signal is reached between 40 and 60 % of cosolvent in the case of Hp, and between 40 and 70% in the case of RVD-Hp. Adding HFIP above these values caused a reduction in the signal, probably due to little destabilisation of this conformation in low polar environment.

A comparison of the spectra recorded in HFIP/NaP 50% v/v at both the explored pHs is shown in figure 5.4. Also in this mixture, Hp is more sensitive to pH change, showing a signal definitely higher at pH 7.4 with respect to pH 3.0; in the case of RVD-Hp, there is a similar effect, although with smaller changes. Moreover, the two peptides show a similar spectrum at neutral pH, both in terms of lineshape and intensity.

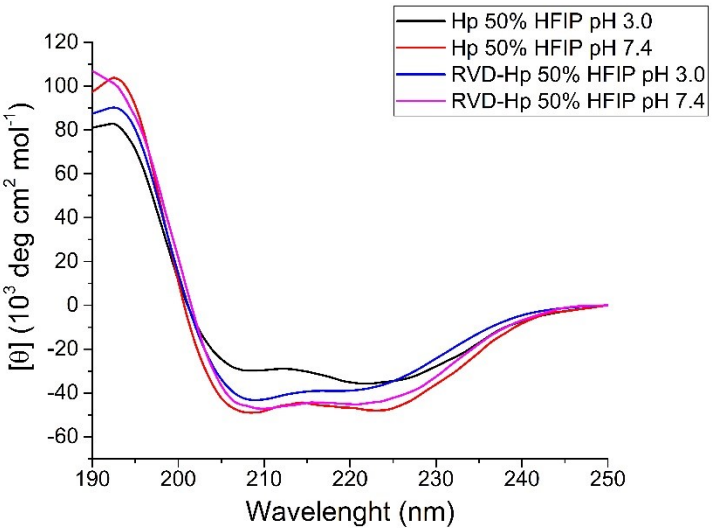

Figure 5.4 *CD spectra comparison of the two peptides dissolved in the mixture 50/50 % v/v of HFIP/NaP at two different pHs.*

5.3 NMR analysis

5.3.1 Aqueous environments

For each condition explored, a set of two-dimensional homonuclear experiments (TOCSY, NOESY, ROESY and COSY), and one carbon-correlated heteronuclear experiment were recorded for both Hp and RVD-Hp, at pH 3.0 and pH 7.4.. The experiments were carried-out at the Bijvoet Center for Biomolecular Research (Utrecht, The Netherland) on a 900 MHz instruments equipped with a cryoprobe, in order to maximize sensitivity and resolution. More details about the experiments set-up are reported in the experimental section. Most of proton and carbon atoms (beside carbons involved in CO groups) were assigned with the dataset recorded; the chemical shift tables for each condition are reported in Appendix A. For sake of simplicity, the RVD-Hp residues numbering will be used for both peptides.

Unfortunately, very few NOE crosspeaks are present in the NOESY spectra, due to a bad combination of instrument magnetic field and peptides tumbling times, but also due to the lack of ordered structure, as expected for small-size linear peptides in aqueous media [194].

Surprisingly, during the long time necessary for NMR data acquisition, the spectra of both the peptides when dissolved at pH 3.0 showed clear changes with the time. The comparison of the amide region of 1D proton spectra of Hp at pH 3.0 recorded at different time and reported in figure 5.5, highlights these changes. A similar effect was detected also for RVD-Hp at pH 3.0, but the effect was less pronounced (figure 5.6). On the other hand, no changes in the spectra were detected at pH 7.4. A possible explanation of this behaviour is that Hp undergoes a slow transition between two different conformations during the experiment timeframe; thus, the spectrum recorded just upon dissolution slowly disappears, and different signals arise from the baseline, corresponding to a new conformation. Moreover, in the spectrum recorded after two days the presence of both initial and final conformation spectra is visible. The

assignment of the second conformation of Hp dissolved at pH 3.0 is complicated due to this conversion, and is still in progress.

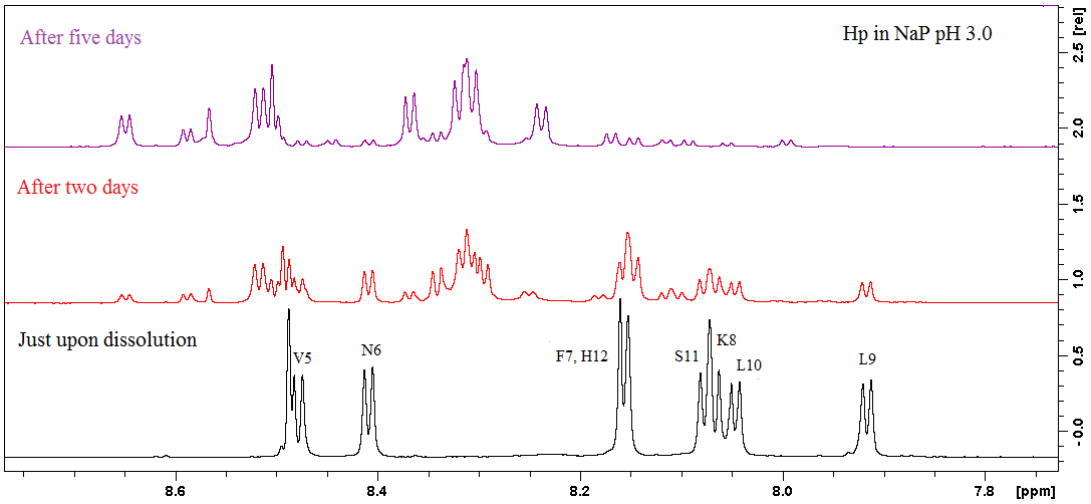

Figure 5.5 *Comparison of the amide region of Hp dissolved in NaP 20 mM pH 3.0 of 1D proton spectra recorded at different time points.*

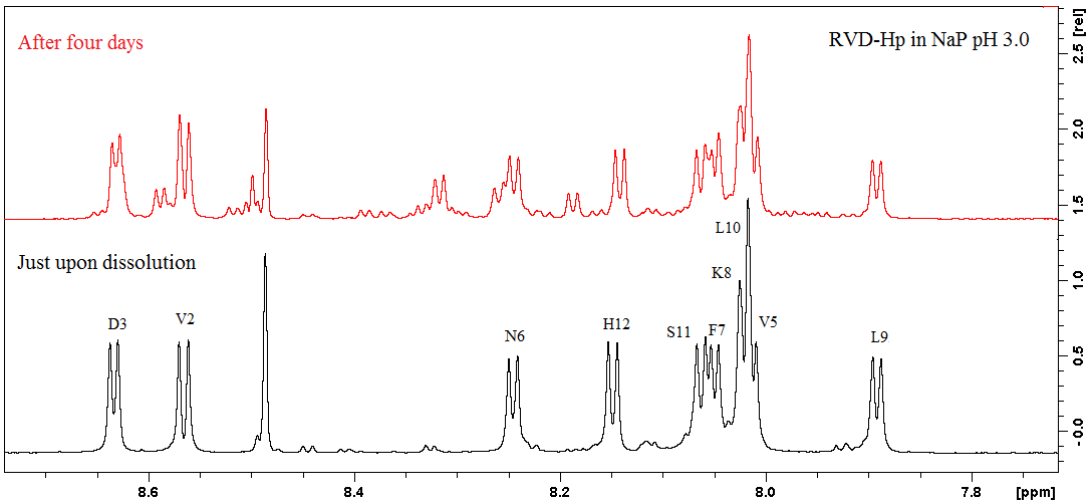

Figure 5.6 *Comparison of the amide region of RVD-Hp dissolved in NaP 20 mM pH 3.0 of 1D proton spectra recorded at different time points.*

A preliminary analysis of these data was performed. In particular, the amide protons peak area drop over time was analysed in detail for both peptides. The trends reported in figure 5.7 and figure 5.8, respectively for Hp and RVD-Hp, show that the C-terminal region peaks drop faster with respect to the N-terminal ones, suggesting that those residues drive the conformational transition for both peptides. Notably, the C-terminal region was found to adopt ordered conformations when the peptide is dissolved in less polar environments (see section 5.3.2).

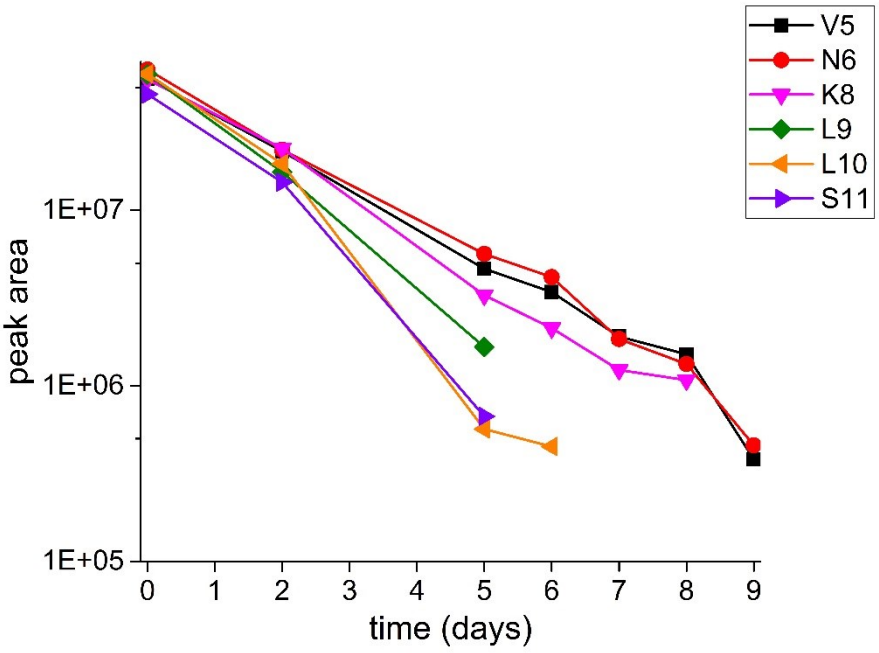

Figure 5.7 *Peak area trends over time of amide proton peaks of Hp dissolved in NaP 20 mM pH 3.0. Only the peaks that could be unambiguously assigned are reported in this graph.*

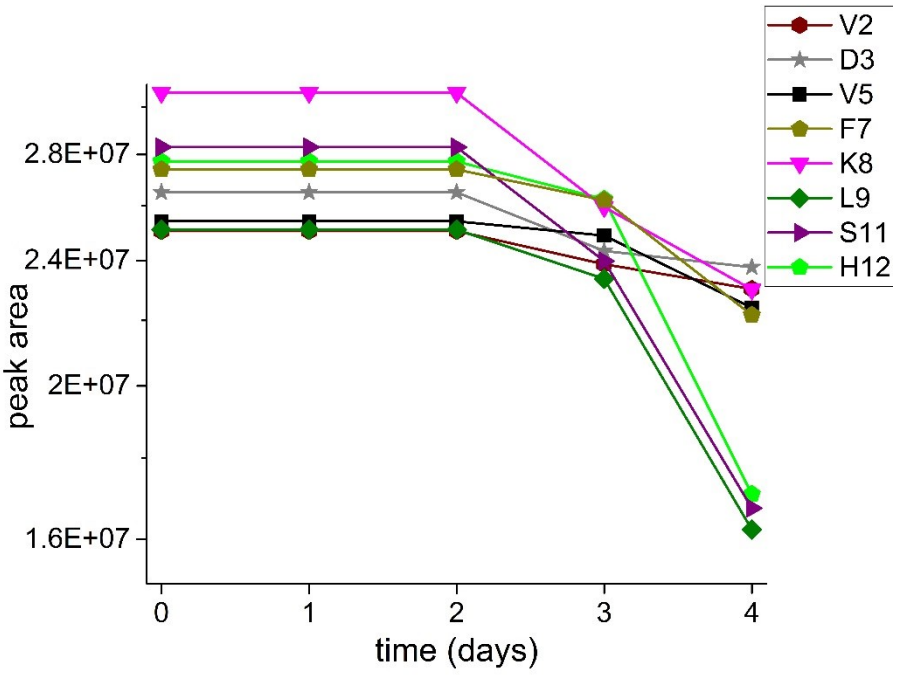

Figure 5.8 *Peak area trends over time of amide proton peaks of RVD-Hp dissolved in NaP 20 mM pH 3.0. Only the peaks that could be unambiguously assigned are reported in this graph.*

5.3.2 Apolar environments

For each condition explored, a similar NMR dataset discussed in section 5.2.2 was recorded (TOCSY, NOESY, ROESY, COSY and ^{13}C-HSQC). Four different conditions were studied: Hp dissolved in either 50/50% v/v HFIP/NaP at pH 3.0 and at pH 7.4; RVD-Hp dissolved in either 50/50% v/v HFIP/NaP at pH 3.0 and at pH 7.4. All protons and carbon atoms (beside carbons involved in CO groups) were assigned with the dataset recorded; the chemical shift tables are reported in Appendix A. Moreover, a peptide structure model was computed for each condition using the NOE restrains obtained. The models were obtained using the ARIA software package, minimised in vacuum; the parameterization of the 50/50% HFIP/Water mixture is

under development. For each condition, the lowest energy structure is reported. The results will be presented separately for each pH condition.

The Hp spectra dissolved at pH 3.0 show a good signal dispersion for NH and α-protons. The bar diagram shows some medium range NOE contacts hinting at a structured region involving the C-terminal residues of the peptide (figure 5.9). The qualitative analysis of the bar diagram, in particular, the low intensity of the αN i,i+1 contacts, the high intensity of the NN i,i+1 and the presence of i,i+3 contacts, points toward the presence of short stretch of a helical/type I β-turn conformation encompassing the residues from 7Phe to 12His.

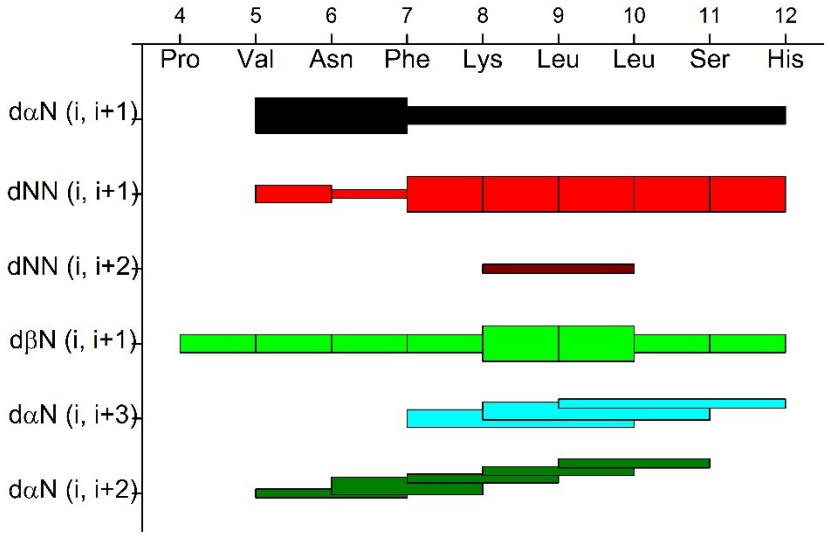

Figure 5.9 *Bar diagram of Hp 500 μM dissolved in HFIP/NaP 20 mM pH 3.0 50/50% v/v; the bar width represent the crosspeak intensity.*

In order to identify a possible structure giving a major contribution to the NOE pattern, the distance restrains were used to generate peptide structure. Even though the final structures bundle is highly variable, as expected on the basis of the short peptide length, the computed structures corroborate the bar diagram analysis, showing a structured α-helical region that resembles an encompassing residues 8Lys to 11Ser; a representative model is shown in figure 5.10.

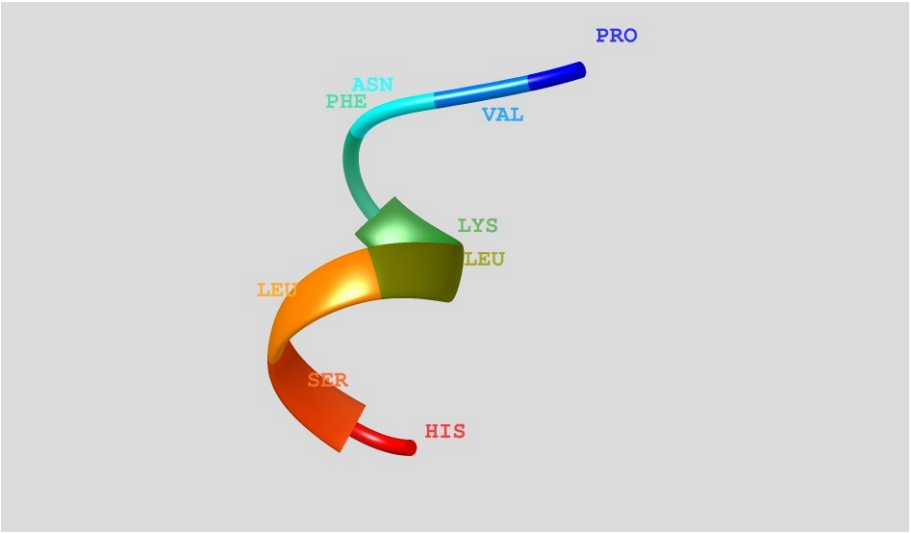

Figure 5.10 *Representative structure model of Hp 500 μM dissolved in HFIP/NaP 20 mM pH 3.0 50/50% v/v.*

In the case of RVD-Hp, at pH 3.0 the 6Asn α-proton is not visible in the TOCSY and NOESY spectra, because it is hidden under the water signal. Moreover, the leucines HN and alpha protons are very close, and for this reason, some sequential NOE contacts cannot be unambiguously assigned (figure 5.11). These missing contacts due to signal overlapping are shown with an empty box. However, more medium-range contacts are present in this condition and the structured region appears to be longer, encompassing residues from 5Val to 12His; also two α-helix diagnostic i,i+4 were detected, encompassing respectively 7Phe to 11Ser and 8Lys to 12His. This data

suggest that the N-terminal extension makes the helix conformation more stable, and slightly longer.

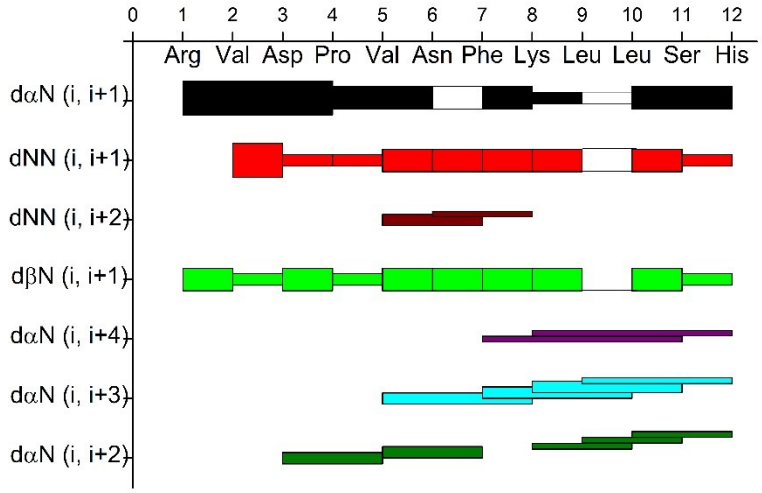

Figure 5.11 *Bar Diagram of RVD-Hp 500 μM dissolved in HFIP/NaP pH 3.0 50/50% v/v.*

The presence of a longer structured region in the peptide core sequence residues is highlighted also by the computed structures, showing an ordered region encompassing residues from 6Asn to 11Ser, as shown by a representative model in figure 5.12.

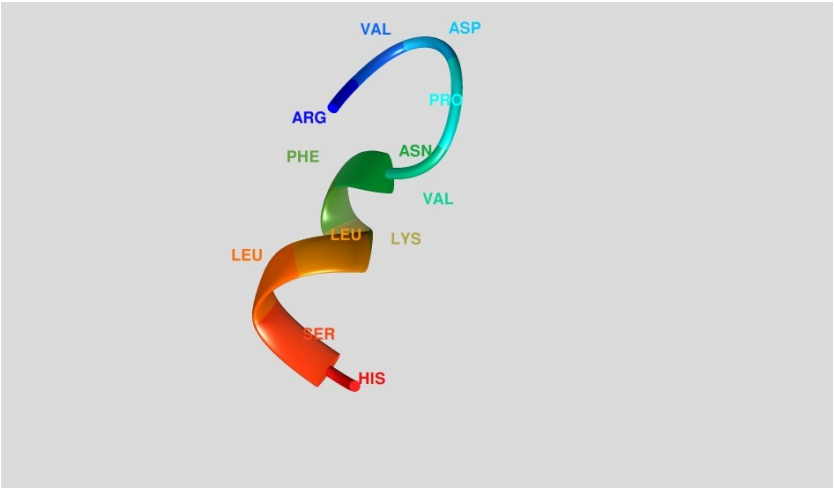

Figure 5.12 *Representative structure model of RVD-Hp 500 μM dissolved in HFIP/NaP 20 mM pH 3.0 50/50% v/v.*

The Hp spectra show good signal dispersion also when dissolved at pH 7.4. However, less NOE contacts, and weaker with respect to the ones measured at pH 3.0 were detected. In particular, diagnostic signals involving 12His disappear, suggesting that the C-terminal end is less structured in this case (figure 5.11). Accordingly, the computed structures suggest the presence of a type I β-turn in this pH condition, involving residues from 7Phe to 10Leu, as shown in figure 5.12.

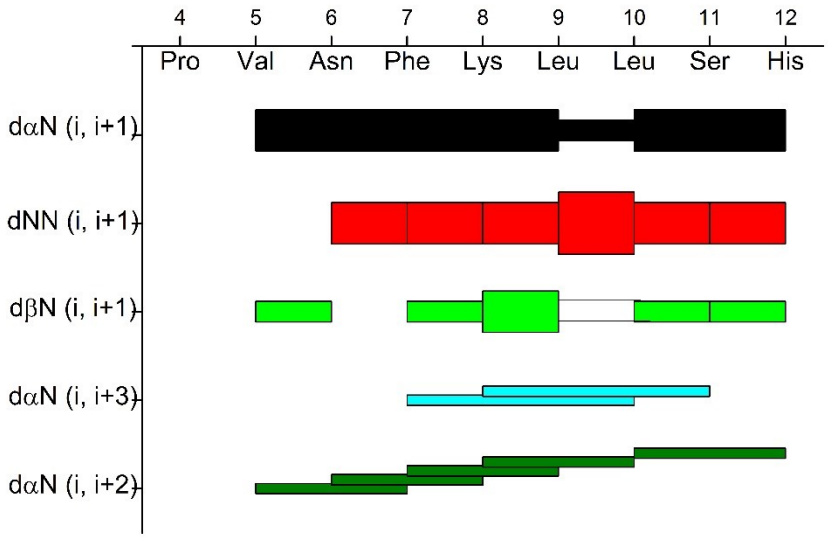

Figure 5.11 *Bar diagram of Hp 500 μM dissolved in HFIP/NaP 20 mM pH 7.4 50/50% v/v.*

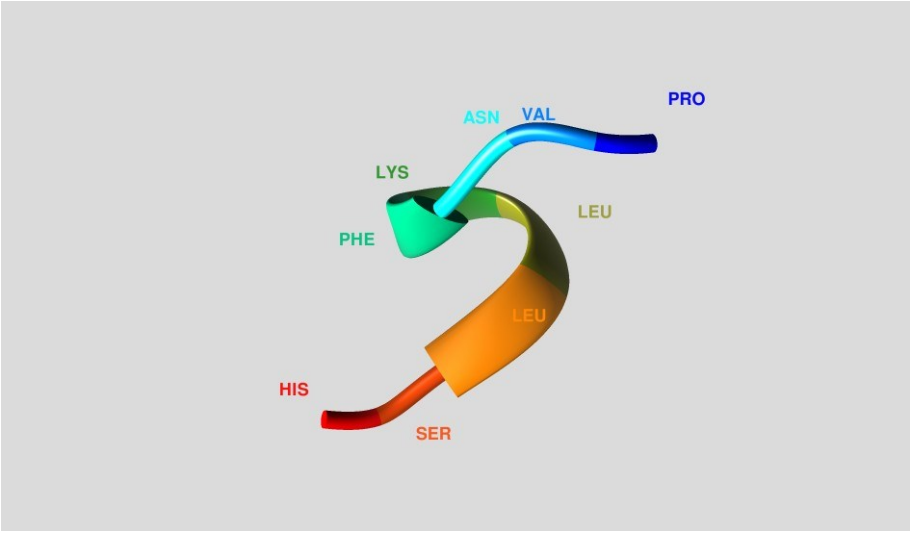

Figure 5.12 *Representative structure model of Hp 500 μM dissolved in HFIP/NaP 20 mM pH 7.4 50/50% v/v.*

In the case of RVD-Hp, at pH 7.4 the HN protons of 6Asn and 7Phe are coincident, as well as and the α-protons of 10Leu and 11Ser. As for the shorter peptide, less medium-range NOE contacts are detected when the peptide is dissolved at neutral pH, indicating a less ordered structure, and the bar diagram appearance points toward the β-turn classification, even though one i,i+3 and one i,i+4 contacts, are still present, as shown in figure 5.13.

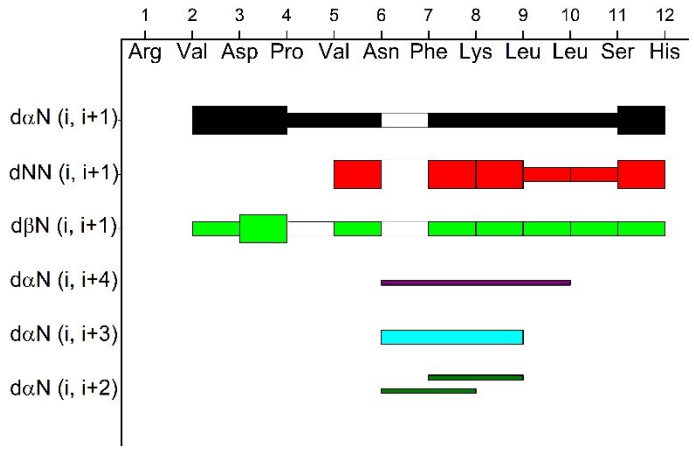

Figure 5.13 *Bar diagram of RVD-Hp 500 μM dissolved in HFIP/NaP 20 mM pH 7.4 50/50% v/v.*

Also in this case the computed structures highlights a shorter structured region at this pH, encompassing residues from 7Phe to 10Leu, as shown by a representative model in figure 5.14.

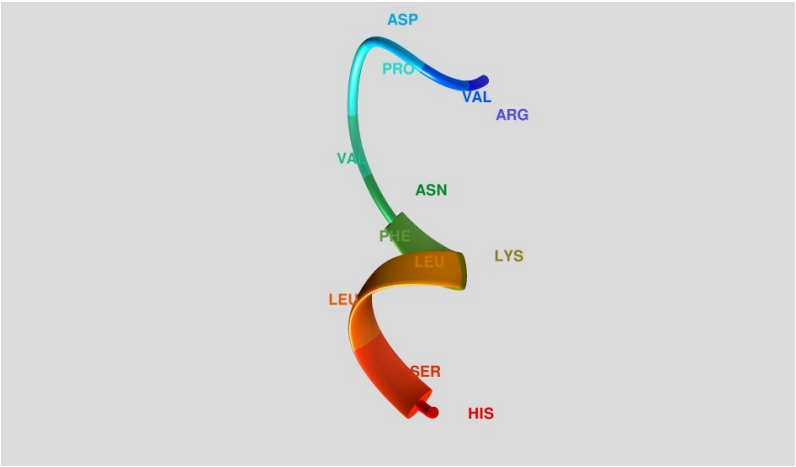

Figure 5.14 *Representative structure model of RVD-Hp 500 μM dissolved in HFIP/NaP 20 mM pH 7.4 50/50% v/v.*

The chemical shift index analysis was performed on the obtained backbone chemical shifts. Unfortunately, there are not reference chemical shift values for random coil conformation in HFIP solution, due to a lack of statistical information in such solutions. Therefore, the results obtained from this analysis are not completely reliable. Still, a comparison of the chemical shift between the two peptides, referred to the same experimental conditions can be used to highlight the main differences explored at local level. To this purpose, the α-proton chemical shifts obtained for the two peptides in the same condition were compared, in order to highlights the differences caused by the N-terminal extension. The secondary shifts of RVD-Hp with respect to Hp are shown in figure 5.15. In both pH conditions, the RVD-Hp shifts are all upfield with respect to Hp, indicating that the longer peptide has a more pronounced tendency to the helical conformation, in agreement with the other results presented in this chapter. Moreover, this kind of analysis shows that at pH 3.0 the peptides conformation are similar, as indicated by the lower values of the difference between the respective secondary shifts; at neutral pH the differences obtained are higher, indicating a more structured conformation for RVD-Hp, even though the high

dynamicity of these peptides hampered the confident identification of these conformational differences at atomic resolution.

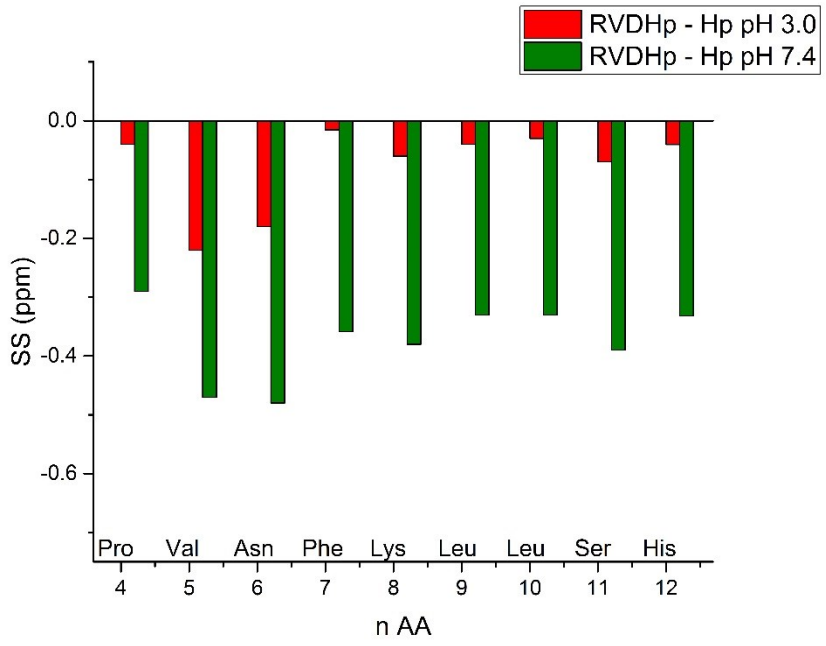

Figure 5.15 *α-proton chemical shifts comparison between RVD-Hp and Hp at the pH conditions studied.*

5.4 Conclusions

In conclusion, a conformational screening of the two hemopressin peptides Hp and RVD-Hp was performed in this thesis, studying the effect of pH and solvent polarity on peptides structure. In aqueous environments, the peptides were found to be unstructured, as expected on the base of their short length, although the recorded CD spectra suggest that the two peptides are able to explore more ordered conformations in this kind of solutions. Interestingly, NMR analysis highlighted that both Hp and RVD-Hp undergo a very slow conformational transition at acidic pH 3.0. More experiments will be performed in this condition to fully characterise this behaviour.

In less polar environments, obtained by different HFIP/NaP buffer mixtures, hemopressin peptides adopt a helical conformation, clearly evidenced by both CD and NMR spectroscopy. The qualitative analysis of the NOE patterns and the structures computed using the obtained distance restrains shown that acidic pH promotes this helical conformation. Moreover, the N-terminal extension present in RVD-Hp was found to stabilise this conformation with respect to Hp at both pHs considered; this could be a possible explanation of the different aggregation properties and biological activity of the two peptides.

5.5 Experimental section

5.5.1 Materials

The hemopressin peptides Hp and RVD-Hp were synthetised by solid phase peptide synthesis by Professor Remo Guerrini of Univerisity of Ferrara. HFIP, both protonated and deuterated, and other laboratory reagents were purchased from Sigma-Aldrich (St. Louis, Missouri, USA).

5.5.2 CD spectroscopy

Stock solution of Hp and RVD-Hp were prepared at 2 mM concentration in HCl 10 mM. The two peptides were diluted in NaP 20 mM buffer solution at pH 3.0 and 7.4 to the final concentration of 20 μM. The same peptides concentration was used for the HFIP titration as well. CD were taken using Jasco J-810 spectropolarimeter (Jasco international Co. Ltd, Tokyo, Japan) in the range of 190–260 nm using a 0.1 cm path length quartz cuvette at 20 °C in continuous scanning mode (20 nm/min, with a 4.0 s response and a 1.0 nm band width). Spectra corresponding only to the solvent was subtracted from the corresponding spectrum. The data were accumulated over 3 runs, the presented data being the average. The results are expressed in term of molar ellipticity [θ], in unit of deg cm^2/mol.

5.5.3 NMR spectroscopy

The two peptides were diluted in NaP 20 mM buffer solution, and in HFIP/NaP 50% v/v, at both pH 3.0 and 7.4 to the final concentration of 500 μM. The NMR spectra were recorded on a Bruker 900 MHz instrument with cryoprobe in collaboration with Dr. Wienk at the Bijvoet Center for Biomolecular Research of the University of Utrecht, wherein a proposal submitted and accepted by the iNEXT platform. For each condition, a dataset comprising several two-dimensional homonuclear correlation spectra and one proton-carbon heteronuclear correlation spectrum were recorded. In details, one TOCSY spectrum (80 ms mixing time), two NOESY spectra (200 and 300 ms mixing time), one ROESY spectrum (100 ms spinlock time) and a ^{13}C-HSQC spectrum were recorded for each sample. The temperature was 298 K for all recorded spectra. The chemical shifts were referenced with respect to the water signal. The spectra were processed using TopSpin software package (Bruker, Billerica, Massachusetts, USA) and NMRPipe software package [195]. The data assignment and analysis were performed using the CCPN software package [196]. The peptides structure models were obtained using the ARIA software package [197].

Chapter 6 – Aggregation propensity study of the sweet protein Y65R-MNEI

6.1 Work outline

In this chapter, the aggregation propensity of Y65R-MNEI was investigated by screening different conditions of temperature, pH and ionic strength. It is known that for the parent proteins, monellin and MNEI [19,160], a first partial denaturation step is needed to trigger the fibrillar aggregation event. Starting from this hypothesis, the stability of Y65R-MNEI in function of temperature was studied by Circular Dichroism spectroscopy. Two different pH were explored: an acidic one (pH 2.5) and a nearly neutral one (pH 6.8). Considering that previous studies have shown that the ion strength is critical for fibril formation [19], two different conditions of ionic strength, 0 and 150 mM of NaCl were explored.

Using the thermal stability data as starting point, different aggregation conditions were evaluated by ThT assay for both pH studied, and the aggregation kinetics were compared. The end-point of the aggregation process was investigated by Atomic Force Microscopy (AFM), in order to study the different aggregate morphologies obtained in each condition.

6.2 Thermal stability

The far-UV CD spectra of Y65R-MNEI, recorded in 20 mM sodium phosphate buffer at pH 2.5 and 6.8, in the presence and in the absence of 150 mM NaCl, are reported in Figure 6.1. In agreement with previous data [198], the CD spectra indicate that the protein is well folded and it presents the typical features of a protein with a high content of β-sheets and a low content of α-helices, as expected on the high similarity with the structure of MNEI determined by NMR [199], and X-ray crystallography [200]. The presence of NaCl does not affect the secondary structure content of the protein. Interestingly, the CD signal is lower at acidic pH.

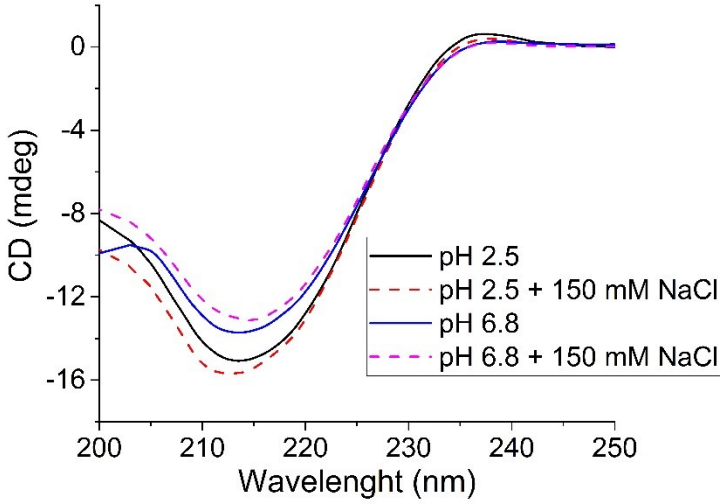

Figure 6.1 *Comparison of CD spectra of Y65R-MNEI in 20 mM NaP at two different pHs and ionic strengths. Protein concentration was 0.2 mg/ml and the temperature 20 °C for all spectra.*

The thermal stability of Y65R-MNEI was investigated by measuring the CD thermal denaturation profiles in the different pH and ionic strength conditions explored, reported in Figure 6.2. Data obtained indicate that the protein is more stable at neutral pH, showing a higher melting temperature (Tm); moreover, NaCl influences the Tm of Y65R-MNEI only at pH 2.5. Indeed, at acidic pH, the presence of the salt leads to a protein stabilization of about 4°C, while no effect is observed at neutral pH. The measured Tm were: 66 ± 1 and 69 ± 1 °C at acidic pH respectively in absence and in presence of NaCl; 71 ± 1 °C at neutral pH, with no influence of ionic strength.

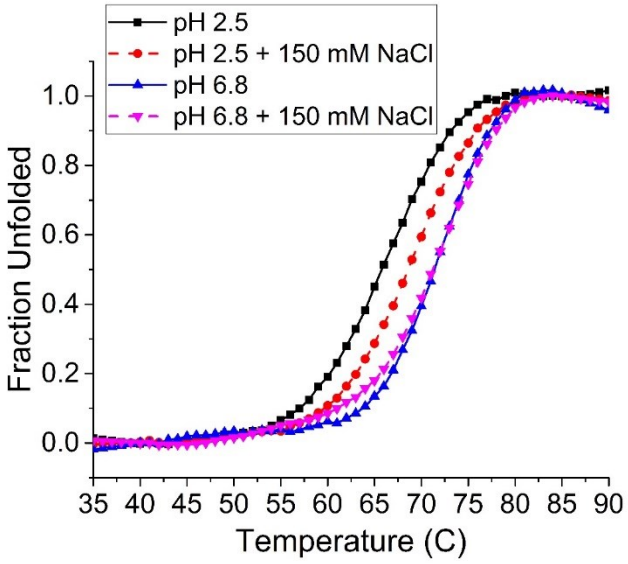

Figure 6.2 *Thermal denaturation profiles of Y65R-MNEI in 20 mM NaP at two different pHs and ionic strengths, as followed by CD spectroscopy signal at 215 nm; the heating rate was 1 °C/min, protein concentration 0.2 mg/ml.*

6.3 Thioflavin T assays

Thermal denaturation data provide a rational basis to select incubation temperatures suitable to prompt protein aggregation, since partial protein unfolding represents a preliminary step in the formation of amyloid-like protein fibrils [201]. Based on the results of the CD thermal denaturation profiles, two different temperatures were selected: 70°C, which corresponds to the Tm of Y65R-MNEI at pH 2.5 with 150 mM NaCl and at pH 6.8; 75 °C, which is a temperature higher than Tm in all conditions explored. Moreover, the latter temperature corresponds to the almost complete denaturation of the protein at pH 2.5 without any salt, i.e. to the state of the parent protein MNEI in the reference experiments [160]. A preliminary investigation of the aggregation process was performed by ThT fluorescence assay at the two selected temperatures, using a protein sample dissolved at 3 mg/ml in 20 mM sodium phosphate at pH 2.5 and pH 6.8, with and without 150 mM NaCl. The time course of the aggregation reaction has been followed for one week, i.e. until a clear ThT

fluorescence intensity plateau was detected. ThT fluorescence intensities in function of time are reported in figure 6.3. Some differences in the kinetics of ThT binding are revealed by these experiments:

- The pH strongly influence ThT behaviour. At neutral pH, the fluorescence reaches a plateau very quickly, i.e. within 24 hours of incubation, and the measured intensity is definitely lower with respect to acidic pH, for both studied temperature. Moreover, these samples show visible aggregates since the first day of incubation.

- At both temperatures studied, only at pH 2.5 without NaCl the curves show a kind of sigmoidal lineshape, formed by a lag, elongation and plateau phase, as expected for amyloid fibrils formation by a nucleation dependent mechanism [202]. Moreover, raising the temperature from 70 to 75 °C decrease the length of the lag phase (from about one day to about 6 hours), speeding up the aggregation process.

- The ion strength has no effect on the neutral pH kinetic, as for the thermal stability. On the other hand, it has a huge effect at acidic pH. At both temperature studied, no lag phase is detected when NaCl is present in the samples. Moreover, this condition shows the highest fluorescence intensity end-point at both temperature.

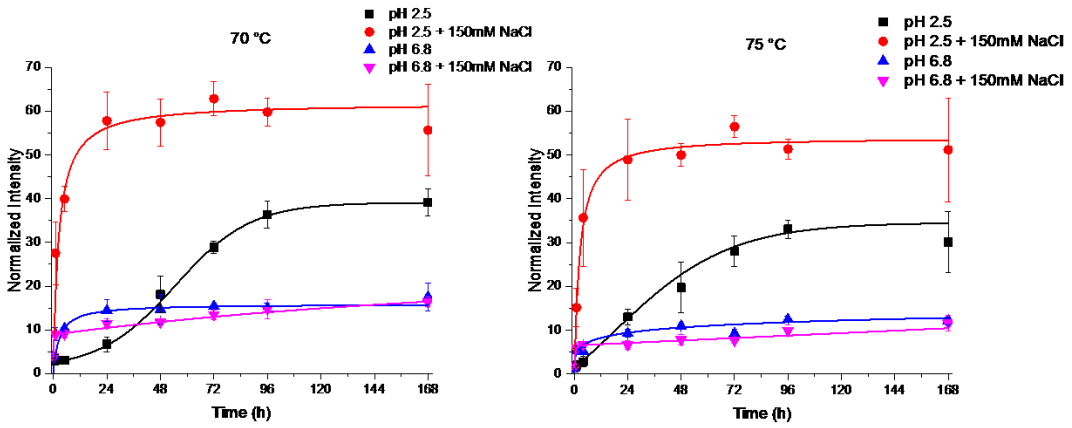

Figure 6.3 *ThT binding assay of Y65R-MNEI. Fluorescence values were recorded at 485 nm at the time indicated upon incubation of the protein at 70 °C (left panel) and 75 °C (right panel) for one week.*

6.4 Atomic Force Microscopy

In order to reveal the nature of the aggregates that are formed at 70 and 75°C, the protein samples after 1 week of incubation for each condition studied (different temperatures, pHs and ionic strength) have been analysed by atomic force microscopy (AFM). Protein samples were also investigated before starting the incubation at high temperature, and no aggregates were detected (data not shown). Coexistence of fibril morphology and amorphous aggregates was detected in only two conditions: at pH 2.5, without NaCl, both at 70 and 75 °C. On the other hand, only amorphous aggregates were detected in all the other conditions explored.

The fibrils width and height were analysed in details; AFM images of Y65R-MNEI fibrils and the height profiles obtained are reported in figure 6.5. The fibrils obtained in the two conditions show a similar width around 50 nm, but different heights: fibrils formed at lower temperature (70 °C) are higher with respect to the ones formed at 75 °C. The height ranges are respectively between 4-8 nm for the former and of about 3 nm for the latter. Considering the amyloid fibril models already published, the aggregates dimensions observed are in good agreement with fibrils formed by other

proteins. The detected fibril morphologies could be related respectively to protofibril and protofilament stages, even if fibrils dimension can differ widely investigating different proteins [203].

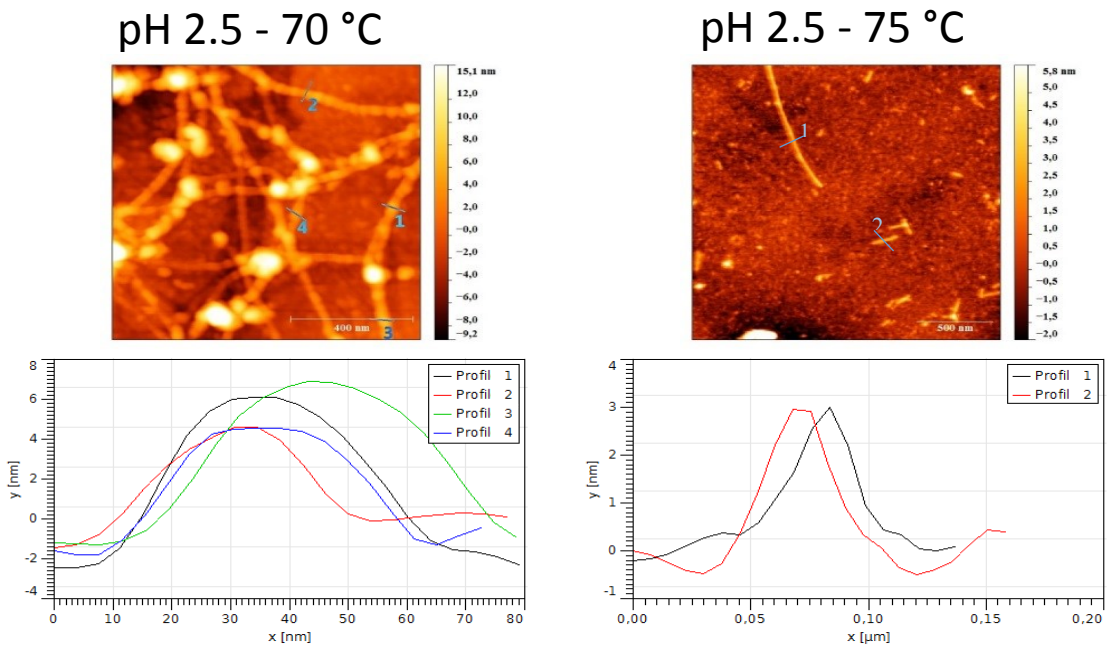

Figure 6.5 *AFM images and height profiles of fibrils formed by Y65R-MNEI at acidic pH at 70 °C (left panel) and 75 °C (right panel). The segments from which the profiles were extracted are highlighted in the figures.*

AFM data actually show amorphous aggregates also at acidic pH in presence of NaCl, at both temperature; the ThT assay performed on these samples showed the highest fluorescence intensity. A possible explanation for these false positives could be found considering that also the Y65R-MNEI native structure is rich in β-sheet [200], thus is possible that these kind of aggregates are characterized by a β-sheet based quartenary structure, to which ThT binds. On the other hand, the kinetic of ThT binding, shown in figure 6.3, revealed to be diagnostic of fibrils formation. Indeed, only in the conditions that shown a sigmoidal lineshape, fibril morphologies was detected. This

kind of kinetics indicates a nucleation dependent mechanism for the aggregation, which is by now the most accepted kinetics model for amyloid fibril formation [202].

6.5 Conclusions

In conclusion, the aggregation propensity of Y65R-MNEI in different conditions of pH, temperature and ionic strength were investigated, identifying for the first time two conditions in which the sweet protein forms aggregate with fibril morphology. The first one is 20 mM NaP pH 2.5, no NaCl at 70 °C; the second one is 20 mM NaP pH 2.5, no NaCl at 75 °C. These fibrils aggregates enhance ThT fluorescence, with a sigmoidal kinetics lineshape compatible with a nucleation dependent mechanism, and the aggregates dimensions compatible with that of amyloid fibrils. Even if a first thermal denaturation step is needed to trigger Y65R-MNEI aggregation, the temperature was not a critical parameter for fibrils formation. Instead, pH had a dramatic influence on Y65R-MNEI aggregation behaviour. At acidic pH, Y65R-MNEI forms aggregated rich in β-sheet, as detected by ThT assays, showing fibrillar morphology at low ionic strength (0 mM NaCl) and amorphous morphology at high ionic strength (150 mM NaCl). The faster aggregation kinetics (with no lag phase) in presence of salt could promote the formation of off-pathway aggregates, still detected by ThT due to the high β-sheet content. At neutral pH, although the protein undergoes aggregation, visible also by eye, these species do not show the typical amyloid properties as evidenced by ThT fluorescence and AFM analysis.

6.6 Experimental Section

6.6.1 Materials

Recombinant Y65R-MNEI was expressed in *E.Coli* as described elsewhere [159]. AFM accessories (sample supports, mica sheets, AFM tips) were purchased from Bruker (Billerica, Massachusetts, USA). ThioflavinT and other laboratory reagents were purchased from Sigma-Aldrich (St. Louis, Missouri, USA).

6.6.2 Circular Dichroism

Circular dichroism (CD) measurements have been performed on a Jasco J815 spectropolarimeter (Jasco, Essex, UK), equipped with a temperature control system, using a 1-mm quartz cell in the far-UV range 200–250 nm (20 nm/min scan speed). Raw spectra have been corrected for buffer contribution. The thermal denaturation curves have been obtained at different pH and ionic strength conditions: 20 mM NaP pH 2.5; 20 mM NaP pH 2.5 with 150 mM NaCl; 20 mM NaP pH 6.8; 20 mM NaP pH 6.8 with 150 mM NaCl. The CD signal at 215 nm (β-sheet minimum) was followed in the thermal denaturation experiments, with a heating speed of 1 °C/min, from 35 to 90 °C. The data were converted into protein unfolded fraction as reported in literature [204]. In all experiments, protein concentration was 0.2 mg/ml.

6.6.3 ThioflavinT assay

The protein (3 mg/ml) were incubated at 70 and 75°C in 20 mM phosphate buffer at pH 2.5 and 6.8 in absence and in presence of 150 mM of NaCl. At each aggregation kinetics time point, a sample aliquot of 15 µl was withdrawn and diluted to 10 µM in 20 mM NaP pH 6.8 containing 30 µM of ThT just before the spectral acquisition. Fluorescence emission spectra were acquired on a HORIBA Fluoromax-4 in the range 460–600 nm with scan speed of 100 nm/min, upon excitation at 440 nm. Excitation and emission slits were both set at 5 nm. Fluorescence intensity values at 485 nm were normalized with respect to the values obtained for a 30 µM ThT sample recorded in the same day, and plotted as a function of time. The reported values represent the means from three independent experiments.

6.6.4 Atomic Force Microscopy

The protein (3 mg/ml) was incubated at 70 and 75°C in 20 mM phosphate buffer at pH 2.5 and 6.8 in absence and in presence of 150 mM of NaCl. Just before and after one week of incubation, a sample aliquot was withdrawn and diluted 100-fold (0.03

mg/ml) in ultrapure water, deposited on a clean mica sheet and gently dried. The mica was then washed with ultrapure water to remove any deposited salt (phosphate or NaCl) and gently dried again. AFM measurements were carried out in collaboration with the research group of Prof. Claudio De Rosa and Dr. Rocco Di Girolamo of University of Naples "Federico II", on a Bruker Multimode 8, in tapping mode, using a silicon cantilevers TESP-MT, tip with radius of about 8 nm, at resonance frequency and force constant of about 250 kHz and 50 N/m, respectively. Images were taken in air under ambient conditions at a scan frequency of 1 Hz. Scans size were varied from 2 x 2 μm to 0.5 x 0.5 μm, depending on sample homogeneity.

Final Remarks

Amyloid fibrils are involved in a wide range of cellular processes, both functional and pathological. Several human diseases are related to the formation of amyloid aggregates, including very severe neurodegenerative diseases, such as Alzheimer disease. The exact processes that lead to the polymerization of such different polypeptides and also their relationship with the toxicity mechanisms are poorly understood. A better understanding of the amyloid aggregation process would be very helpful for the identification of the key therapeutic targets of amyloidosis.

To provide structural and biophysical insights on the molecular mechanism of amyloid aggregation, in this thesis, different hallmarks that affects the polypeptide aggregation process were studied, using an integrated biophysical approach. Three different molecular models were chosen for these studies. All of them are able to form amyloid fibrillar aggregates, and they were studied at different levels of deepness in literature, with a wide range of biophysical techniques. The first model is represented by amyloid beta peptides, Abeta40 and Abeta42, which are related to AD. From the discovery of their relation with AD, the structures and the aggregation properties of these peptides were extensively studied in literature; however, Abeta peptides properties are strictly related to the surrounding environment. Therefore, the effect of interaction with membranes model systems and of glycation, a non-enzymatic post-translational modification occurring in vivo, on Abeta peptides structure and aggregation properties were analysed in this work.

The oligomeric state of Abeta42 interacting with lipids depends dramatically on bilayer composition: simple liposomes formed by POPC were found to stabilise soluble Abeta42 oligomers, while a bilayer mimicking neuronal membranes lipid composition is not able to solubilise the peptide, likely promoting the formation of insoluble aggregates. Interestingly, the presence of Omega3 lipids in the biomimetic

bilayer promotes the formation of Abeta oligomers, which were deeply inserted in the liposomes.

The glycation reaction with MGO was found to hinder the aggregation of Abeta40 and Abeta42 peptides, even though with different degrees. Upon addition of the glycating agent, Abeta40 showed a faster reaction kinetics, and the modification induced by this reaction inhibits peptide ability to assume a β-sheet conformation. On the other hand, Abeta42 showed a slower kinetics, and is still able to undergo the conformational transition to β-sheet also upon modification, although the aggregation propensity of the glycated peptide was found lower with respect to the unmodified Abeta42. The reaction was studied also in HFIP/phosphate buffer mixture; this kind of solution stabilises soluble Abeta peptides in α-helix conformation, avoiding any aggregation event. Abeta peptides appears to be glycated also in this condition, but the presence of HFIP promotes MGO side reactions that likely interfere with AGEs formation. More work is needed to characterise and set up the glycation reaction in this solution.

The second model is represented by hemopressin peptides, two short molecules deriving from hemoglobin, whose sequence differs only for a RVD N-terminal extension in the longer peptide, showing completely different aggregation properties. The ability of hemopressin to form amyloid aggregates was characterized only very recently, and in literature only a few information are available about the biophysical properties of these peptides.

The effect of different pH and solvent polarity conditions were analysed in this thesis on both hemopressin peptides, Hp and the N-terminal extended RVD-Hp. In aqueous environments, these peptides are mainly unstructured, even though the CD spectra suggest the presence of some ordered conformations. Surprisingly, when dissolved at acidic pH, both peptides undergo a slow conformational transition detectable by NMR, which is still under investigation. In less polar environments, mimicked by

HFIP/phosphate buffer mixtures, the peptides assume more ordered conformations, as resulted by both CD and NMR analysis. The three extra residues present in RVD-Hp sequence stabilise more ordered conformations, even though in all explored conditions the two peptides show a high conformational dynamicity.

The third model is an engineered sweet protein, called Y65R-MNEI, derived for the plant protein monellin. The parent proteins monellin and MNEI were known to form amyloid fibrils upon thermal unfolding but no information was available on the amyloid aggregation of Y65R-MNEI.

In this thesis, a preliminary study of Y65R-MNEI aggregation properties in function of pH, temperature and ionic strength was performed, to identify how these crucial factors modulate the protein aggregation. Experimental data indicate that the crucial parameters affecting the aggregation mechanism is pH. Indeed, pH dramatically change Y65R-MNEI aggregation properties, as an acidic pH promotes the formation of amyloid fibrils, while neutral pH promotes the formation of amorphous, off-pathway aggregates.

In conclusion, the choice of these molecular models to investigate amyloid aggregation allowed the study of this process from different points of view, using several biophysical techniques. This thesis can represent a little step towards the elucidation of this process, whose relevance is more and more evident in biological and biotechnological processes.

Appendix A – Hemopressin peptides chemical shifts tables

A-I Hp in NaP pH 3.0

Residue	NH	αH	βH	δH	εH	γH	zH	αC	βC	δC	εC	γC
4-Pro		4.34	2.37, 1.93	3.31		1.97, 1.91		62.21	32.60	49.38		26.42
5-Val	8.48	3.96	1.85		0.80, 0.71			62.61	32.73			20.44, 20.97
6-Asn	8.41	4.61	2.71, 2.63	7.52					38.76			
7-Phe	8.15	4.44	2.94, 3.04	7.38	7.27		7.23	58.26	39.53			
8-Lys	8.06	4.13	1.67, 1.62	1.57	2.89	1.26		56.44	32.90	29.04	42.04	24.73
9-Leu	7.91	4.22	1.52	0.86, 0.80		1.51		55.08	42.24	24.79, 23.52		26.94
10-Leu	8.04	4.30	1.49, 1.57	0.83, 0.77		1.54		54.94	42.32	24.96, 23.30		26.84
11-Ser	8.07	4.32	3.75					58.19	63.87			
12-His	8.15	4.52	3.21, 3.07	8.49	7.19			55.89	29.46			

A-II Hp in NaP pH 7.4

Residue	NH	αH	βH	δH	εH	γH	zH	αC	βC	δC	εC	γC
4-Pro		4.31	2.35, 1.91	3.28		1.89, 1.95		62.19	32.64	49.37		26.49
5-Val	8.40	3.96	1.86		0.80, 0.71			62.55	32.71			20.43, 20.98
6-Asn			2.71, 2.62						38.82			
7-Phe	8.18	4.46	2.92, 3.03					58.01	39.55			
8-Lys	8.04	4.14	1.67, 1.60	1.56	2.88	1.24		56.29	33.0	29.05	42.05	24.70
9-Leu	7.96	4.21	1.51	0.85, 0.79		1.49		55.13	42.27	24.80, 23.55		26.99
10-Leu	8.06	4.30	1.47, 1.56	0.83, 0.77		1.53		54.85	42.42	24.93, 23.32		26.88
11-Ser		4.32	3.73					58.05	63.91			
12-His	7.83	4.36	3.09, 2.95					57.31	30.86			

A-III RVD-Hp in NaP pH 3.0

Residue	NH	αH	βH	δH	εH	γH	zH	αC	βC	δC	εC	γC
1-Arg		3.99	1.83	3.13	7.15	1.52		55.36	30.84	43.20		26.11
2-Val	8.56	4.06	1.93			0.82, 0.84		62.15	32.76			20.45
3-Asp	8.63	4.85	2.59, 2.79					51.36	38.59			
4-Pro		4.32	2.17, 1.84	3.75		1.92		63.16	32.09	50.70		27.22
5-Val	8.02	3.88	1.87		0.72			62.66	32.57			
6-Asn	8.24	4.60	2.71, 2.60	6.81, 7.52				52.73	38.67			
7-Phe	8.05	4.41	2.96, 3.04	7.15	7.27		7.22	58.43	39.39			
8-Lys	8.01	4.12	1.67, 1.61	1.56	2.89	1.25		56.47	32.02	29.02	42.05	24.74
9-Leu	7.89	4.20	1.51	0.86, 0.79		1.52		55.09	42.21	24.77, 23.52		26.87
10-Leu	8.02	4.29	1.48, 1.55	0.83, 0.77		1.50		54.91	42.35	24.93, 23.28		26.93
11-Ser	8.06	4.31	3.74					58.25	63.85			
12-His	8.15	4.51	3.07, 3.21	7.18	8.48			55.88	29.43			

A-IV RVD-Hp in NaP pH 7.4

Residue	NH	αH	βH	δH	εH	γH	zH	αC	βC	δC	εC	γC
1-Arg		3.80	1.74	3.11		1.49		55.76	31.93	43.28		26.36
2-Val		4.11	1.93			0.82, 0.83		61.81	32.90			20.40, 20.98
3-Asp	8.47	4.79	2.40, 2.63					63.23	41.13			
4-Pro		4.29	2.19, 1.85	3.65		1.93		63.23	32.13	50.69		27.23
5-Val	8.11	3.87	1.91		0.74, 0.84			62.99	32.38			20.91, 20.96
6-Asn	8.19	4.59	2.70, 2.62	6.81, 7.56				52.97	38.76			
7-Phe	7.99	4.42	2.98, 3.04	7.14	7.23		7.26	58.31	39.25			
8-Lys	7.96	4.14	1.68, 1.61	1.57	2.88	1.26		56.32	32.95	29.03	42.07	24.72
9-Leu	7.93	4.21	1.51	0.86, 0.80		1.52		55.09	42.23	24.77, 23.55		26.89
10-Leu	8.03	4.30	1.47, 1.56	0.83, 0.77		1.50		54.93	42.41	24.98, 23.28		26.97
11-Ser	8.07	4.31	3.74					58.17	63.90			
12-His	7.84	4.36	3.10, 2.97	6.99	8.03			57.42	30.72			

A-V Hp in HFIP/NaP 50/50 % v/v pH 3.0

Residue	NH	αH	βH	δH	εH	γH	zH	αC	βC	δC	εC	γC
4-Pro		4.58	2.23, 2.27	3.59		2.70		62.57	26.44	49.70		32.59
5-Val	8.07	4.20	2.07			0.92, 1.06		63.03	33.41			20.40, 19.98
6-Asn	7.80	4.89	2.88, 3.20	6.39, 7.22				52.59	38.06			
7-Phe	7.95	4.53	3.39, 3.21	7.41				60.57	39.21	51.18		
8-Lys	8.16	4.29	1.67, 2.09	1.92	3.20	1.64, 1.69		58.91	31.99	29.02	42.31	25.06
9-Leu	7.63	4.40	1.87	1.08, 1.14		1.81		57.12	42.28	22.31, 24.03		27.32
10-Leu	7.70	4.45	1.94	1.08, 1.10		1.87		56.57	42.50	22.72, 24.45		27.15
11-Ser	7.87	4.55	4.03, 4.16					58.91	64.14			
12-His	8.08	4.81	3.48, 3.59	7.50				55.98	28.75	51.62		

A-VI Hp in HFIP/NaP 50/50 % v/v pH 7.4

Residue	NH	αH	βH	δH	εH	γH	zH	αC	βC	δC	εC	γC
4-Pro		4.47	2.16, 2.21	3.07, 3.51		2.64		62.53	26.65	49.59		32.71
5-Val		4.16	2.07			0.92, 1.04		63.09	33.22			20.37, 19.98
6-Asn	7.88	4.83	3.11, 2.84	6.37, 7.17				52.91	38.05			
7-Phe	7.87	4.54	3.19, 3.38	7.52	7.39			60.15	39.11	69.67	69.59	
8-Lys	8.10	4.32	2.05, 1.79	1.64, 1.90	3.17	1.64		58.33	32.06	28.93	42.31	24.90
9-Leu	7.63	4.38	1.79	1.05, 1.12		1.99		56.84	42.28	22.42, 24.20		27.32
10-Leu	7.58	4.49	1.93	1.05, 1.09		1.87		56.06	42.38	22.22, 24.50		24.50
11-Ser	7.83	4.55	4.02, 4.12					58.68	64.20			
12-His	7.94	4.64	3.49, 3.59	7.50	7.50			57.67	29.70			

A-VII RVD-Hp HFIP/NaP 50/50 % v/v pH 3.0

Residue	NH	αH	βH	δH	εH	γH	zH	αC	βC	δC	εC	γC
1-Arg		4.30	2.18	3.44	7.43	1.88, 1.91		55.76	31.15	43.27		26.31
2-Val	8.42	4.36	2.25			1.13, 1.17		62.88	33.05			20.61, 20.31
3-Asp	8.49	5.25	3.03, 3.15					51.19	39.16			
4-Pro		4.54	2.52	4.02		2.20, 2.27		64.90	31.96	50.84		27.07
5-Val	7.61	3.99	2.21			1.05, 1.15		64.94	32.05			20.43, 20.31
6-Asn	7.90	4.72	2.95, 3.00	6.73, 7.23				54.94	38.23			
7-Phe	8.05	4.52	3.30, 3.36	7.37			7.26	60.86	39.05			
8-Lys	8.21	4.23	2.17	1.92	3.19	1.71		58.91	31.93	28.90	42.31	24.82
9-Leu	7.95	4.37	1.82, 1.99	1.06, 1.16				57.64	42.22	22.37, 24.17		
10-Leu	7.94	4.42	1.80, 1.95	1.07, 1.09				56.77	42.45	22.19, 24.38		
11-Ser	7.87	4.48	3.89, 4.10					58.99	64.03			
12-His	8.02	4.77	3.48, 3.58	7.41	7.47			56.01	28.61		51.32	

A-VIII RVD-Hp HFIP/NaP 50/50 % v/v pH 7.4

Residue	NH	αH	βH	δH	εH	γH	zH	αC	βC	δC	εC	γC
1-Arg		3.65	1.69, 1.74	3.19	7.19	1.52, 1.91		55.99	32.42	43.05		26.26
2-Val		4.08	1.90			0.81, 0.84		62.19	32.75			20.33, 19.80
3-Asp	8.07	4.84	2.60, 2.67					52.11	41.41			
4-Pro		4.18	2.23	3.70		1.86, 2.27		60.61	31.70	50.54		26.86
5-Val	7.68	3.69	1.99			0.78, 0.85		65.18	31.74			20.06, 20.92
6-Asn	7.94	4.36	2.65, 2.67	6.41, 7.08				54.80	37.99			
7-Phe	7.94	4.18	3.03, 3.05	7.06			7.26	64.84	38.75	50.85		
8-Lys	7.78	3.95	1.88	1.63	2.89	1.42		58.32	31.69	28.51	42.04	24.40
9-Leu	7.72	4.06	1.49, 1.72	0.76		1.63		57.23	41.92	21.91		26.81
10-Leu	7.59	4.16	1.47, 1.63	0.76, 0.77				56.04	42.26	23.93, 24.22		
11-Ser	7.51	4.17	3.57, 3.74					58.65	63.74			
12-His	7.54	4.30	3.09, 3.19	7.41	7.10			57.44	29.21	50.88	49.59	

Appendix B – PhD Course Activity Summary

Candidate: Alessandro Emendato **Supervisor: Prof. Delia Picone**

1) **Attended Courses:**

- **Corso avanzato di spettrometria di massa**, Lecturer: Prof. Piero Pucci, from 30th June to 4th July 2014.
- **Analisi strutturale di materiali su scala nanometrica tramite diffusione di raggi X a basso angolo,** Lecturer: Prof. Finizia Auriemma, from 4th to 18th September 2015.
- **Applications of neutron scattering techniques in soft matter and bio-relevant systems. How to study their structure and dynamics,** Lecturer: Dott. Yuri Gerelli, from 9th to 13th November 2015.
- **Studi NMR di sistemi paramagnetici e di interazioni bio-macromolecolari allo stato solido,** Lecturer Dott. Guido Pintacuda, from 22nd to 24th February 2016.
- **Le tecniche di estrazione solido-liquido impiegate nella preparazione del campione per l'analisi chimica e nella produzione di estratti per usi industriali,** Lecturer: Prof. Daniele Naviglio, from 29th February to 3rd March 2016.
- **Chimica fisica degli acidi nucleici,** Lecturer: Prof. Luigi Petraccone, from 11th to 14th July 2016.

2) Attended Seminars:

Title	Speaker	Date	Place
Incontro con la Peroni: azienda alimentare leader nel settore birraio	Luigi Serino	12/05/2014	Monte Sant'Angelo, Naples
DNA aptamers as new type of drugs	Vera A. Spiridova	22/05/2014	Monte Sant'Angelo, Naples
Protein symmetrisation as a novel tool in structural biology	Francesca Coscia	28/05/2014	Monte Sant'Angelo, Naples
Impact factors, citations, journal reputation, editorial policies	Thierry Tron, Danilo Porro	26/06/2014	Monte Sant'Angelo, Naples
Material design of transition metal oxide alloys	Mayal Caspary Toroker	08/07/2014	Monte Sant'Angelo, Naples
NMR study of bioactive protein conformation	Giuseppe Nicastro	20/11/2014	National Institute for Medical Research, London
The conformation of enkephalin bound to its receptor: an "elusive goal" beyond reality	Domenico Sanfelice	03/12/2014	National Institute for Medical Research, London
Iron sulfor cluster protein: ISCA	Matija Popovic	12/02/2015	National Institute for Medical Research, London
Mechanistic and structural aspects of M. tb alanine racemase inhibition by D-cycloserine	Cesira De Chiara	12/03/2015	National Institute for Medical Research, London
Structural architecture of Trim32: a member of the tripartite motif E3-ligases family	Diego Esposito	12/03/2015	National Institute for Medical Research, London
A new cellular model to follow Friedreich's ataxia development in a time-resolved way	Tommaso Vannocci	30/04/2015	National Institute for Medical Research, London

Microscopia a forza atomica – applicazioni biologiche	Alex Winkel, Benjamin L. Holmes	19/11/2015	Monte Sant'Angelo, Naples
Computational Chemistry beyond molecules	Alessio Petrone	07/01/2016	Monte Sant'Angelo, Naples
Biopesticides which target voltage-gates ion channels: efficacy and biosafety	Angharad M.R. Gatehouse	14/01/2016	Monte Sant'Angelo, Naples
Functionalized and artificial enzymes: new bioderived catalysts	Thierry Tron	14/01/2016	Monte Sant'Angelo, Naples
Multimodal approaches for preclinical molecular imaging	Luca Menichetti, Mario Chiariello	02/02/2016	Monte Sant'Angelo, Naples
Probing molecular and supramolecular chirality by chiroptical response of porphyrins and metalloporphyrins	Nina Berova	13/09/2016	Monte Sant'Angelo, Naples
Biomolecular interaction analytics using microscale thermophoresis	Francesca Viganò	26/10/2016	Monte Sant'Angelo, Naples
Modified nucleosides and oligonucleotides for biomedical applications	Daniela Montesarchio	18/01/2017	Monte Sant'Angelo, Naples

3) Attended Integration Exams (for candidates not graduated in Chemical Science):

Title	Professor	Date

4) Visiting periods in Institutions different from University of Naples "Federico II":

Host Institution	Country	Start Date	End Date
National Institute for Medical Research	London, England	15th September 2014	31st August 2015

5) Publications (include submitted and in preparation):

- Alessandro Emendato, Roberta Spadaccini, Augusta De Santis, Remo Guerrini, Gerardino D'Errico, Delia Picone; *Preferential interaction of the Alzheimer peptide Aβ-(1-42) with Omega-3-containing lipid bilayers: structure and interaction studies*, (2016), FEBS Letters, 590, (4), 582-91, doi: 10.1002/1873-3468.12082.
- Rosario Oliva, Alessandro Emendato, Giuseppe Vitiello, Manuela Grimaldi, Anna Maria D'Ursi, Pompea Del Vecchio, Luigi Petraccone, Gerardino D'Errico; *On the microscopic and mesoscopic perturbations of lipid bilayers upon interaction with the MPER domain of the HIV glycoprotein gp41*, (2016), BBA-Biomembranes, 1858 (8), 1904-1913, doi:10.1016/j.bbamem.2016.05.007.
- Andrea Pica, Federica Donnarumma, Alessandro Emendato, Serena Leone, Michele Fortunato Rega, Rocco Di Girolamo, Antonello Merlino, Delia Picone; *Structure and aggregation propensity of the super-sweet protein Y65R-MNEI,* Manuscript in preparation.
- Alessandro Emendato, Giulia Milordini, Miquel Adrover, Annalisa Pastore, Delia Picone; *The effect of glycation on the aggregation properties of the Abeta peptides,* Manuscript in preparation.

6) Attended congresses/workshops/summer schools/contribution:

- May 25-26, 2014: Biophysics of Amyloids and Prions, Naples, Italy.
  Poster communication: *Interaction between amyloid peptide Aβ (1-42) with model phospholipid bilayers,* poster award winner.
- October, 27-29, 2015: Sigma-Aldrich Young Chemist Symposium, Rimini, Italy. Poster communication: *Omega3 lipid amount in liposomes modulates their interaction with Aβ (1-42) peptide.*
- June, 23-25, 2016: 15th Naples Workshop on Bioactive Peptides, Naples, Italy.
  Poster communication: *High resolution NMR study of endocannabinoid peptides.*
- November, 7-11, 2016: Helmholtz Training Course on Integrative Structural Biology, Braunschweig, Germany.
- February, 11-15, 2017: Biophysical Society 61th Annual Meeting, New Orleans, USA.
  Poster communication: *Sweeter and stronger: structure-driven molecular design to enhance sweetness and stability of the single chain monellin MNEI.*

7) Other Activities:

- Didactic support for the course "NMR di biomolecule", held by Prof. Delia Picone, year 2015/2016.
- PhD student representative in High School Students Orientation Commission, year 2016.
- Participation at orientation event Porte Aperte: Scienze si presenta, 22nd - 23rd Febraury 2016.
- Participation at orientation/divulgation event Futuro Remoto, 7th – 10th October 2016.

- Didactic support for the course “NMR di biomolecule”, held by Prof. Delia Picone, year 2016/2017.

References

[1] Knowles, T.P., Vendruscolo, M. and Dobson, C.M. (2014). The amyloid state and its association with protein misfolding diseases. Nat Rev Mol Cell Biol 15, 384-96.

[2] Bucciantini, M., Giannoni, E., Chiti, F., Baroni, F., Formigli, L., Zurdo, J., Taddei, N., Ramponi, G., Dobson, C.M. and Stefani, M. (2002). Inherent toxicity of aggregates implies a common mechanism for protein misfolding diseases. Nature 416, 507-11.

[3] Harrison, R.S., Sharpe, P.C., Singh, Y. and Fairlie, D.P. (2007). Amyloid peptides and proteins in review. Rev Physiol Biochem Pharmacol 159, 1-77.

[4] Chiti, F. and Dobson, C.M. (2006). Protein misfolding, functional amyloid, and human disease. Annu Rev Biochem 75, 333-66.

[5] Huff, M.E., Balch, W.E. and Kelly, J.W. (2003). Pathological and functional amyloid formation orchestrated by the secretory pathway. Curr Opin Struct Biol 13, 674-82.

[6] Maji, S.K., Perrin, M.H., Sawaya, M.R., Jessberger, S., Vadodaria, K., Rissman, R.A., Singru, P.S., Nilsson, K.P., Simon, R., Schubert, D., Eisenberg, D., Rivier, J., Sawchenko, P., Vale, W. and Riek, R. (2009). Functional amyloids as natural storage of peptide hormones in pituitary secretory granules. Science 325, 328-32.

[7] Kim, Y.S., Randolph, T.W., Manning, M.C., Stevens, F.J. and Carpenter, J.F. (2003). Congo red populates partially unfolded states of an amyloidogenic protein to enhance aggregation and amyloid fibril formation. J Biol Chem 278, 10842-50.

[8] Turnell, W.G. and Finch, J.T. (1992). Binding of the dye congo red to the amyloid protein pig insulin reveals a novel homology amongst amyloid-forming peptide sequences. J Mol Biol 227, 1205-23.

[9] LeVine, H., 3rd. (1999). Quantification of beta-sheet amyloid fibril structures with thioflavin T. Methods Enzymol 309, 274-84.

[10] Lashuel, H.A., Labrenz, S.R., Woo, L., Serpell, L.C. and Kelly, J.W. (2000). Protofilaments, filaments, ribbons, and fibrils from peptidomimetic self-assembly: implications for amyloid fibril formation and materials science. J Am Chem Soc 122, 5262-77.

[11] Zurdo, J., Guijarro, J.I. and Dobson, C.M. (2001). Preparation and characterization of purified amyloid fibrils. J Am Chem Soc 123, 8141-2.

[12] Kirschner, D.A., Abraham, C. and Selkoe, D.J. (1986). X-ray diffraction from intraneuronal paired helical filaments and extraneuronal amyloid fibers in Alzheimer disease indicates cross-beta conformation. Proc Natl Acad Sci U S A 83, 503-7.

[13] Tycko, R. (2004). Progress towards a molecular-level structural understanding of amyloid fibrils. Curr Opin Struct Biol 14, 96-103.

[14] Benilova, I., Karran, E. and De Strooper, B. (2012). The toxic Abeta oligomer and Alzheimer's disease: an emperor in need of clothes. Nat Neurosci 15, 349-57.

[15] Yamaguchi, T., Yagi, H., Goto, Y., Matsuzaki, K. and Hoshino, M. (2010). A disulfide-linked amyloid-beta peptide dimer forms a protofibril-like oligomer through a distinct pathway from amyloid fibril formation. Biochemistry 49, 7100-7.

[16] Crescenzi, O., Tomaselli, S., Guerrini, R., Salvadori, S., D'Ursi, A.M., Temussi, P.A. and Picone, D. (2002). Solution structure of the Alzheimer amyloid beta-peptide (1-42) in an apolar microenvironment. Similarity with a virus fusion domain. Eur J Biochem 269, 5642-8.

[17] Coles, M., Bicknell, W., Watson, A.A., Fairlie, D.P. and Craik, D.J. (1998). Solution structure of amyloid beta-peptide(1-40) in a water-micelle environment. Is the membrane-spanning domain where we think it is? Biochemistry 37, 11064-77.

[18] Bomar, M.G., Samuelsson, S.J., Kibler, P., Kodukula, K. and Galande, A.K. (2012). Hemopressin forms self-assembled fibrillar nanostructures under physiologically relevant conditions. Biomacromolecules 13, 579-83.

[19] Konno, T. (2001). Multistep nucleus formation and a separate subunit contribution of the amyloidgenesis of heat-denatured monellin. Protein Sci 10, 2093-101.

[20] Glenner, G.G. and Wong, C.W. (1984). Alzheimer's disease: initial report of the purification and characterization of a novel cerebrovascular amyloid protein. Biochem Biophys Res Commun 120, 885-90.

[21] Masters, C.L., Simms, G., Weinman, N.A., Multhaup, G., McDonald, B.L. and Beyreuther, K. (1985). Amyloid plaque core protein in Alzheimer disease and Down syndrome. Proc Natl Acad Sci U S A 82, 4245-9.

[22] Mori, H., Takio, K., Ogawara, M. and Selkoe, D.J. (1992). Mass spectrometry of purified amyloid beta protein in Alzheimer's disease. J Biol Chem 267, 17082-6.

[23] Citron, M., Diehl, T.S., Gordon, G., Biere, A.L., Seubert, P. and Selkoe, D.J. (1996). Evidence that the 42- and 40-amino acid forms of amyloid beta protein are generated from the beta-amyloid precursor protein by different protease activities. Proc Natl Acad Sci U S A 93, 13170-5.

[24] Saitoh, T., Sundsmo, M., Roch, J.M., Kimura, N., Cole, G., Schubert, D., Oltersdorf, T. and Schenk, D.B. (1989). Secreted form of amyloid beta protein precursor is involved in the growth regulation of fibroblasts. Cell 58, 615-22.

[25] Mattson, M.P., Cheng, B., Culwell, A.R., Esch, F.S., Lieberburg, I. and Rydel, R.E. (1993). Evidence for excitoprotective and intraneuronal calcium-

regulating roles for secreted forms of the beta-amyloid precursor protein. Neuron 10, 243-54.

[26] Hesse, L., Beher, D., Masters, C.L. and Multhaup, G. (1994). The beta A4 amyloid precursor protein binding to copper. FEBS Lett 349, 109-16.

[27] Barrett, P.J., Song, Y., Van Horn, W.D., Hustedt, E.J., Schafer, J.M., Hadziselimovic, A., Beel, A.J. and Sanders, C.R. (2012). The amyloid precursor protein has a flexible transmembrane domain and binds cholesterol. Science 336, 1168-71.

[28] Esler, W.P. and Wolfe, M.S. (2001). A portrait of Alzheimer secretases--new features and familiar faces. Science 293, 1449-54.

[29] Haass, C., Schlossmacher, M.G., Hung, A.Y., Vigo-Pelfrey, C., Mellon, A., Ostaszewski, B.L., Lieberburg, I., Koo, E.H., Schenk, D., Teplow, D.B. and et al. (1992). Amyloid beta-peptide is produced by cultured cells during normal metabolism. Nature 359, 322-5.

[30] Axelsen, P.H., Komatsu, H. and Murray, I.V. (2011). Oxidative stress and cell membranes in the pathogenesis of Alzheimer's disease. Physiology (Bethesda) 26, 54-69.

[31] Mattson, M.P. (1997). Cellular actions of beta-amyloid precursor protein and its soluble and fibrillogenic derivatives. Physiol Rev 77, 1081-132.

[32] Alzheimer, A., Stelzmann, R.A., Schnitzlein, H.N. and Murtagh, F.R. (1995). An English translation of Alzheimer's 1907 paper, "Uber eine eigenartige Erkankung der Hirnrinde". Clin Anat 8, 429-31.

[33] Tanzi, R.E., McClatchey, A.I., Lamperti, E.D., Villa-Komaroff, L., Gusella, J.F. and Neve, R.L. (1988). Protease inhibitor domain encoded by an amyloid protein precursor mRNA associated with Alzheimer's disease. Nature 331, 528-30.

[34] Selkoe, D.J. (1991). The molecular pathology of Alzheimer's disease. Neuron 6, 487-98.

[35] Mattson, M.P. (2004). Pathways towards and away from Alzheimer's disease. Nature 430, 631-9.

[36] Lin, H., Bhatia, R. and Lal, R. (2001). Amyloid beta protein forms ion channels: implications for Alzheimer's disease pathophysiology. FASEB J 15, 2433-44.

[37] Kremer, J.J., Pallitto, M.M., Sklansky, D.J. and Murphy, R.M. (2000). Correlation of beta-amyloid aggregate size and hydrophobicity with decreased bilayer fluidity of model membranes. Biochemistry 39, 10309-18.

[38] Muller, W.E., Eckert, G.P., Scheuer, K., Cairns, N.J., Maras, A. and Gattaz, W.F. (1998). Effects of beta-amyloid peptides on the fluidity of membranes from frontal and parietal lobes of human brain. High potencies of A beta 1-42 and A beta 1-43. Amyloid 5, 10-5.

[39] Butterfield, D.A., Yatin, S.M., Varadarajan, S. and Koppal, T. (1999). Amyloid beta-peptide-associated free radical oxidative stress, neurotoxicity, and Alzheimer's disease. Methods Enzymol 309, 746-68.

[40] Koudinov, A.R., Berezov, T.T. and Koudinova, N.V. (1998). Alzheimer's amyloid beta and lipid metabolism: a missing link? FASEB J 12, 1097-9.

[41] Loo, D.T., Copani, A., Pike, C.J., Whittemore, E.R., Walencewicz, A.J. and Cotman, C.W. (1993). Apoptosis is induced by beta-amyloid in cultured central nervous system neurons. Proc Natl Acad Sci U S A 90, 7951-5.

[42] Behl, C., Davis, J.B., Lesley, R. and Schubert, D. (1994). Hydrogen peroxide mediates amyloid beta protein toxicity. Cell 77, 817-27.

[43] Hardy, J. (2006). Alzheimer's disease: the amyloid cascade hypothesis: an update and reappraisal. J Alzheimers Dis 9, 151-3.

[44] Hardy, J.A. and Higgins, G.A. (1992). Alzheimer's disease: the amyloid cascade hypothesis. Science 256, 184-5.

[45] Hardy, J. and Allsop, D. (1991). Amyloid deposition as the central event in the aetiology of Alzheimer's disease. Trends Pharmacol Sci 12, 383-8.

[46] El-Sayed, M.M., Ghareeb, D.A., Talat, H.A. and Sarhan, E.M. (2013). High fat diet induced insulin resistance and elevated retinol binding protein 4 in female rats; treatment and protection with Berberis vulgaris extract and vitamin A. Pak J Pharm Sci 26, 1189-95.

[47] Bush, A.I. and Tanzi, R.E. (2008). Therapeutics for Alzheimer's disease based on the metal hypothesis. Neurotherapeutics 5, 421-32.

[48] Roy, S. and Rauk, A. (2005). Alzheimer's disease and the 'ABSENT' hypothesis: mechanism for amyloid beta endothelial and neuronal toxicity. Med Hypotheses 65, 123-37.

[49] Klug, G.M., Losic, D., Subasinghe, S.S., Aguilar, M.I., Martin, L.L. and Small, D.H. (2003). Beta-amyloid protein oligomers induced by metal ions and acid pH are distinct from those generated by slow spontaneous ageing at neutral pH. Eur J Biochem 270, 4282-93.

[50] Kayed, R., Pensalfini, A., Margol, L., Sokolov, Y., Sarsoza, F., Head, E., Hall, J. and Glabe, C. (2009). Annular protofibrils are a structurally and functionally distinct type of amyloid oligomer. J Biol Chem 284, 4230-7.

[51] Walsh, D.M., Klyubin, I., Fadeeva, J.V., Cullen, W.K., Anwyl, R., Wolfe, M.S., Rowan, M.J. and Selkoe, D.J. (2002). Naturally secreted oligomers of amyloid beta protein potently inhibit hippocampal long-term potentiation in vivo. Nature 416, 535-9.

[52] Walsh, D.M. and Selkoe, D.J. (2004). Oligomers on the brain: the emerging role of soluble protein aggregates in neurodegeneration. Protein Pept Lett 11, 213-28.

[53] Stefani, M. (2012). Structural features and cytotoxicity of amyloid oligomers: implications in Alzheimer's disease and other diseases with amyloid deposits. Prog Neurobiol 99, 226-45.

[54] Babu, M.M., van der Lee, R., de Groot, N.S. and Gsponer, J. (2011). Intrinsically disordered proteins: regulation and disease. Curr Opin Struct Biol 21, 432-40.
[55] Uversky, V.N. (2013). A decade and a half of protein intrinsic disorder: biology still waits for physics. Protein Sci 22, 693-724.
[56] Talafous, J., Marcinowski, K.J., Klopman, G. and Zagorski, M.G. (1994). Solution structure of residues 1-28 of the amyloid beta-peptide. Biochemistry 33, 7788-96.
[57] Tomaselli, S., Esposito, V., Vangone, P., van Nuland, N.A., Bonvin, A.M., Guerrini, R., Tancredi, T., Temussi, P.A. and Picone, D. (2006). The alpha-to-beta conformational transition of Alzheimer's Abeta-(1-42) peptide in aqueous media is reversible: a step by step conformational analysis suggests the location of beta conformation seeding. Chembiochem 7, 257-67.
[58] Barrow, C.J., Yasuda, A., Kenny, P.T. and Zagorski, M.G. (1992). Solution conformations and aggregational properties of synthetic amyloid beta-peptides of Alzheimer's disease. Analysis of circular dichroism spectra. J Mol Biol 225, 1075-93.
[59] Soto, C., Castano, E.M., Kumar, R.A., Beavis, R.C. and Frangione, B. (1995). Fibrillogenesis of synthetic amyloid-beta peptides is dependent on their initial secondary structure. Neurosci Lett 200, 105-8.
[60] Zagorski, M.G., Yang, J., Shao, H., Ma, K., Zeng, H. and Hong, A. (1999). Methodological and chemical factors affecting amyloid beta peptide amyloidogenicity. Methods Enzymol 309, 189-204.
[61] Luhrs, T., Ritter, C., Adrian, M., Riek-Loher, D., Bohrmann, B., Dobeli, H., Schubert, D. and Riek, R. (2005). 3D structure of Alzheimer's amyloid-beta(1-42) fibrils. Proc Natl Acad Sci U S A 102, 17342-7.
[62] Colvin, M.T., Silvers, R., Ni, Q.Z., Can, T.V., Sergeyev, I., Rosay, M., Donovan, K.J., Michael, B., Wall, J., Linse, S. and Griffin, R.G. (2016). Atomic Resolution Structure of Monomorphic Abeta42 Amyloid Fibrils. J Am Chem Soc 138, 9663-74.
[63] Lu, J.X., Qiang, W., Yau, W.M., Schwieters, C.D., Meredith, S.C. and Tycko, R. (2013). Molecular structure of beta-amyloid fibrils in Alzheimer's disease brain tissue. Cell 154, 1257-68.
[64] Walti, M.A., Ravotti, F., Arai, H., Glabe, C.G., Wall, J.S., Bockmann, A., Guntert, P., Meier, B.H. and Riek, R. (2016). Atomic-resolution structure of a disease-relevant Abeta(1-42) amyloid fibril. Proc Natl Acad Sci U S A 113, E4976-84.
[65] Nelson, R. and Eisenberg, D. (2006). Recent atomic models of amyloid fibril structure. Curr Opin Struct Biol 16, 260-5.
[66] Antzutkin, O.N., Balbach, J.J., Leapman, R.D., Rizzo, N.W., Reed, J. and Tycko, R. (2000). Multiple quantum solid-state NMR indicates a parallel, not

antiparallel, organization of beta-sheets in Alzheimer's beta-amyloid fibrils. Proc Natl Acad Sci U S A 97, 13045-50.

[67] Buchete, N.V., Tycko, R. and Hummer, G. (2005). Molecular dynamics simulations of Alzheimer's beta-amyloid protofilaments. J Mol Biol 353, 804-21.

[68] Ionescu-Zanetti, C., Khurana, R., Gillespie, J.R., Petrick, J.S., Trabachino, L.C., Minert, L.J., Carter, S.A. and Fink, A.L. (1999). Monitoring the assembly of Ig light-chain amyloid fibrils by atomic force microscopy. Proc Natl Acad Sci U S A 96, 13175-9.

[69] Harper, J.D., Lieber, C.M. and Lansbury, P.T., Jr. (1997). Atomic force microscopic imaging of seeded fibril formation and fibril branching by the Alzheimer's disease amyloid-beta protein. Chem Biol 4, 951-9.

[70] Mithu, V.S., Sarkar, B., Bhowmik, D., Chandrakesan, M., Maiti, S. and Madhu, P.K. (2011). Zn(++) binding disrupts the Asp(23)-Lys(28) salt bridge without altering the hairpin-shaped cross-beta Structure of Abeta(42) amyloid aggregates. Biophys J 101, 2825-32.

[71] Petkova, A.T., Leapman, R.D., Guo, Z., Yau, W.M., Mattson, M.P. and Tycko, R. (2005). Self-propagating, molecular-level polymorphism in Alzheimer's beta-amyloid fibrils. Science 307, 262-5.

[72] Qiang, W., Yau, W.M., Luo, Y., Mattson, M.P. and Tycko, R. (2012). Antiparallel beta-sheet architecture in Iowa-mutant beta-amyloid fibrils. Proc Natl Acad Sci U S A 109, 4443-8.

[73] Xiao, Y., Ma, B., McElheny, D., Parthasarathy, S., Long, F., Hoshi, M., Nussinov, R. and Ishii, Y. (2015). Abeta(1-42) fibril structure illuminates self-recognition and replication of amyloid in Alzheimer's disease. Nat Struct Mol Biol 22, 499-505.

[74] Liu, R.Q., Zhou, Q.H., Ji, S.R., Zhou, Q., Feng, D., Wu, Y. and Sui, S.F. (2010). Membrane localization of beta-amyloid 1-42 in lysosomes: a possible mechanism for lysosome labilization. J Biol Chem 285, 19986-96.

[75] Lansbury, P.T. and Lashuel, H.A. (2006). A century-old debate on protein aggregation and neurodegeneration enters the clinic. Nature 443, 774-9.

[76] Qiang, W., Yau, W.M. and Schulte, J. (2015). Fibrillation of beta amyloid peptides in the presence of phospholipid bilayers and the consequent membrane disruption. Biochim Biophys Acta 1848, 266-76.

[77] Martins, I.C., Kuperstein, I., Wilkinson, H., Maes, E., Vanbrabant, M., Jonckheere, W., Van Gelder, P., Hartmann, D., D'Hooge, R., De Strooper, B., Schymkowitz, J. and Rousseau, F. (2008). Lipids revert inert Abeta amyloid fibrils to neurotoxic protofibrils that affect learning in mice. EMBO J 27, 224-33.

[78] Sabate, R. and Estelrich, J. (2005). Evidence of the existence of micelles in the fibrillogenesis of beta-amyloid peptide. J Phys Chem B 109, 11027-32.

[79] McLaurin, J. and Chakrabartty, A. (1997). Characterization of the interactions of Alzheimer beta-amyloid peptides with phospholipid membranes. Eur J Biochem 245, 355-63.

[80] Kremer, J.J. and Murphy, R.M. (2003). Kinetics of adsorption of beta-amyloid peptide Abeta(1-40) to lipid bilayers. J Biochem Biophys Methods 57, 159-69.

[81] Lin, M.S., Chiu, H.M., Fan, F.J., Tsai, H.T., Wang, S.S., Chang, Y. and Chen, W.Y. (2007). Kinetics and enthalpy measurements of interaction between beta-amyloid and liposomes by surface plasmon resonance and isothermal titration microcalorimetry. Colloids Surf B Biointerfaces 58, 231-6.

[82] Yip, C.M., Darabie, A.A. and McLaurin, J. (2002). Abeta42-peptide assembly on lipid bilayers. J Mol Biol 318, 97-107.

[83] Kayed, R., Sokolov, Y., Edmonds, B., McIntire, T.M., Milton, S.C., Hall, J.E. and Glabe, C.G. (2004). Permeabilization of lipid bilayers is a common conformation-dependent activity of soluble amyloid oligomers in protein misfolding diseases. J Biol Chem 279, 46363-6.

[84] Sokolov, Y., Kozak, J.A., Kayed, R., Chanturiya, A., Glabe, C. and Hall, J.E. (2006). Soluble amyloid oligomers increase bilayer conductance by altering dielectric structure. J Gen Physiol 128, 637-47.

[85] Williams, T.L., Day, I.J. and Serpell, L.C. (2010). The effect of Alzheimer's Abeta aggregation state on the permeation of biomimetic lipid vesicles. Langmuir 26, 17260-8.

[86] Engel, M.F., Khemtemourian, L., Kleijer, C.C., Meeldijk, H.J., Jacobs, J., Verkleij, A.J., de Kruijff, B., Killian, J.A. and Hoppener, J.W. (2008). Membrane damage by human islet amyloid polypeptide through fibril growth at the membrane. Proc Natl Acad Sci U S A 105, 6033-8.

[87] Ambroggio, E.E., Kim, D.H., Separovic, F., Barrow, C.J., Barnham, K.J., Bagatolli, L.A. and Fidelio, G.D. (2005). Surface behavior and lipid interaction of Alzheimer beta-amyloid peptide 1-42: a membrane-disrupting peptide. Biophys J 88, 2706-13.

[88] Mason, R.P., Shoemaker, W.J., Shajenko, L., Chambers, T.E. and Herbette, L.G. (1992). Evidence for changes in the Alzheimer's disease brain cortical membrane structure mediated by cholesterol. Neurobiol Aging 13, 413-9.

[89] Beel, A.J., Mobley, C.K., Kim, H.J., Tian, F., Hadziselimovic, A., Jap, B., Prestegard, J.H. and Sanders, C.R. (2008). Structural studies of the transmembrane C-terminal domain of the amyloid precursor protein (APP): does APP function as a cholesterol sensor? Biochemistry 47, 9428-46.

[90] D'Errico, G., Vitiello, G., Ortona, O., Tedeschi, A., Ramunno, A. and D'Ursi, A.M. (2008). Interaction between Alzheimer's Abeta(25-35) peptide and phospholipid bilayers: the role of cholesterol. Biochim Biophys Acta 1778, 2710-6.

[91] Ji, S.R., Wu, Y. and Sui, S.F. (2002). Cholesterol is an important factor affecting the membrane insertion of beta-amyloid peptide (A beta 1-40), which may potentially inhibit the fibril formation. J Biol Chem 277, 6273-9.

[92] Subasinghe, S., Unabia, S., Barrow, C.J., Mok, S.S., Aguilar, M.I. and Small, D.H. (2003). Cholesterol is necessary both for the toxic effect of Abeta peptides on vascular smooth muscle cells and for Abeta binding to vascular smooth muscle cell membranes. J Neurochem 84, 471-9.

[93] Ashley, R.H., Harroun, T.A., Hauss, T., Breen, K.C. and Bradshaw, J.P. (2006). Autoinsertion of soluble oligomers of Alzheimer's Abeta(1-42) peptide into cholesterol-containing membranes is accompanied by relocation of the sterol towards the bilayer surface. BMC Struct Biol 6, 21.

[94] Micelli, S., Meleleo, D., Picciarelli, V. and Gallucci, E. (2004). Effect of sterols on beta-amyloid peptide (AbetaP 1-40) channel formation and their properties in planar lipid membranes. Biophys J 86, 2231-7.

[95] Di Scala, C., Chahinian, H., Yahi, N., Garmy, N. and Fantini, J. (2014). Interaction of Alzheimer's beta-amyloid peptides with cholesterol: mechanistic insights into amyloid pore formation. Biochemistry 53, 4489-502.

[96] Fishman, P.H. and Brady, R.O. (1976). Biosynthesis and function of gangliosides. Science 194, 906-15.

[97] Hakomori, S. (2003). Structure, organization, and function of glycosphingolipids in membrane. Curr Opin Hematol 10, 16-24.

[98] Chi, E.Y., Frey, S.L. and Lee, K.Y. (2007). Ganglioside G(M1)-mediated amyloid-beta fibrillogenesis and membrane disruption. Biochemistry 46, 1913-24.

[99] Valdes-Gonzalez, T., Inagawa, J. and Ido, T. (2001). Neuropeptides interact with glycolipid receptors: a surface plasmon resonance study. Peptides 22, 1099-106.

[100] McLaurin, J., Franklin, T., Fraser, P.E. and Chakrabartty, A. (1998). Structural transitions associated with the interaction of Alzheimer beta-amyloid peptides with gangliosides. J Biol Chem 273, 4506-15.

[101] Choo-Smith, L.P., Garzon-Rodriguez, W., Glabe, C.G. and Surewicz, W.K. (1997). Acceleration of amyloid fibril formation by specific binding of Abeta-(1-40) peptide to ganglioside-containing membrane vesicles. J Biol Chem 272, 22987-90.

[102] Matsuzaki, K. (2007). Physicochemical interactions of amyloid beta-peptide with lipid bilayers. Biochim Biophys Acta 1768, 1935-42.

[103] Calamai, M., Evangelisti, E., Cascella, R., Parenti, N., Cecchi, C., Stefani, M. and Pavone, F. (2016). Single molecule experiments emphasize GM1 as a key player of the different cytotoxicity of structurally distinct Abeta1-42 oligomers. Biochim Biophys Acta 1858, 386-92.

[104] Matsuzaki, K., Kato, K. and Yanagisawa, K. (2010). Abeta polymerization through interaction with membrane gangliosides. Biochim Biophys Acta 1801, 868-77.
[105] Hebda, J.A. and Miranker, A.D. (2009). The interplay of catalysis and toxicity by amyloid intermediates on lipid bilayers: insights from type II diabetes. Annu Rev Biophys 38, 125-52.
[106] Arispe, N., Pollard, H.B. and Rojas, E. (1993). Giant multilevel cation channels formed by Alzheimer disease amyloid beta-protein [A beta P-(1-40)] in bilayer membranes. Proc Natl Acad Sci U S A 90, 10573-7.
[107] Quist, A., Doudevski, I., Lin, H., Azimova, R., Ng, D., Frangione, B., Kagan, B., Ghiso, J. and Lal, R. (2005). Amyloid ion channels: a common structural link for protein-misfolding disease. Proc Natl Acad Sci U S A 102, 10427-32.
[108] Strodel, B., Lee, J.W., Whittleston, C.S. and Wales, D.J. (2010). Transmembrane structures for Alzheimer's Abeta(1-42) oligomers. J Am Chem Soc 132, 13300-12.
[109] Shafrir, Y., Durell, S., Arispe, N. and Guy, H.R. (2010). Models of membrane-bound Alzheimer's Abeta peptide assemblies. Proteins 78, 3473-87.
[110] Shai, Y. (1999). Mechanism of the binding, insertion and destabilization of phospholipid bilayer membranes by alpha-helical antimicrobial and cell non-selective membrane-lytic peptides. Biochim Biophys Acta 1462, 55-70.
[111] Lis, H. and Sharon, N. (1993). Protein glycosylation. Structural and functional aspects. Eur J Biochem 218, 1-27.
[112] Hodge, J.E. (1955). The Amadori rearrangement. Adv Carbohydr Chem 10, 169-205.
[113] Chen, K., Maley, J. and Yu, P.H. (2006). Potential inplications of endogenous aldehydes in beta-amyloid misfolding, oligomerization and fibrillogenesis. J Neurochem 99, 1413-24.
[114] Munch, G., Mayer, S., Michaelis, J., Hipkiss, A.R., Riederer, P., Muller, R., Neumann, A., Schinzel, R. and Cunningham, A.M. (1997). Influence of advanced glycation end-products and AGE-inhibitors on nucleation-dependent polymerization of beta-amyloid peptide. Biochim Biophys Acta 1360, 17-29.
[115] Woltjer, R.L., Maezawa, I., Ou, J.J., Montine, K.S. and Montine, T.J. (2003). Advanced glycation endproduct precursor alters intracellular amyloid-beta/A beta PP carboxy-terminal fragment aggregation and cytotoxicity. J Alzheimers Dis 5, 467-76.
[116] Vitek, M.P., Bhattacharya, K., Glendening, J.M., Stopa, E., Vlassara, H., Bucala, R., Manogue, K. and Cerami, A. (1994). Advanced glycation end products contribute to amyloidosis in Alzheimer disease. Proc Natl Acad Sci U S A 91, 4766-70.

[117] Ko, S.Y., Lin, Y.P., Lin, Y.S. and Chang, S.S. (2010). Advanced glycation end products enhance amyloid precursor protein expression by inducing reactive oxygen species. Free Radic Biol Med 49, 474-80.
[118] Ahmed, N., Ahmed, U., Thornalley, P.J., Hager, K., Fleischer, G. and Munch, G. (2005). Protein glycation, oxidation and nitration adduct residues and free adducts of cerebrospinal fluid in Alzheimer's disease and link to cognitive impairment. J Neurochem 92, 255-63.
[119] Li, X.H., Du, L.L., Cheng, X.S., Jiang, X., Zhang, Y., Lv, B.L., Liu, R., Wang, J.Z. and Zhou, X.W. (2013). Glycation exacerbates the neuronal toxicity of beta-amyloid. Cell Death Dis 4, e673.
[120] Cerami, A., Vlassara, H. and Brownlee, M. (1987). Glucose and aging. Sci Am 256, 90-6.
[121] Rabbani, N. and Thornalley, P.J. (2012). Glycation research in amino acids: a place to call home. Amino Acids 42, 1087-96.
[122] Baynes, J.W. (1991). Role of oxidative stress in development of complications in diabetes. Diabetes 40, 405-12.
[123] Iannuzzi, C., Irace, G. and Sirangelo, I. (2014). Differential effects of glycation on protein aggregation and amyloid formation. Front Mol Biosci 1, 9.
[124] Delpierre, G., Rider, M.H., Collard, F., Stroobant, V., Vanstapel, F., Santos, H. and Van Schaftingen, E. (2000). Identification, cloning, and heterologous expression of a mammalian fructosamine-3-kinase. Diabetes 49, 1627-34.
[125] Delplanque, J., Delpierre, G., Opperdoes, F.R. and Van Schaftingen, E. (2004). Tissue distribution and evolution of fructosamine 3-kinase and fructosamine 3-kinase-related protein. J Biol Chem 279, 46606-13.
[126] Baba, S.P., Barski, O.A., Ahmed, Y., O'Toole, T.E., Conklin, D.J., Bhatnagar, A. and Srivastava, S. (2009). Reductive metabolism of AGE precursors: a metabolic route for preventing AGE accumulation in cardiovascular tissue. Diabetes 58, 2486-97.
[127] Foyer, C.H., Faragher, R. and Thornalley, P. (2009). Redox metabolism and longevity relationships in animals and plants. Preface. SEB Exp Biol Ser 62, xix-xx.
[128] Ahmed, N., Babaei-Jadidi, R., Howell, S.K., Beisswenger, P.J. and Thornalley, P.J. (2005). Degradation products of proteins damaged by glycation, oxidation and nitration in clinical type 1 diabetes. Diabetologia 48, 1590-603.
[129] Agalou, S., Ahmed, N., Babaei-Jadidi, R., Dawnay, A. and Thornalley, P.J. (2005). Profound mishandling of protein glycation degradation products in uremia and dialysis. J Am Soc Nephrol 16, 1471-85.
[130] Chen, F., Wollmer, M.A., Hoerndli, F., Munch, G., Kuhla, B., Rogaev, E.I., Tsolaki, M., Papassotiropoulos, A. and Gotz, J. (2004). Role for glyoxalase I in Alzheimer's disease. Proc Natl Acad Sci U S A 101, 7687-92.

[131] Rabbani, N., Chittari, M.V., Bodmer, C.W., Zehnder, D., Ceriello, A. and Thornalley, P.J. (2010). Increased glycation and oxidative damage to apolipoprotein B100 of LDL cholesterol in patients with type 2 diabetes and effect of metformin. Diabetes 59, 1038-45.

[132] Hambsch, B., Chen, B.G., Brenndorfer, J., Meyer, M., Avrabos, C., Maccarrone, G., Liu, R.H., Eder, M., Turck, C.W. and Landgraf, R. (2010). Methylglyoxal-mediated anxiolysis involves increased protein modification and elevated expression of glyoxalase 1 in the brain. J Neurochem 113, 1240-51.

[133] Kurz, A., Rabbani, N., Walter, M., Bonin, M., Thornalley, P., Auburger, G. and Gispert, S. (2011). Alpha-synuclein deficiency leads to increased glyoxalase I expression and glycation stress. Cell Mol Life Sci 68, 721-33.

[134] Vagelatos, N.T. and Eslick, G.D. (2013). Type 2 diabetes as a risk factor for Alzheimer's disease: the confounders, interactions, and neuropathology associated with this relationship. Epidemiol Rev 35, 152-60.

[135] Moloney, A.M., Griffin, R.J., Timmons, S., O'Connor, R., Ravid, R. and O'Neill, C. (2010). Defects in IGF-1 receptor, insulin receptor and IRS-1/2 in Alzheimer's disease indicate possible resistance to IGF-1 and insulin signalling. Neurobiol Aging 31, 224-43.

[136] Craft, S., Baker, L.D., Montine, T.J., Minoshima, S., Watson, G.S., Claxton, A., Arbuckle, M., Callaghan, M., Tsai, E., Plymate, S.R., Green, P.S., Leverenz, J., Cross, D. and Gerton, B. (2012). Intranasal insulin therapy for Alzheimer disease and amnestic mild cognitive impairment: a pilot clinical trial. Arch Neurol 69, 29-38.

[137] Carvalho, C., Cardoso, S., Correia, S.C., Santos, R.X., Santos, M.S., Baldeiras, I., Oliveira, C.R. and Moreira, P.I. (2012). Metabolic alterations induced by sucrose intake and Alzheimer's disease promote similar brain mitochondrial abnormalities. Diabetes 61, 1234-42.

[138] Heimann, A.S., Gomes, I., Dale, C.S., Pagano, R.L., Gupta, A., de Souza, L.L., Luchessi, A.D., Castro, L.M., Giorgi, R., Rioli, V., Ferro, E.S. and Devi, L.A. (2007). Hemopressin is an inverse agonist of CB1 cannabinoid receptors. Proc Natl Acad Sci U S A 104, 20588-93.

[139] Rioli, V., Gozzo, F.C., Heimann, A.S., Linardi, A., Krieger, J.E., Shida, C.S., Almeida, P.C., Hyslop, S., Eberlin, M.N. and Ferro, E.S. (2003). Novel natural peptide substrates for endopeptidase 24.15, neurolysin, and angiotensin-converting enzyme. J Biol Chem 278, 8547-55.

[140] Bomar, M.G. and Galande, A.K. (2013). Modulation of the cannabinoid receptors by hemopressin peptides. Life Sci 92, 520-4.

[141] Dodd, G.T., Mancini, G., Lutz, B. and Luckman, S.M. (2010). The peptide hemopressin acts through CB1 cannabinoid receptors to reduce food intake in rats and mice. J Neurosci 30, 7369-76.

[142] Scrima, M., Di Marino, S., Grimaldi, M., Mastrogiacomo, A., Novellino, E., Bifulco, M. and D'Ursi, A.M. (2010). Binding of the hemopressin peptide to the cannabinoid CB1 receptor: structural insights. Biochemistry 49, 10449-57.
[143] Gomes, I., Grushko, J.S., Golebiewska, U., Hoogendoorn, S., Gupta, A., Heimann, A.S., Ferro, E.S., Scarlata, S., Fricker, L.D. and Devi, L.A. (2009). Novel endogenous peptide agonists of cannabinoid receptors. FASEB J 23, 3020-9.
[144] Marcus, F. (1985). Preferential cleavage at aspartyl-prolyl peptide bonds in dilute acid. Int J Pept Protein Res 25, 542-6.
[145] Temussi, P.A. (2006). Natural sweet macromolecules: how sweet proteins work. Cell Mol Life Sci 63, 1876-88.
[146] Picone, D. and Temussi, P.A. (2012). Dissimilar sweet proteins from plants: oddities or normal components? Plant Sci 195, 135-42.
[147] Nelson, G., Hoon, M.A., Chandrashekar, J., Zhang, Y., Ryba, N.J. and Zuker, C.S. (2001). Mammalian sweet taste receptors. Cell 106, 381-90.
[148] Chandrashekar, J., Hoon, M.A., Ryba, N.J. and Zuker, C.S. (2006). The receptors and cells for mammalian taste. Nature 444, 288-94.
[149] Morris, J.A. and Cagan, R.H. (1972). Purification of monellin, the sweet principle of Dioscoreophyllum cumminsii. Biochim Biophys Acta 261, 114-22.
[150] van der Wel, H. and Loeve, K. (1972). Isolation and characterization of thaumatin I and II, the sweet-tasting proteins from Thaumatococcus daniellii Benth. Eur J Biochem 31, 221-5.
[151] Ming, D. and Hellekant, G. (1994). Brazzein, a new high-potency thermostable sweet protein from Pentadiplandra brazzeana B. FEBS Lett 355, 106-8.
[152] Theerasilp, S., Hitotsuya, H., Nakajo, S., Nakaya, K., Nakamura, Y. and Kurihara, Y. (1989). Complete amino acid sequence and structure characterization of the taste-modifying protein, miraculin. J Biol Chem 264, 6655-9.
[153] Ogata, C., Hatada, M., Tomlinson, G., Shin, W.C. and Kim, S.H. (1987). Crystal structure of the intensely sweet protein monellin. Nature 328, 739-42.
[154] Murzin, A.G. (1993). Sweet-tasting protein monellin is related to the cystatin family of thiol proteinase inhibitors. J Mol Biol 230, 689-94.
[155] Patra, A.K. and Udgaonkar, J.B. (2007). Characterization of the folding and unfolding reactions of single-chain monellin: evidence for multiple intermediates and competing pathways. Biochemistry 46, 11727-43.
[156] Kim, S.H., Kang, C.H., Kim, R., Cho, J.M., Lee, Y.B. and Lee, T.K. (1989). Redesigning a sweet protein: increased stability and renaturability. Protein Eng 2, 571-5.
[157] Tancredi, T., Pastore, A., Salvadori, S., Esposito, V. and Temussi, P.A. (2004). Interaction of sweet proteins with their receptor. A conformational study of

peptides corresponding to loops of brazzein, monellin and thaumatin. Eur J Biochem 271, 2231-40.

[158] Esposito, V., Gallucci, R., Picone, D., Saviano, G., Tancredi, T. and Temussi, P.A. (2006). The importance of electrostatic potential in the interaction of sweet proteins with the sweet taste receptor. J Mol Biol 360, 448-56.

[159] Leone, S., Pica, A., Merlino, A., Sannino, F., Temussi, P.A. and Picone, D. (2016). Sweeter and stronger: enhancing sweetness and stability of the single chain monellin MNEI through molecular design. Sci Rep 6, 34045.

[160] Esposito, V., Guglielmi, F., Martin, S.R., Pauwels, K., Pastore, A., Piccoli, R. and Temussi, P.A. (2010). Aggregation mechanisms of cystatins: a comparative study of monellin and oryzacystatin. Biochemistry 49, 2805-10.

[161] Walsh, D.M., Thulin, E., Minogue, A.M., Gustavsson, N., Pang, E., Teplow, D.B. and Linse, S. (2009). A facile method for expression and purification of the Alzheimer's disease-associated amyloid beta-peptide. FEBS J 276, 1266-81.

[162] Hu, N., Yu, J.T., Tan, L., Wang, Y.L., Sun, L. and Tan, L. (2013). Nutrition and the risk of Alzheimer's disease. Biomed Res Int 2013, 524820.

[163] Reitz, C., Brayne, C. and Mayeux, R. (2011). Epidemiology of Alzheimer disease. Nat Rev Neurol 7, 137-52.

[164] Singh, B., Parsaik, A.K., Mielke, M.M., Erwin, P.J., Knopman, D.S., Petersen, R.C. and Roberts, R.O. (2014). Association of mediterranean diet with mild cognitive impairment and Alzheimer's disease: a systematic review and meta-analysis. J Alzheimers Dis 39, 271-82.

[165] Cunnane, S.C., Plourde, M., Pifferi, F., Begin, M., Feart, C. and Barberger-Gateau, P. (2009). Fish, docosahexaenoic acid and Alzheimer's disease. Prog Lipid Res 48, 239-56.

[166] Bazinet, R.P. and Laye, S. (2014). Polyunsaturated fatty acids and their metabolites in brain function and disease. Nat Rev Neurosci 15, 771-85.

[167] Hjorth, E., Zhu, M., Toro, V.C., Vedin, I., Palmblad, J., Cederholm, T., Freund-Levi, Y., Faxen-Irving, G., Wahlund, L.O., Basun, H., Eriksdotter, M. and Schultzberg, M. (2013). Omega-3 fatty acids enhance phagocytosis of Alzheimer's disease-related amyloid-beta42 by human microglia and decrease inflammatory markers. J Alzheimers Dis 35, 697-713.

[168] Williamson, R. and Sutherland, C. (2011). Neuronal membranes are key to the pathogenesis of Alzheimer's disease: the role of both raft and non-raft membrane domains. Curr Alzheimer Res 8, 213-21.

[169] Stillwell, W., Shaikh, S.R., Zerouga, M., Siddiqui, R. and Wassall, S.R. (2005). Docosahexaenoic acid affects cell signaling by altering lipid rafts. Reprod Nutr Dev 45, 559-79.

[170] Wassall, S.R. and Stillwell, W. (2009). Polyunsaturated fatty acid-cholesterol interactions: domain formation in membranes. Biochim Biophys Acta 1788, 24-32.

[171] Escriba, P.V., Busquets, X., Inokuchi, J., Balogh, G., Torok, Z., Horvath, I., Harwood, J.L. and Vigh, L. (2015). Membrane lipid therapy: Modulation of the cell membrane composition and structure as a molecular base for drug discovery and new disease treatment. Prog Lipid Res 59, 38-53.

[172] Prasad, M.R., Lovell, M.A., Yatin, M., Dhillon, H. and Markesbery, W.R. (1998). Regional membrane phospholipid alterations in Alzheimer's disease. Neurochem Res 23, 81-8.

[173] Vitiello, G., Di Marino, S., D'Ursi, A.M. and D'Errico, G. (2013). Omega-3 fatty acids regulate the interaction of the Alzheimer's abeta(25-35) peptide with lipid membranes. Langmuir 29, 14239-45.

[174] Calderon, R.O., Attema, B. and DeVries, G.H. (1995). Lipid composition of neuronal cell bodies and neurites from cultured dorsal root ganglia. J Neurochem 64, 424-9.

[175] Soderberg, M., Edlund, C., Kristensson, K. and Dallner, G. (1991). Fatty acid composition of brain phospholipids in aging and in Alzheimer's disease. Lipids 26, 421-5.

[176] Hennebelle, M., Plourde, M., Chouinard-Watkins, R., Castellano, C.A., Barberger-Gateau, P. and Cunnane, S.C. (2014). Ageing and apoE change DHA homeostasis: relevance to age-related cognitive decline. Proc Nutr Soc 73, 80-6.

[177] Vitiello, G., Grimaldi, M., D'Ursi, A.M. and D'Errico, G. (2012). The iAbeta5p beta-breaker peptide regulates the Abeta(25-35) interaction with lipid bilayers through a cholesterol-mediated mechanism. Biochem Biophys Res Commun 417, 88-92.

[178] Vitiello G., F.G., Petruk A.A., Falanga A., Galdiero S., D'Ursi A.M., Merlino A., D'Errico G. (2013). Cholesterol modulates the fusogenic activity of a membranotropic domain of the FIV glycoprotein gp36. Soft Matter 9, 6442-6456.

[179] Georgieva, R., Chachaty, C., Hazarosova, R., Tessier, C., Nuss, P., Momchilova, A. and Staneva, G. (2015). Docosahexaenoic acid promotes micron scale liquid-ordered domains. A comparison study of docosahexaenoic versus oleic acid containing phosphatidylcholine in raft-like mixtures. Biochim Biophys Acta 1848, 1424-35.

[180] Brzustowicz, M.R., Cherezov, V., Zerouga, M., Caffrey, M., Stillwell, W. and Wassall, S.R. (2002). Controlling membrane cholesterol content. A role for polyunsaturated (docosahexaenoate) phospholipids. Biochemistry 41, 12509-19.

[181] Shaikh, S.R., Kinnun, J.J., Leng, X., Williams, J.A. and Wassall, S.R. (2015). How polyunsaturated fatty acids modify molecular organization in membranes: insight from NMR studies of model systems. Biochim Biophys Acta 1848, 211-9.

[182] Puff, N., Watanabe, C., Seigneuret, M., Angelova, M.I. and Staneva, G. (2014). Lo/Ld phase coexistence modulation induced by GM1. Biochim Biophys Acta 1838, 2105-14.
[183] Vitiello, G., Falanga, A., Petruk, A.A., Merlino, A., Fragneto, G., Paduano, L., Galdiero, S. and D'Errico, G. (2015). Fusion of raft-like lipid bilayers operated by a membranotropic domain of the HSV-type I glycoprotein gH occurs through a cholesterol-dependent mechanism. Soft Matter 11, 3003-16.
[184] Rasti, B., Jinap, S., Mozafari, M.R. and Yazid, A.M. (2012). Comparative study of the oxidative and physical stability of liposomal and nanoliposomal polyunsaturated fatty acids prepared with conventional and Mozafari methods. Food Chem 135, 2761-70.
[185] Parente, R.A., Nir, S. and Szoka, F.C., Jr. (1990). Mechanism of leakage of phospholipid vesicle contents induced by the peptide GALA. Biochemistry 29, 8720-8.
[186] Bustamante, C., Tinoco, I., Jr. and Maestre, M.F. (1983). Circular differential scattering can be an important part of the circular dichroism of macromolecules. Proc Natl Acad Sci U S A 80, 3568-72.
[187] Williams, T.L., Johnson, B.R., Urbanc, B., Jenkins, A.T., Connell, S.D. and Serpell, L.C. (2011). Abeta42 oligomers, but not fibrils, simultaneously bind to and cause damage to ganglioside-containing lipid membranes. Biochem J 439, 67-77.
[188] Williams, T.L., Urbanc, B., Marshall, K.E., Vadukul, D.M., Jenkins, A.T. and Serpell, L.C. (2015). Europium as an inhibitor of Amyloid-beta(1-42) induced membrane permeation. FEBS Lett 589, 3228-36.
[189] Ellens, H., Bentz, J. and Szoka, F.C. (1984). pH-induced destabilization of phosphatidylethanolamine-containing liposomes: role of bilayer contact. Biochemistry 23, 1532-8.
[190] Oya, T., Hattori, N., Mizuno, Y., Miyata, S., Maeda, S., Osawa, T. and Uchida, K. (1999). Methylglyoxal modification of protein. Chemical and immunochemical characterization of methylglyoxal-arginine adducts. J Biol Chem 274, 18492-502.
[191] Coussons, P.J., Jacoby, J., McKay, A., Kelly, S.M., Price, N.C. and Hunt, J.V. (1997). Glucose modification of human serum albumin: a structural study. Free Radic Biol Med 22, 1217-27.
[192] Watkins, N.G., Neglia-Fisher, C.I., Dyer, D.G., Thorpe, S.R. and Baynes, J.W. (1987). Effect of phosphate on the kinetics and specificity of glycation of protein. J Biol Chem 262, 7207-12.
[193] Remelli, M., Ceciliato, C., Guerrini, R., Kolkowska, P., Krzywoszynska, K., Salvadori, S., Valensin, D., Watly, J. and Kozlowski, H. (2016). DOES hemopressin bind metal ions in vivo? Dalton Trans 45, 18267-18280.
[194] Balboni, G., Marastoni, M., Picone, D., Salvadori, S., Tancredi, T., Temussi, P.A. and Tomatis, R. (1990). New features of the delta opioid receptor:

conformational properties of deltorphin I analogues. Biochem Biophys Res Commun 169, 617-22.

[195] Delaglio, F., Grzesiek, S., Vuister, G.W., Zhu, G., Pfeifer, J. and Bax, A. (1995). NMRPipe: a multidimensional spectral processing system based on UNIX pipes. J Biomol NMR 6, 277-93.

[196] Vranken, W.F., Boucher, W., Stevens, T.J., Fogh, R.H., Pajon, A., Llinas, M., Ulrich, E.L., Markley, J.L., Ionides, J. and Laue, E.D. (2005). The CCPN data model for NMR spectroscopy: development of a software pipeline. Proteins 59, 687-96.

[197] Rieping, W., Habeck, M., Bardiaux, B., Bernard, A., Malliavin, T.E. and Nilges, M. (2007). ARIA2: automated NOE assignment and data integration in NMR structure calculation. Bioinformatics 23, 381-2.

[198] Rega, M.F., Di Monaco, R., Leone, S., Donnarumma, F., Spadaccini, R., Cavella, S. and Picone, D. (2015). Design of sweet protein based sweeteners: hints from structure-function relationships. Food Chem 173, 1179-86.

[199] Spadaccini, R., Crescenzi, O., Tancredi, T., De Casamassimi, N., Saviano, G., Scognamiglio, R., Di Donato, A. and Temussi, P.A. (2001). Solution structure of a sweet protein: NMR study of MNEI, a single chain monellin. J Mol Biol 305, 505-14.

[200] Hobbs, J.R., Munger, S.D. and Conn, G.L. (2007). Monellin (MNEI) at 1.15 A resolution. Acta Crystallogr Sect F Struct Biol Cryst Commun 63, 162-7.

[201] Kelly, J.W. (1998). The alternative conformations of amyloidogenic proteins and their multi-step assembly pathways. Curr Opin Struct Biol 8, 101-6.

[202] Yoshimura, Y., Lin, Y., Yagi, H., Lee, Y.H., Kitayama, H., Sakurai, K., So, M., Ogi, H., Naiki, H. and Goto, Y. (2012). Distinguishing crystal-like amyloid fibrils and glass-like amorphous aggregates from their kinetics of formation. Proc Natl Acad Sci U S A 109, 14446-51.

[203] Khurana, R., Ionescu-Zanetti, C., Pope, M., Li, J., Nielson, L., Ramirez-Alvarado, M., Regan, L., Fink, A.L. and Carter, S.A. (2003). A general model for amyloid fibril assembly based on morphological studies using atomic force microscopy. Biophys J 85, 1135-44.

[204] Pace, C.N., Laurents, D.V. and Thomson, J.A. (1990). pH dependence of the urea and guanidine hydrochloride denaturation of ribonuclease A and ribonuclease T1. Biochemistry 29, 2564-72.